**Title**
Optical Modulation and Detection Techniques for High-Spectral Efficiency



**Author**
Chien, Cheng-Chung

**Publication Date**
2008

Peer reviewed|Thesis/dissertation

UNIVERSITY OF CALIFORNIA
RIVERSIDE

# Optical Modulation and Detection Techniques for High-Spectral Efficiency

A Dissertation submitted in partial satisfaction
of the requirements for the degree of

Doctor of Philosophy

in

Electrical Engineering

by

Cheng-Chung Chien

December 2008

Dissertation Committee:
Dr. Ilya Lyubomirsky Chairperson
Dr. Ilya Dumer
Dr. Zhengyuan Xu

The Dissertation of Cheng-Chung Chien is approved:

______________________________

/Ilya Dumer/
______________________________

______________________________
Committee Chairperson

University of California, Riverside

# ACKNOWLEDGMENTS

First of all, I would like to thank my supervisor, Dr. Ilya Lyubomirsky, for his kind guidance, supports, and helpful advices for my research over the years. Without these, this dissertation would not have been possible.

I also would like to thank Dr. Ilya Dumer and Dr. Zhengyuan Xu for their time and efforts on serving as my committee.

I would also like to thank my colleagues and friends, Sean Wang, Dan Giles, Paul Stovall, Frank MacDonald, Elmar Palma, Kyle Pi, Eric Cheung and Wu-Feng Ya, and my climbing partners, Ola Ween, Gregory Gibson, and Diane Menuz. Their friendships really enrich my life at UCR.

Last but not least, I thank my wife, Vivienne Wang, my son, Matt Chien, and my parents for their love and unlimited support.

# ABSTRACT OF THE DISSERTATION

## Optical Modulation and Detection Techniques for High-Spectral Efficiency

by

Cheng-Chung Chien

Doctor of Philosophy, Graduate Program in Electrical Engineering
University of California, Riverside, December 2008
Dr. Ilya Lyubomirsky, Chairperson

The development of advanced multilevel modulation and detection technologies is important for enabling efficient lightwave transmission of high-bit rate services, such as 40G Synchronous Optical Network (SONET/SDH) and 100G Ethernet. In this dissertation, we proposed and experimentally demonstrated several modulation and detection techniques for different optical modulation formats.

Optimal duobinary was achieved by optimizing LPF, transmitter and receiver bandpass filter, which gains 4.4 dB better receiver sensitivity compared with conventional duobinary. The optimum RZ-duobinary was demonstrated and its performances of receiver sensitivity, fiber chromatic dispersion tolerance, and self-phase modulation nonlinearity tolerance were compared with NRZ-duobinary's. Surprisingly, and contrary to the case of on–off keying, we find the NRZ pulse shape

to be superior, compared with RZ, for duobinary transmission in all the cases that were studied.

A new DPSK demodulation scheme employing a frequency discriminator filter followed by direct detection (FD-DD) was proposed, which achieved a 1.2 dB better sensitivity compared with NRZ-OOK. DQPSK operating at 20 Gb/s doubles the spectral efficiency. Our proposed FD-DD demodulation scheme offers 2 times better chromatic dispersion tolerance than conventional delay interferometer followed by balanced detection (DI-BD) scheme. FD-DD demodulation scheme for PolMux DQPSK operating at 40 Gb/s not only quadruples the spectral efficiency of NRZ-DPSK, but also maintains roughly the same chromatic dispersion tolerance of a 20 Gb/s DQPSK.

This research work improves system performances for more efficient next generation fiber communication.

# TABLE OF CONTENTS

# LIST OF FIGURES

# LIST OF TABLES

# Chapter 1

# Introduction

## 1.1 Background

An optical modulation format is the method used to impress data (i.e. information) on an optical carrier wave for transmission. The simple Non-Return-to-Zero (NRZ) On-Off Keying (OOK) and Return-to-Zero (RZ) OOK modulation formats are a natural choice when bandwidth is plentiful. Indeed, the immense intrinsic bandwidth of optical fiber (~ 25 THz) has enabled an exponential growth in transmission capacity at a rate that even surpasses Moore's Law for electronic computers [1]. The development of wavelength division multiplexing (WDM) and all-optical amplification technology based on erbium doped fiber amplifier (EDFA) made it possible to transmit multiple channels on a single strand of optical fiber as well as amplify these signals in different channels simultaneously without electrical regeneration. However, the demand of optical fiber communication capacity has been increased dramatically over the past few years and expected to keep this trend in the near future. The usage of simple OOK modulation formats is questionable.

## 1.2 Motivation

In most transmission channel, bandwidth is at a premium. The usage of optical fiber between transmitters and receivers provides a vast channel bandwidth for communication. But a good signaling scheme plays an important role to make efficient use of the bandwidth. As the demand of capacity growths, further capacity increases could be achieved by, first, laying down more optical fiber links, second, by increasing higher bit rate per channel (10 Gb/s toward 40 Gb/s, even 100 Gb/s), and third, by applying more efficient use of the available fiber links, [2, 3, 4, 5, 6]. The first method requires a lot of infrastructural works and is extremely costly. The second method is limited by the speed of commercially available electric devices, which is limited to 40 GHz/s nowadays. The third method, applying advanced multilevel modulation formats with better spectral efficiency, provides a more cost-effective solution to achieve desired capacity. The overall capacity (b/s) of a WDM transmission system is governed by the available bandwidth (Hz) and by the achievable spectral efficiency (b/s/Hz). By applying advanced multilevel modulation formats and packing channels more closely (channel spacing from 100 GHz toward 12.5 GHz), the spectral efficiency of fiber optic communication is pushing from 0.4 toward 1.6 (b/s/Hz) and beyond. In this dissertation, we focus on applying novel modulation and demodulation techniques for higher spectral efficiency and optimizing fiber optic communication system.

## 1.3 Organization of this Dissertation

An introduction is given in chapter one. Optical modulation formats and performance evaluation parameters are covered in chapter two. Intensity modulations are described in chapter three, which includes NRZ- and RZ-OOK as a baseline for comparison with other advanced formats. Duobinary is also presented after OOK in chapter four. The optimal NRZ- and RZ-duobinary are demonstrated and their performances are compared. In chapter five, phase modulation formats (DPSK, DQPSK and PolMux DQPSK) are included. The final chapter summarizes the conclusions.

# Chapter 2

# Optical Modulation Formats and Performance Evaluations

## 2.1 Introduction to Optical Modulation Formats

An optical modulation format is the method used to impress data (i.e. information) on an optical carrier wave for transmission over optical fiber. The simplest optical modulation format is on-off-keying (OOK) intensity modulation, which can take either of two forms: non-return-to-zero (NRZ) or return-to-zero (RZ) [7, 8, 9]. NRZ requires roughly half the bandwidth of RZ, and is thus easier to implement, and is less costly. The receiver for both NRZ and RZ modulation is based on a square-law (intensity) photodetector.

To achieve high-speed modulation, an external modulator, typically based on the Mach-Zehnder modulator (MZM) structure, is often used instead of modulating the laser source directly. Figure 2.1 illustrates how the MZM operates. CW light from a laser is split to follow two separate optical paths. The electrical data signal introduces a $\pi$-phase shift, via electro-optic effect, between the two paths for logical 0 versus logical 1. Light from the two paths is allowed to interfere at the output such that the $\pi$-phase shifts lead to destructive interference for optical logical 0, and constructive interference for optical logical 1. A transmission curve of an optical modulator can be obtained by measuring its optical output power versus bias voltages while keeping its input optical power constant.

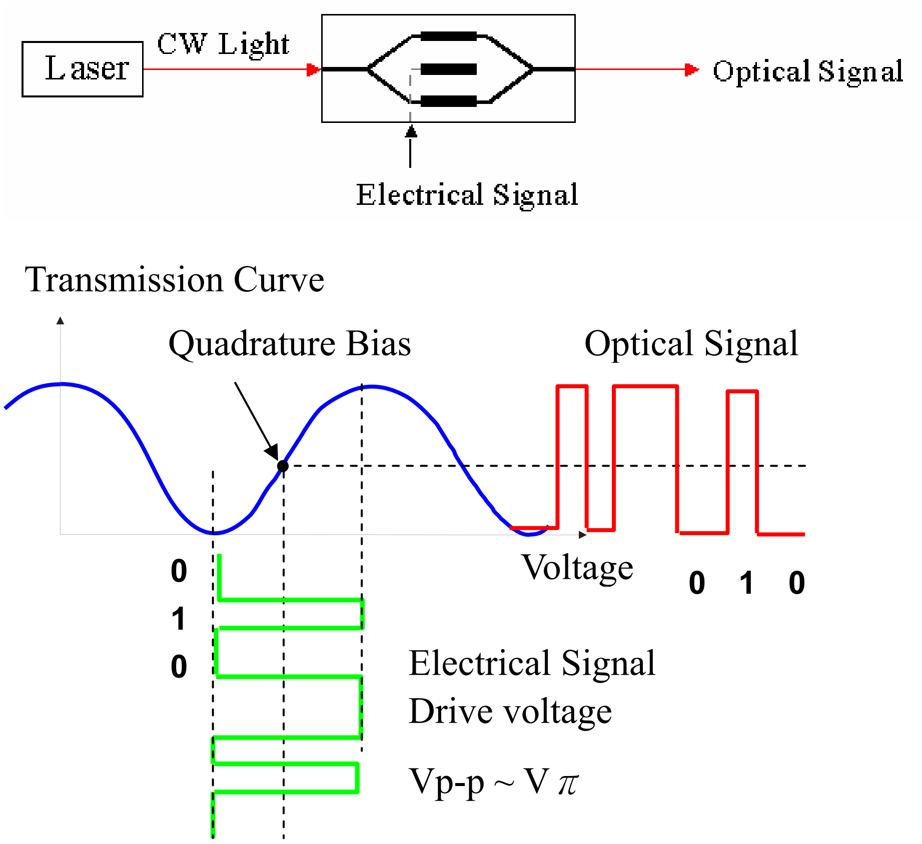


Figure 2.1: Schematic diagram for Mach-Zehnder modulator (MZM). The MZM transmission curve forms periodic interference fringes in the output intensity as a function of applied voltage.

The mathematic formula of a transmission curve of modulator is derived below:

$$E_0 = \frac{1}{\sqrt{2}}(E_1 e^{j\Phi_1} + E_2 e^{j\Phi_2}) \tag{2.1}$$

$$\text{If } \Phi_1 = -\Phi_2 = \frac{\pi}{2}\frac{V(t)}{V_\pi} \text{ and } E_1 = E_2 = \frac{E_i}{\sqrt{2}} \tag{2.2}$$

$$E_0 = \frac{E_i}{2}(e^{j\Phi_1} + e^{j\Phi_2}) = \frac{E_i}{2}(e^{j\frac{\pi}{2}\frac{V(t)}{V_\pi}} + e^{-j\frac{\pi}{2}\frac{V(t)}{V_\pi}}) = E_i[\cos(\frac{\pi}{2}\frac{V(t)}{V_\pi})] \qquad (2.3)$$

$$\frac{|E_o|^2}{|E_i|^2} = \cos^2(\frac{\pi}{2}\frac{V(t)}{V_\pi}) = \frac{1}{2}[1+\cos(\pi\frac{V(t)}{V_\pi})] \qquad (2.4)$$

From (2.4), a transmission curve in figure 2.1 could be obtained. An important parameter for any MZM is $V_\pi$, which is the voltage swing required to go from null to peak in the MZM transmission curve. Thus, to generate NRZ modulation, the RF driver amplifier must provide an output voltage swing of $V_{p-p} \sim V_\pi$. (we shall see below that for some modulation formats a voltage swing of $2V_\pi$ is necessary). Figure 2.1 also shows by properly choosing swing and bias voltages how electrical signals convert to optical signals via transmission curve.

## 2.2 Performance Evaluations

In this section, some important performance evaluation parameters used in this dissertation are introduced and described in order to compare the differences between modulation formats. The parameters covered in this chapter are the bit-error rate, Q parameter, optical signal to noise ratio (OSNR), receiver sensitivity, chromatic dispersion tolerance, spectral efficiency (SE), self-phase modulation and frequency offset tolerance [10].

### 2.2.1 Bit-Error Rate and Q parameter

The fluctuating optical signal caused by all kinds of impairments in fiber link is received by receiver, which converts optical signal to electrical signal. The electrical signal is fed into an error detector, which contains a decision circuit to sample the signal and compares to the transmitted data patterns. A bit-error ratio (BER), sometime refers to bit-error rate, is defined as the ratio of the number of bits incorrectly received to the total number of bits received during a specified time interval. Hence, a BER of $4 \times 10^{-6}$ corresponds to an average 4 errors per million bits. BER can also be defined as the probability of incorrect identification of a bit by the decision circuit of the receiver [10]. The error probability is defined as

$$\text{BER} = p(1)P(0/1)+p(0)P(1/0) \tag{2.5}$$

Where p(1) and p(0) are the probabilities of receiving bits 1 and 0, respectively, P(0/1) is the probably of deciding 0 when 1 is received, and P(1/0) is the probability of deciding 1 when 0 is received. Since 1 and 0 are equally likely to occur, p(1) = p(0) = 1/2, then the BER becomes

$$\text{BER} = 1/2[P(1/0)+P(0/1)] \tag{2.6}$$

Where

$$P(0/1) = \frac{1}{\sigma_1\sqrt{2\pi}}\int_{-\infty}^{I_D}\exp(-\frac{(I-I_1)^2}{2\sigma_1^{\ 2}})dI = \frac{1}{2}erfc(\frac{I_1-I_D}{\sigma_1\sqrt{2}}), \tag{2.7}$$

$$P(1/0) = \frac{1}{\sigma_0\sqrt{2\pi}} \int_{I_D}^{\infty} \exp(-\frac{(I - I_0)^2}{2\sigma_0^{\ 2}}) dI = \frac{1}{2} erfc(\frac{I_D - I_0}{\sigma_0\sqrt{2}}), \qquad (2.8)$$

And *erfc* stands for the complementary error function, defined as

$$erfc(x) = \frac{2}{\sqrt{\pi}} \int_{x}^{\infty} \exp(-y^2) dy \qquad (2.9)$$

By substituting Eqs. (2.7) and (2.8) in Eq. (2.6), the BER is given by

$$\text{BER} = \frac{1}{4}[erfc(\frac{I_1 - I_D}{\sigma_1\sqrt{2}}) + erfc(\frac{I_D - I_0}{\sigma_0\sqrt{2}})] = \frac{1}{4}[P(0/1) + P(1/0)] \qquad (2.10)$$

Equation (2.10) shows the BER depends on the decision threshold $I_D$. In practice, the minimum BER occurs when $I_D$ is chosen such that

$$\frac{(I_D - I_1)^2}{2\sigma_1^{\ 2}} = \frac{(I_D - I_0)^2}{2\sigma_0^{\ 2}} + \ln(\frac{\sigma_1}{\sigma_0}) \qquad (2.11)$$

where $\sigma_0 \cong \sigma_1$ in most practical cases.

$$(\frac{I_1 - I_D}{\sigma_1}) = (\frac{I_D - I_0}{\sigma_0}) \equiv Q \qquad (2.12)$$

An explicit expression for $I_D$ is

$$I_D = \frac{\sigma_0 I_1 + \sigma_1 I_0}{\sigma_0 + \sigma_1} \qquad (2.13)$$

When $\sigma_0 = \sigma_1$, $I_D = (I_0 + I_1)/2$, which corresponds to setting the decision threshold in the middle.

The BER with the optimum setting of the decision threshold is obtained by using Eqs. (2.10) and (2.12) and depends only the Q parameter as

$$\text{BER}= \frac{1}{2} erfc(\frac{Q}{\sqrt{2}}) \tag{2.14}$$

where the parameter Q is obtained from Eqs. (2.12) and (2.13) and is given by

$$Q = \frac{I_1 - I_0}{\sigma_1 + \sigma_0} \tag{2.15}$$

In other words,

$$\text{Q=20*log} \, [\sqrt{2}\ erfc^{-1}(\text{2*BER})] \text{ in dB.} \tag{2.16}$$

where $erfc^{-1}$ represents invert error function. The BER improves as Q increases. The receiver sensitivity corresponds to the average optical power for Q $\approx$ 6, when BER $\approx 10^{-9}$ .

## 2.2.2 Receiver Sensitivity

The performance criterion of a receiver is governed by the bit-error ratio (BER), defined as the probability of incorrect identification of a bit by the decision circuit of the receiver. A receiver is said to be more sensitive if it achieves the same performance with less required incident power. The common receiver sensitivity is defined as the minimum average received power for a receiver to achieve a BER of $10^{-9}$ [10]. Since the forward-error correction coding is well developed, nowadays system designers are more interested in the region of BER down to $10^{-3}$.

### 2.2.3 Chromatic Dispersion

Chromatic Dispersion (CD), also known as Group-Velocity Dispersion (GVD), is a fundamental impairment of fiber communication. In fiber optics, the pulses used to carry information over distances occupy some amount of spectral bandwidth. The frequency dependence of the group velocity leads to pulse broadening, because different spectral components of the pulse travel in slightly different speed and thus do not arrive simultaneously at the fiber output. The Group-Velocity $V_g$ is define as

$$v_g = \frac{\partial \omega}{\partial \beta} = \frac{c}{\bar{n}} \tag{2.17}$$

where $\omega$ is frequency and $\beta$ is defined as propagation constant. $c$ is the speed of light and $\bar{n}$ is mode index.

$$\beta = \bar{n}\frac{\omega}{c} \tag{2.18}$$

$$\beta_2 = \frac{d^2\beta}{d^2\omega} = \frac{d}{d\omega} v_g \tag{2.19}$$

where $\beta_2$ is known as the GVD parameter, which determines how much an optical pulse would broaden on propagation inside the fiber. This pulse broaden effect, which leaks optical power into adjacent bit slots and causes inter-symbol interference (ISI), is proportional to propagated fiber length and requires extra input power (i.e higher optical signal-to-noise ratio) at the receiver end to compensate signal degradation. A system is said to be more tolerant to chromatic dispersion, if less extra power is required at the receiver in order to keep the same performance compared to back-to-back for certain amount of fiber length traveled.

### 2.2.4 Self-Phase Modulation

Although silica-glass has intrinsically low optical nonlinearity, the fiber optical mode is confined to a very small effective area ~ 50-80 μm$^2$, and propagation lengths can be relatively long ~ 1000 km. Thus, when a sufficiently high optical power is launched into the fiber, optical nonlinear effects can occur. The fundamental fiber nonlinearity is due to Kerr Effect, where the refractive index becomes power dependent [16]. The propagation constant also can be written as

$$\beta' = \beta + k_0 \bar{n}_2 P / A_{eff} \equiv \beta + \gamma P \tag{2.20}$$

where $\gamma = 2\pi \bar{n}_2 /(A_{eff}\lambda)$ is an nonlinear parameter depending on effective core area $A_{eff}$ and the wavelength $\lambda$. The nonlinear phase shift produced by $\gamma$ term is given by

$$\Phi_{NL} = \int_0^L (\beta' - \beta) dz = \int_0^L \gamma P(z) dz = \gamma P_{in} L_{eff} \tag{2.21}$$

where $p(z) = P_{in}\exp(-\alpha z)$, $\alpha$ is fiber loss parameter and $L_{eff}$ is effective interaction length defined as $L_{eff} = [1 - \exp(-\alpha L] / \alpha$. Note for an N span transmission system, the total nonlinear phase shift is enhanced by N, which can be as high as ~ 100 for submarine fiber systems. From Eq. 2.21, the nonlinear phase shift $\Phi_{NL}$ varies with time across a pulse dependent on input power $P_{in}$ and causes optical phase changes with time. This nonlinear effect is called self-phase modulation (SPM) due to the self-induced nonlinear phase modulation phenomenon. In OOK systems, the SPM-induced chirp affects the pulse sharp through interaction with GVD and often leads to additional pulse broadening causing considerable penalties and limiting the performance of lightwave system [10]. SPM is also detrimental in systems based on phase modulation because it can convert intensity noise from optical amplifiers into phase noise. This nonlinear phase noise is a major impairment in long haul DPSK/DQPSK systems.

### 2.2.5 Spectral Efficiency

Spectral efficiency (SE) is very important in fiber optics, since the spectral bandwidth affects the number of channels occupied in a single fiber.

$$SE = \frac{C}{\Delta f} \tag{2.22}$$

where $C$ is the capacity per channel with unit of bits per second (b/s) and $\Delta f$ is the channel spacing with unit of bits per second per hertz (b/s/Hz) [10].

### 2.2.6 Frequency Offset Tolerance

The laser frequency and demodulator (i.e. filter or delay interferometer) must be align and stabilized with time. Unfortunately, this is not always the case. The laser frequency can drift with time as well as demodulator. The frequency offset tolerance is measured by the OSNR penalties occurring when the laser frequency and filter center frequency are misaligned. The measurement can be done by varying the laser frequency (i.e. wavelength), but fixing the filter center, or vice versa. Our experiment is done by varying the laser, because the DFB laser provides a more accurate control with temperature stability over detuning the filter. The OSNR penalty is measured versus laser frequency detuning from the optimum.

### 2.2.7 Amplified Spontaneous Emission

The amplified spontaneous emission (ASE) is the main dominated noise source in long haul fiber communication system. ASE is produced by erbium doped fiber amplifier (EDFA) distributed along the optical transmission line to periodically boost signal power. As optical signals propagate through fiber links experiencing multiple optical amplifying, ASE noise is also amplified and accumulated, which degrades optical signal-to-noise ratio along the optical path. Although ASE noise can be reduced by employing proper optical filtering, it can not be eliminated completely, and results in fundamental impairment in optically amplified systems.

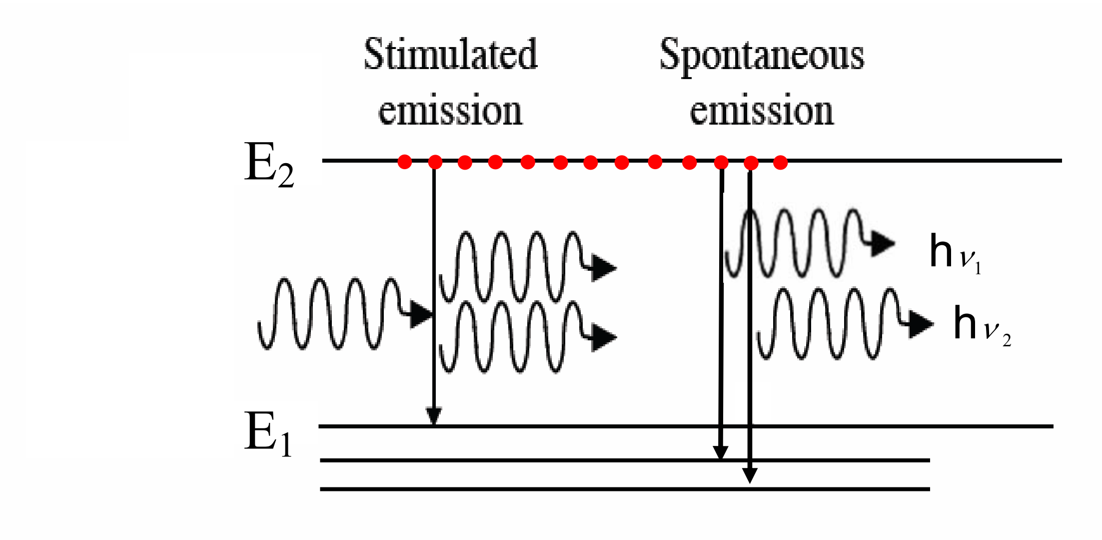


Figure 2.2: Stimulated emission (Gain) and Amplified Spontaneous Emission (ASE) noise of EDFA.

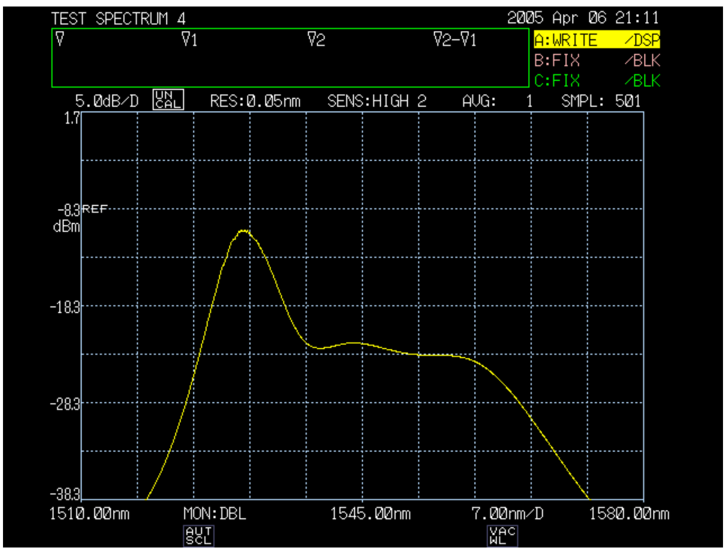


Figure 2.3: Spectrum of amplified spontaneous emission from EDFA measured in our lab.

Fig. 2.2 shows the mechanics of stimulated emission (Gain) and amplified spontaneous emission (ASE) noise of EDFA. Fig. 2.3 shows the measured spectrum of ASE noise in our lab. The gain peak near ~ 1530 nm is due to the erbium gain medium; it is typically flattened out using special gain flattening filters (GFF) inside the amplifiers.

### 2.2.8 Eye Diagram

In telecommunication, an eye diagram is also known as an eye pattern, which is formed by superposing the bit patterns on top of each other. A high speed digital sampling oscilloscope is employed to sample the data stream and display the superposed bit patterns. It is so called because, for several types of modulation formats, the pattern looks like a series of eyes between a pair of rails. A typical eye diagram of Non-Return-to-Zero On-Off-Keying signal is shown in figure 2.6. The eye diagrams are used for system performance evaluations, such as pulse raise/fall time, duty cycle, extinction ratio, jitter, eye height/width, crossing percentage, etc. An open eye pattern corresponds to minimal distortion of the signal. While a closure of the eye pattern reveals the system imperfections or impairments, such as due to ISI.

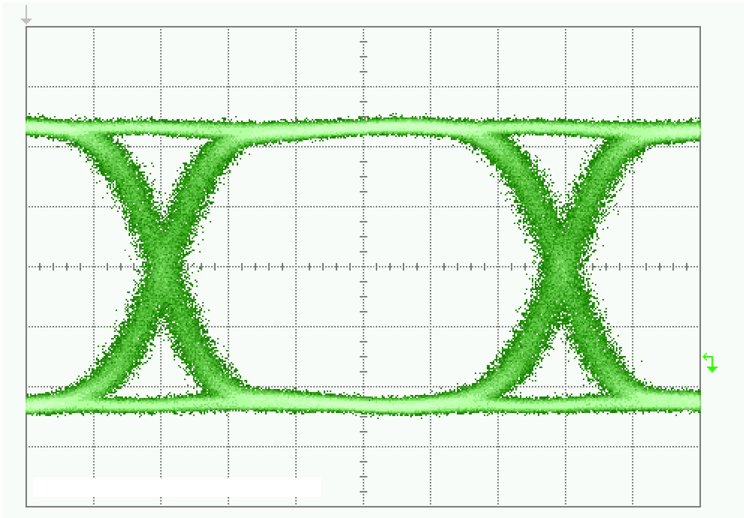

Figure 2.4: Eye diagram of Non-Return-to-Zero On-Off-Keying signal.

# Chapter 3

# Binary Intensity Modulation Formats

Binary intensity modulation or also called amplitude shift keying is the most deployed modulation format nowadays for optical communication system. It's also known as On-Off-Keying (OOK) because the transmitted data are represented by the presence ("On" state) /absence ("Off" state) of laser carrier intensity, which could be realized by either modulating the laser drive current directly or employing an external optical modulator to carve the amplitude of a continuous wave laser output [11]. In modern optical fiber communication system, a MZM made in $LiNbO_3$ material is a typical external modulators operating at higher bit rate and also providing better performance than directly modulated laser [12].

## 3.1 NRZ- and RZ- On-Off Keying

In principle, NRZ and RZ have the same quantum-limited receiver sensitivity [13]. However, RZ is less susceptible to ISI, and in practice achieves 1-2 dB better performance compared to NRZ [14]. RZ pulses also benefit from a soliton-like effect in optical fiber, and suffer less distortion due to fiber nonlinearity compared to NRZ [15]. For these reasons, RZ (or a related format called chirped-RZ) modulation is currently favored in ultra-long haul submarine systems where the use of more costly transmitters and receivers is justified. Terrestrial transmission systems, where cost is a primary driving factor, typically employ simple NRZ modulation.

### 3.1.1 NRZ OOK Encoder

In high-speed transmission of 10 Gb/s or greater, RZ and NRZ modulation is most easily realized using the Mach-Zehnder modulator (MZM) [11, 12, 17]. Both NRZ and RZ modulation formats are realized in our laboratory. The schematic diagram for the 10 Gb/s NRZ transmitter, and measured eye are shown in figure 3.1. The NRZ transmitter using a single MZM was described in chapter 2.1.

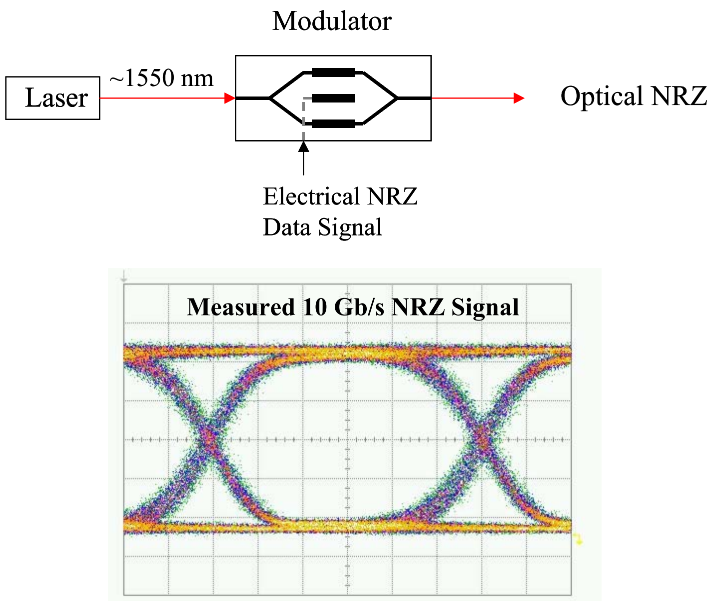


Figure 3.1: Experimental 10 Gb/s NRZ transmitter, and measured NRZ eye diagram.

### 3.1.2 RZ OOK Encoder

The experimental RZ transmitter requires two MZM modulators. The first MZM is called a “pulse carver.” It produces a periodic RZ pulse train at the bitrate since the drive signal is a sine wave with frequency equal to bitrate (i.e. clock signal). The second MZM is a gating modulator, used to impress the data on the RZ pulse train. The gating modulator is synchronized with the pulse carver modulator by adjusting the phase of either clock or data signal. Figure 3.2 shows the experimental 10 Gb/s RZ transmitter realized in our laboratory, and the measured RZ eye diagram.

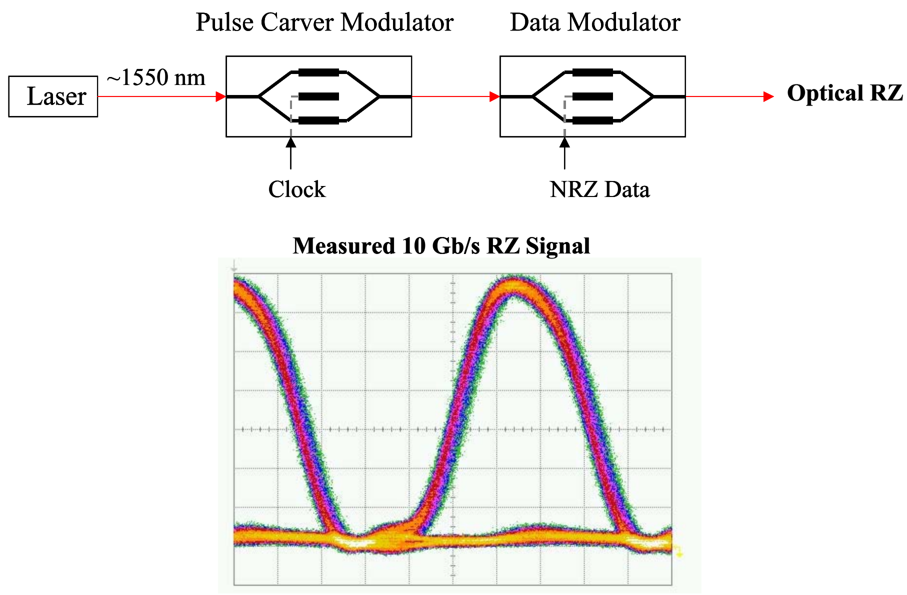


Figure 3.2: Experimental 10 Gb/s RZ transmitter, and measured RZ eye diagram.

## 3.2 On-Off-Keying Decoder

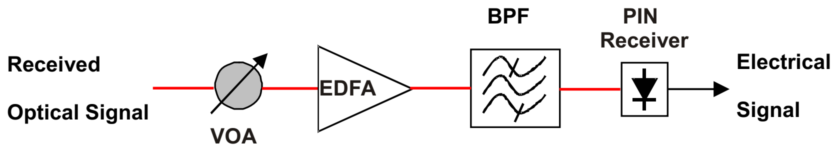


Figure 3.3: Scheme diagram of On-Off-Keying decoder

Fig. 3.3 shows a typical on-off keying receiver. The optical signal is passing through a variable optical attenuator which controls the input power to the next step, an optical amplifier. The amplifier boosts the power of incoming optical signal. EDFAs are usually employed and are commonly used to improve the receiver sensitivity. An optical bandpass filter is then used to shape the signal and eliminate undesired noise getting into receiver. The receiver is based on a square-law photodetector, which is sensitive to optical intensity. The main function of receiver is converting optical signal into electrical signal.

## 3.3 Results

Figure 3.4 shows our experimental setup for the ASE noise-limited OOK system measurements. An Optical OOK modulation format is produced at 10 Gb/s by a zero-chirp Lithium Niobate modulator, with the pulse pattern generator (PPG) set to produce PRBS patterns of length $2^{23}$-1. Two modulator schemes as shown in previous

OOK encoder section are employed to produce NRZ- and RZ- OOK modulation formats. After modulation, the optical signal passes through a variable optical attenuator (VOA), and an erbium doped fiber amplifier (EDFA). The VOA is used to set the average power input into the optically pre-amplified receiver. The EDFA pre-amplifier is followed by an Agilent 86146B unit, which is used to realize the tunable bandwidth receiver optical bandpass filter (Rx BPF). The receiver in the experimental setup is based on a conventional 10 Gb/s p-i-n photodetector with integrated trans-impedance amplifier (TIA), and limiting amplifier (LA), and is specified to have a bandwidth of ~ 7 GHz. The receiver output is fed into a 12.5 GHz error detector for bit error rate measurement.

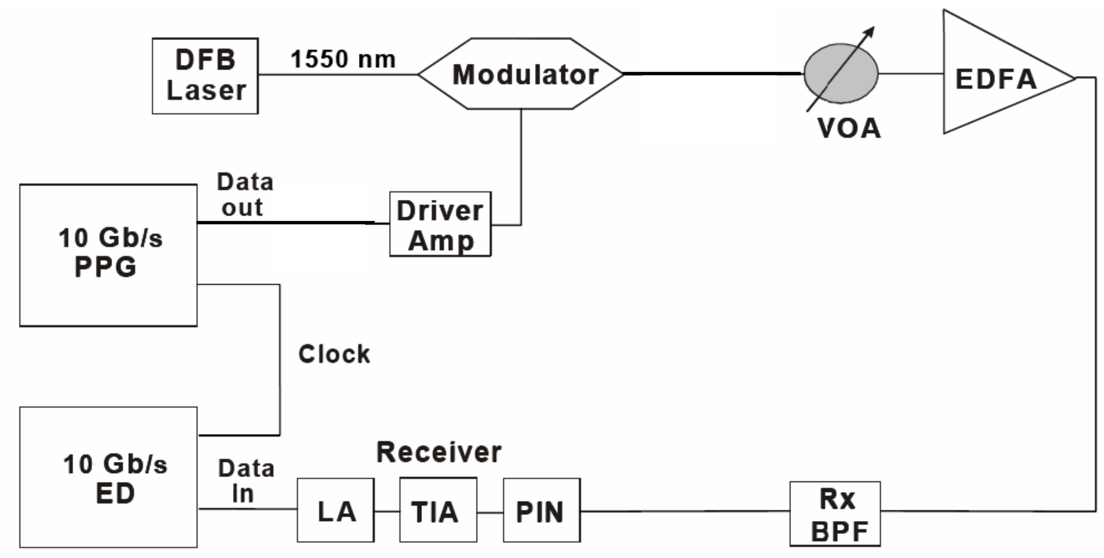


Figure 3.4: Experimental setup of our OOK system realized in the lab.

Figure 3.5 presents the experimental results that determine the optimum Rx bandpass filter bandwidths for NRZ- and RZ- OOK in ASE noise-limited system, which shows the BER as a function of Rx BPF bandwidth while OSNR is kept fixed at 14 dB/0.1nm and 13 dB/0.1nm for NRZ- and RZ- OOK respectively. The lines drawn through the data points serve as guides for the eye. The optimum Rx BPF bandwidth is found to be $B_{opt} \sim$ 12 GHz for NRZ-OOK and 25 GHz for RZ-OOK. This figure also shows RZ- enjoys slightly larger than 1 dB OSNR advantage over NRZ-OOK for the same BER.

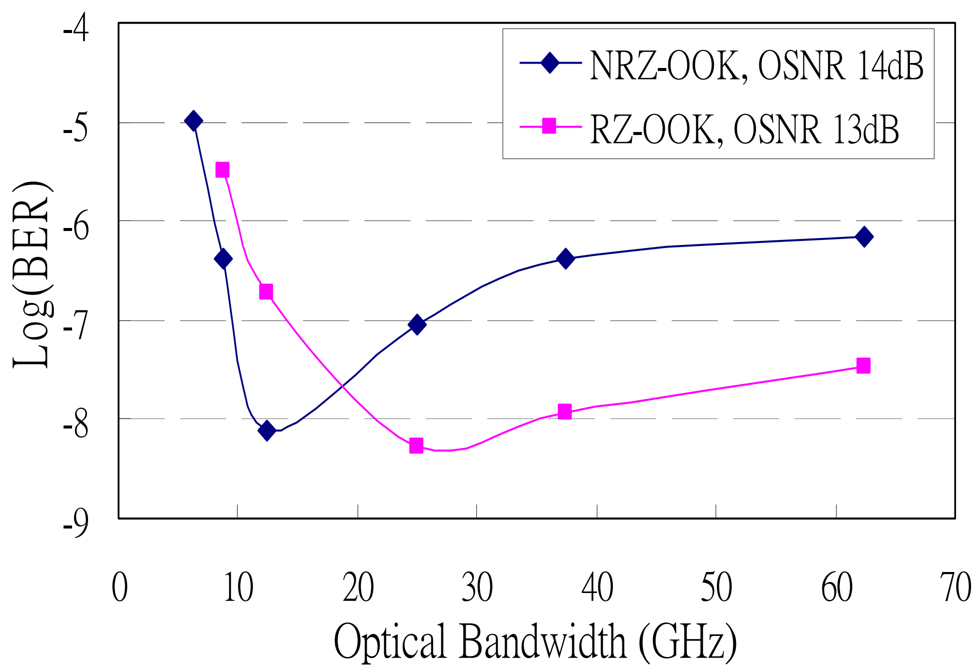


Figure 3.5: Optimization of receiver bandpass filter bandwidth for NRZ- and RZ-OOK.

Figure 3.6 shows our results for back-to-back optically pre-amplified receiver sensitivity measurements, while the receiver bandpass filters set in their optimum bandwidth as shown in Fig. 3.5. The receiver sensitivity (BER = $10^{-9}$) is measured to be –38, -37.5 for RZ- and NRZ-OOK, respectively. Thus, RZ performs 1.5 dB better compared with NRZ, which is typically observed in practice.

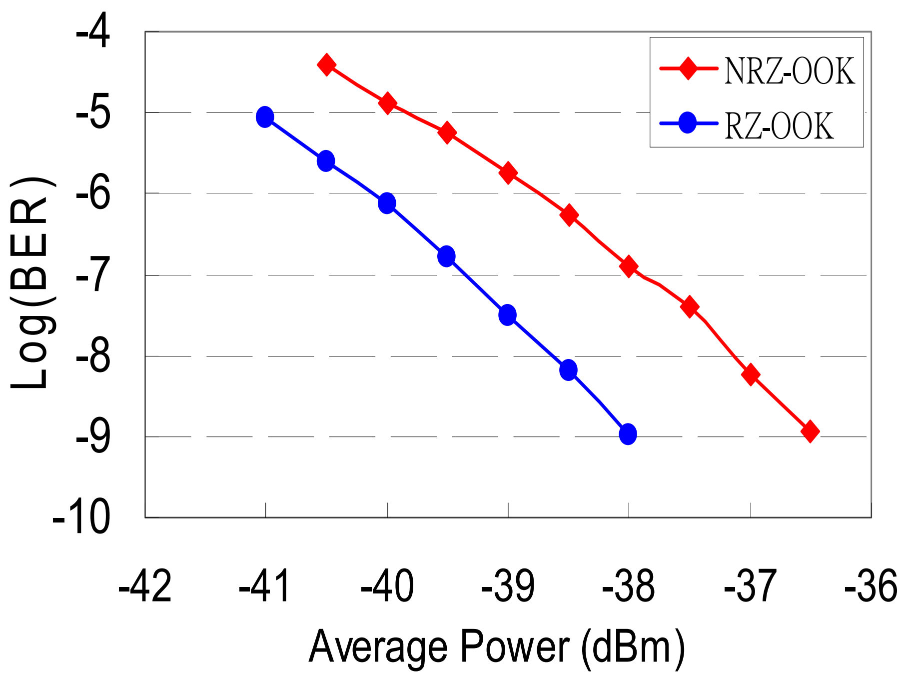


Figure 3.6: Receiver sensitivity of NRZ- and RZ-OOK

The dispersion tolerance is obtained by measuring receiver sensitivity with different lengths of conventional single mode fiber (SMF) inserted between transmitter and VOA. The launch power is fixed at a relatively low value of – 6.5 dBm to avoid self-phase modulation effects in the fiber. Figure 3.7 shows the measured dispersion tolerance of RZ- and NRZ-OOK modulation formats. RZ-OOK has worse dispersion tolerance with 2 dB OSNR penalty happened at 26 Km SMF. NRZ-OOK reaches 2 dB OSNR penalty at 45 Km SMF. This can be explained due to the naturally wider spectrum bandwidth of RZ-OOK which contains higher spectrum frequency components resulting in severer chromatic dispersion.

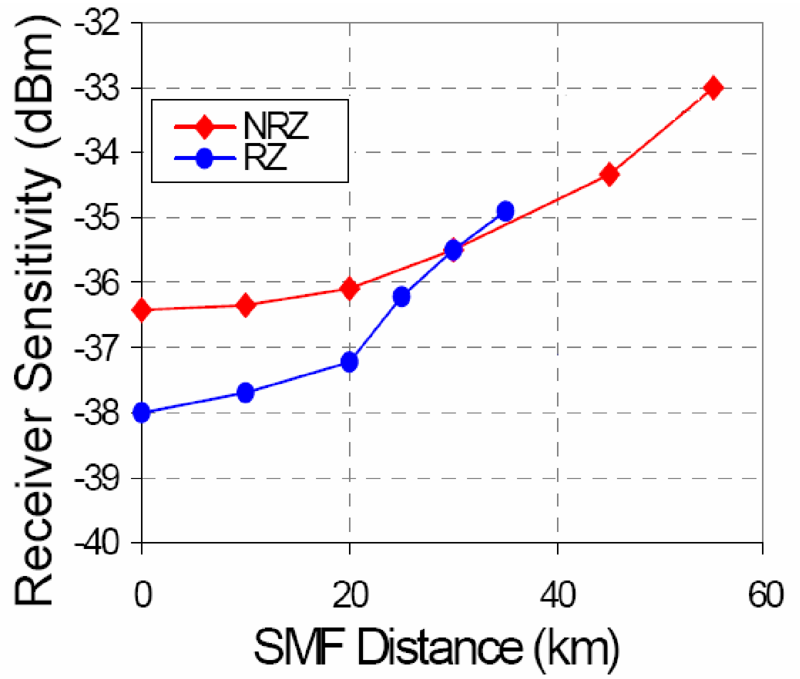


Figure 3.7: Comparison of chromatic dispersion for NRZ- and RZ-OOK

Figure 3.8 shows measured optical spectra for 10 Gb/s NRZ and 50% duty cycle RZ. As seen in figure 3.8, RZ occupies roughly twice as much bandwidth as NRZ.

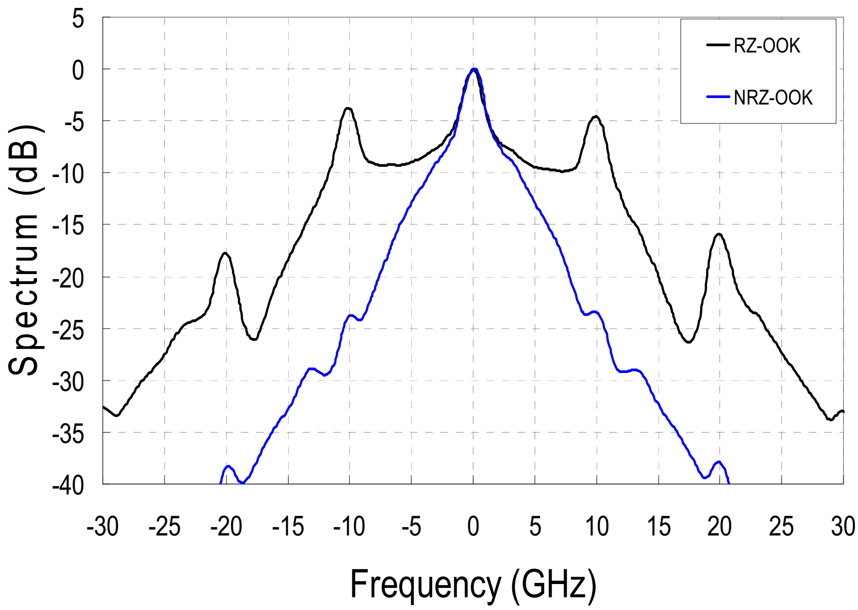


Figure 3.8: Spectra of NRZ-OOK and 50% duty cycle RZ-OOK.

The results on OOK represented in this chapter serves as a baseline for comparison with more advanced modulation formats described in the following chapters.

# Chapter 4

# Optical Duobinary Modulation Formats

In wavelength-division multiplexing (WDM) transmission systems, the total capacity is rapidly approaching 10 Tb/s. This Moore's Law-like growth in transmission capacity is fast exhausting the bandwidth of current optical amplifier technologies [93]. If the progress is to continue, new spectrally more efficient modulation formats must be developed. In this respect, optical duobinary modulation, also known as phase shaped binary modulation, is an attractive modulation format for attaining high spectral efficiency in WDM transmission systems [20]. Duobinary modulation results in a narrower optical signal spectrum compared to non-return-to-zero (NRZ) modulation, which is beneficial for ameliorating the effects of fiber dispersion [18, 23], as well as for reducing adjacent channel crosstalk in ultra-dense WDM (UDWDM) systems [28]. Duobinary systems also enjoy a cost advantage over other advanced modulation formats, such as return-to-zero (RZ) and differential phase shift keying (DPSK), since duobinary requires less dispersion compensation with transmitters and receivers that are comparable in cost to those used in NRZ systems [29, 66, 91]. Previous studies also showed its good tolerant of intersymbol interference (ISI) as well [24, 25, 26].

## 4.1 NRZ-Duobinary

Electrical duobinary has a long history in RF communications, where it is known to give a factor of ~ 2 better spectral efficiency compared to NRZ. When the need of lightwave communication system capacity increases, optical NRZ-duobinary is also attractive due to its narrow spectral bandwidth, which is about half the bandwidth of a conventional binary NRZ intensity modulation (IM) [19, 20, 21].

A practical approach of an optical duobinary system consists of a precoder logical circuit, an encoder realized by a duobinary filter, which converts binary signals into three-level electrical duobinary signals, an electrical modulator driver amplifier used to amplify to electrical duobinary signal to drive the optical MZM, and a decoder to extract the data from optical duobinary signal.

### 4.1.1 NRZ-Duobinary Precoder

The differential precoder is used to avoid recursive decoding in the receiver thus avoiding error propagation and reducing hardware complexity [20, 29, 30]. The duobinary precoder contains a logic XOR gate with a one bit delay/feedback loop. The precoding function can be expressed as:

$$a_n = b_n \oplus a_{n-1} \tag{4.1}$$

where $b_n$ is the transmitted binary data sequence. $a_n$ is the precoded binary sequence and $\oplus$ is the logic XOR gate. In our setup precoder is ignored due to the common usage of pseudo-random bit sequences (PRBS) pattern where the precoded bit stream is a time-delayed and logic inverted version of the input PRBS bit stream. A logic inverter can be put in front of precoder or receiver to correct this issue. Fortunately, the logic inversion causes on problem in laboratory setup. Since error detectors can still recognize and convert the received inverted data.

An electrical duobinary precoder and bit sequences at different stages are shown in figure 4.1.

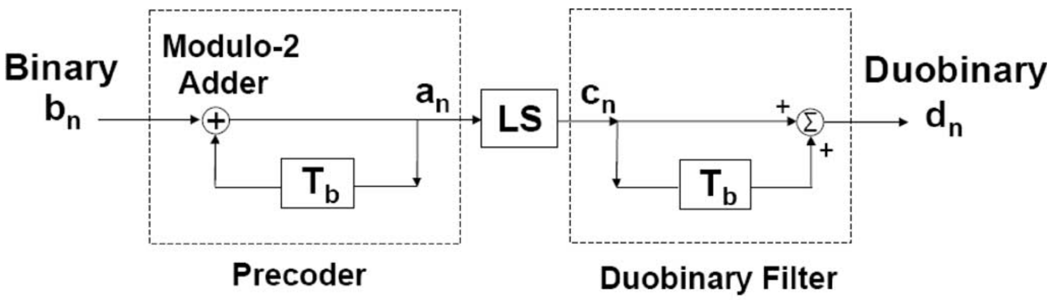


| | | | | | | | | |
|---|---|---|---|---|---|---|---|---|
| $b_n$ | | 0 | 0 | 1 | 0 | 1 | 1 | 0 |
| $a_n$ | 1 | 1 | 1 | 0 | 0 | 1 | 0 | 0 |
| $c_n$ | +1 | +1 | +1 | -1 | -1 | +1 | -1 | -1 |
| $d_n$ | | 2 | 2 | 0 | -2 | 0 | 0 | -2 |

Figure 4.1: The production of electrical duobinary signals.

### 4.1.2 NRZ-Duobinary Encoder

Two optical duobinary encoding schemes, the conventional electrical one bit delay-and-add method [18, 23] and a low-pass filtering (LPF) method [31, 32], are commonly used. In our experiment we employ a LPF method, which requires a LPF with a 3dB bandwidth approximately equal to one quarter of the bit rate. This LPF is equivalent to a one bit delay-and-add operation similar to the conventional scheme. The main purpose of this encoding process is converting an electrical binary signal to a normalized three levels {0, 1, 2} electrical signal. The equation is shown below by adding the current bit to the previous bit.

$$d_n = c_n + c_{n-1} \tag{4.2}$$

A DC-block is used to remove the DC component, resulting a level shift to normalized three levels {-2, 0, 2}. The optical duobinary signals generated using the LPF method suppress the optical spectrum sidelobes better than the duobinary one-bit delay and add method. Therefore it tolerates more chromatic dispersion. A drawback of the LPF method generated optical duobinary signal is that it has worse eye opening, poor tolerance to noise, and worse back-to-back receiver sensitivity compared to the one-bit-delay and add method [5, 7, 25, 21, 33, 34].

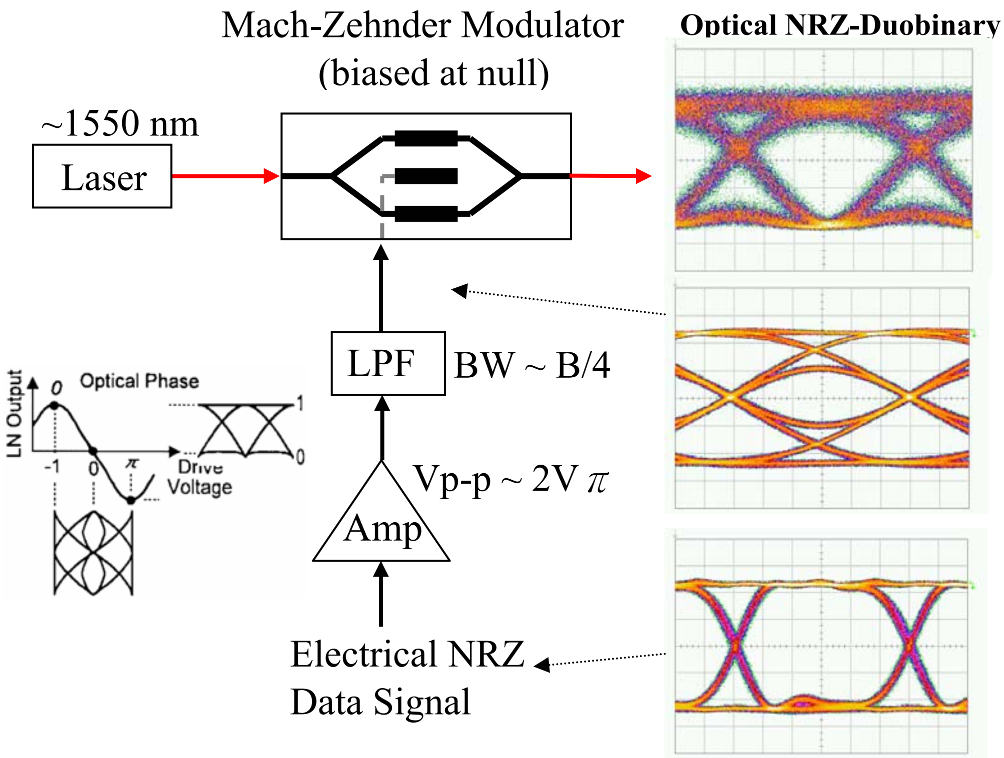


Figure 4.2: Experimental 10 Gb/s duobinary transmitter, and measured eye diagram at different stages.

An optical duobinary transmitter can be realized with a single MZM. The electrical NRZ drive signal is first amplified up to $V_{p\text{-}p} \sim 2\,V_{\pi}$. The MZM is biased at a null, so that electrical logical +/- 1 is converted to optical +/- E, where E is the optical field amplitude, and electrical logical 0 is converted to optical logical 0. Figure 4.2 shows the experimental realization of a 10 Gb/s optical duobinary transmitter in our laboratory. Note that the optical duobinary levels +/- E both correspond to logical 1. The phase of the 1 bits is being modulated between 0 and $\pi$ according to the electrical duobinary drive signal, while actually no useful information is encoded in this phase modulation [65]. Thus, a conventional square-law intensity photodetector can still be used for the duobinary receiver. However, this scheme requires differential encoding of the data source. So why use duobinary modulation? By modulating the phase of the logical one bits, duobinary modulation produces a narrower spectrum compared to NRZ. ISI distortion is also reduced since bit patterns such as {1 0 1} have the ones with opposite phase (i.e. the corresponding optical field amplitude is {–E, 0, E}). Thus, if the pulses corresponding to the ones spread out into the zero bit time-slot (for example due to fiber dispersion), they tend to cancel each other out. It was also shown recently that the quantum limit of an optically pre-amplified receiver is about 1 dB better for duobinary compared to NRZ. This again follows from the narrow duobinary spectrum, which allows for a much narrower optical filter to be used in front of the receiver. Thus, less amplified spontaneous emission (ASE) noise enters the receiver for duobinary compared to NRZ.

### 4.1.3 NRZ-Duobinary Decoder

A simple decoder by using a square-law detection as simple as OOK decoder can be used to receive duobinary signal, shown in figure 4.3. A photodiode can convert {-E, 0, +E} optical duobinary signals to binary signals with normalized amplitudes {0, 1}, which {-E, +E} all represent logic 1.

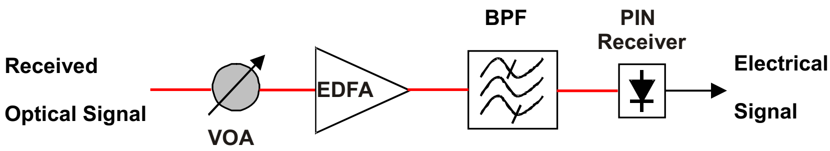


Figure 4.3: Decoder/demodulator of optical duobinary

### 4.1.4 Results

Figure 4.4 shows our experimental setup for the ASE noise-limited duobinary system measurements. Optical duobinary modulation at 10 Gb/s is produced by a combination of electrical and optical filtering at the transmitter. The LPF bandwidth is fixed at 3.6 GHz, which is close to the theoretical optimum [36]. We employ a zero-chirp Lithium Niobate modulator, with the pulse pattern generator (PPG) set to produce PRBS patterns of length $2^{23}$-1. The optical bandpass filter at the transmitter (Tx BPF) is realized with an Agilent 86146B optical spectrum analyzer (OSA), operated in WDM filter mode [92]. The 86146B can be used as a tunable bandwidth optical filter by varying the OSA resolution. After modulation, the optical signal passes through a variable optical attenuator (VOA), and an erbium doped fiber amplifier (EDFA). The VOA is used to set the average power input into the optically pre-amplified receiver. The EDFA pre-amplifier is followed by a second 86146B unit, which is used to realize the tunable bandwidth receiver optical bandpass filter (Rx

BPF). The receiver in the experimental setup is based on a conventional 10 Gb/s p-i-n photodetector with integrated trans-impedance amplifier (TIA), and limiting amplifier (LA), and is specified to have a bandwidth of ~ 7 GHz. We also employ a second similar receiver with ~ 9 GHz bandwidth in some of the measurements. The receiver output is fed into a 12.5 GHz error detector (ED) for BER measurement.

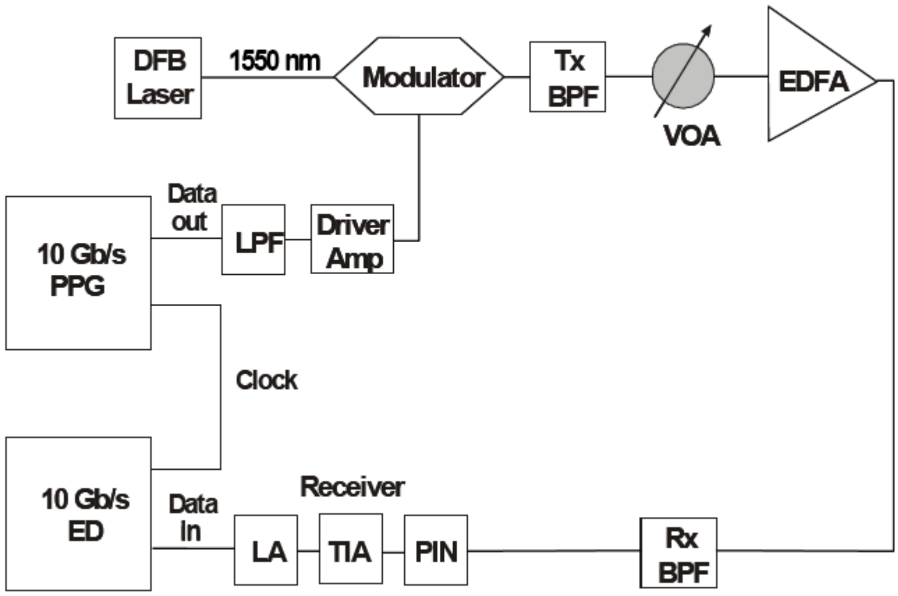


Figure 4.4: Experimental setup for ASE noise-limited measurements.

The experiments that determine the optimum Tx and Rx BPF bandwidths for the ASE noise-limited duobinary system are conducted. Figure 4.5 shows the Q factor, obtained by measuring BER versus receiver threshold [35], as a function of Rx BPF bandwidth. OSNR is kept fixed at 17 dB/0.1nm. The lines drawn through the data points serve as guides for the eye. Several sets of data are shown in Figure 4.5, corresponding to different values of Tx BPF bandwidth. The optimum Rx BPF bandwidth is found to be $B_{opt} \sim 0.85R$, and is relatively independent of Tx BPF bandwidth. Thus, in ASE noise-limited regime, the spectrally narrow duobinary signal is always best matched by a similarly narrow Rx BPF. However, the performance enhancement from narrow optical filtering at the receiver is more dramatic for wider Tx BPF bandwidths, which is an indication of additional beneficial pulse shaping effects due to narrow optical filtering.

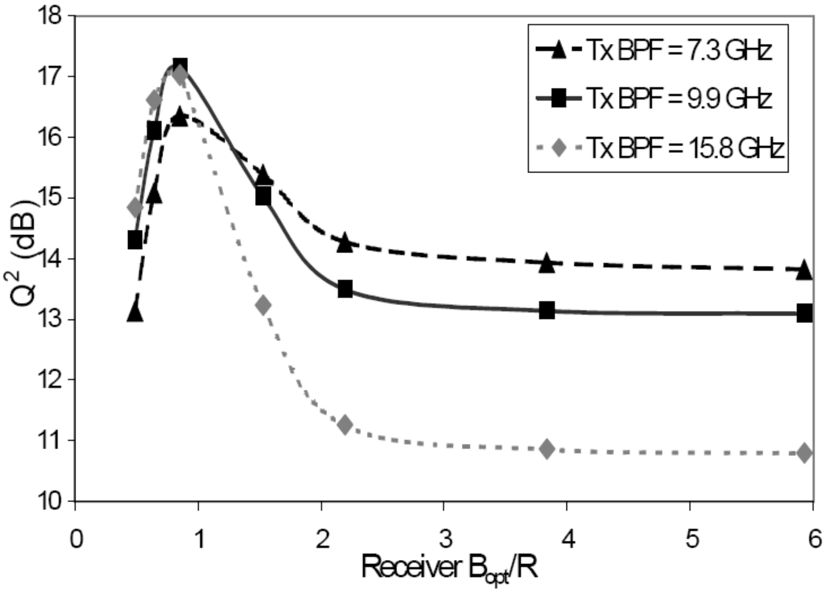


Figure 4.5: Measured Q versus receiver optical BPF bandwidth. OSNR is kept fixed at 17 dB/0.1nm.

Figure 4.6 shows the measured Q factor as a function of Tx BPF bandwidth. Several curves are shown, but this time parameterized with different values of Rx BPF bandwidth. In this case, the optimum Tx BPF bandwidth is seen to vary, depending on the value of Rx BPF bandwidth. As the Rx BPF bandwidth is increased, the optimum Tx BPF bandwidth is reduced. Narrow optical filtering at the transmitter results in a dramatic improvement in performance when the Rx BPF bandwidth is relatively wide ( i.e. > R ). Both Tx and Rx BPFs play a part in optimally shaping the duobinary pulse. The optimum point is reached when both Tx and Rx BPF bandwidths are near or slightly less than ~ R in agreement with theory [36].

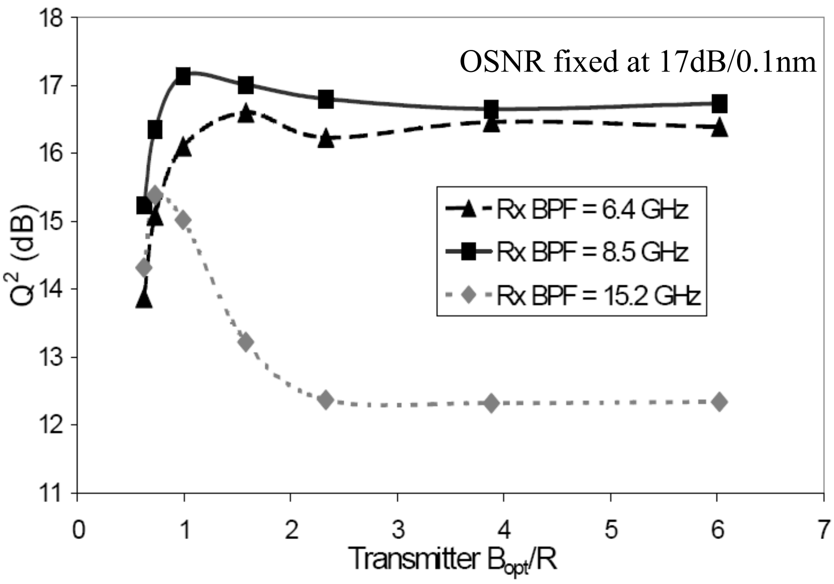


Figure 4.6: Measured Q versus transmitter optical BPF bandwidth. OSNR is kept fixed at 17 dB/0.1nm.

Figure 4.7 shows the optimum Tx and Rx BPF amplitude response, measured with 10 pm resolution, as well as the corresponding duobinary spectrum at output of Rx BPF. Note that the optical filters, corresponding to the optimum bandwidth points, also provide ~ 30 dB isolation at +/- 12.5 GHz. Thus, the same filters could serve as the multiplexers and de-multiplexers in UDWDM transmission with 12.5 GHz channel spacing at 10 Gb/s per channel. This implies that the duobinary modulation format is particularly well suited for UDWDM systems since the ultra-narrow UDWDM filter shapes required to suppress adjacent channel crosstalk are also optimum for duobinary ASE noise-limited operation.

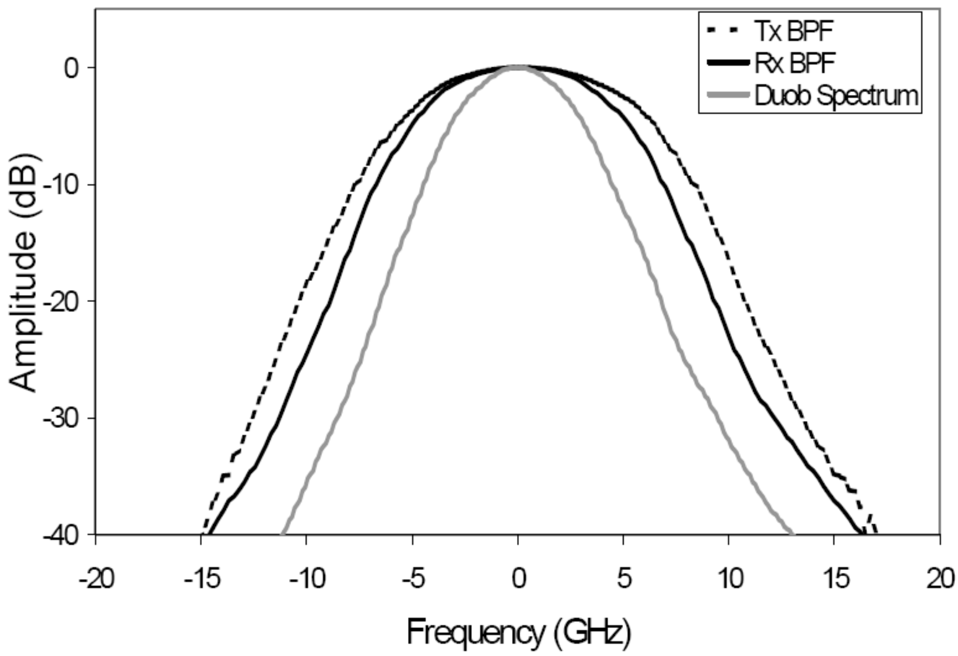


Figure 4.7 Measured amplitude response for Tx and Rx BPF, and optical signal spectrum after Rx BPF for the optimum duobinary system. The frequency axis is displayed relative to carrier frequency.

In all measurements presented thus far, the duobinary electrical LPF bandwidth was fixed at 0.36R to correspond as closely as possible to the theoretical optimum value determined in [36]. However, one might expect that the exact optimum value for the LPF bandwidth would vary depending on the shape of the optical filters used in the experiment (or simulation). Figure 4.8 shows a measurement of Q versus LPF bandwidth. The optical filters used in this experiment are the same as those shown in figure 4.7, with Tx and Rx optical BPF bandwidths equal to R and 0.85R, respectively. OSNR is held constant at 15 dB/0.1nm. As seen in figure 4.8, the optimum LPF bandwidth is near ~ 4.5 GHz for the optical filter shapes used in our experiments. However, using the theoretically optimum LPF value found in [36] gives a nearly optimum performance, the difference being only ~ 0.3 dB Q.

Interestingly, there is a wide range of LPF bandwidth values ~ 0.36R to 0.6R that give roughly similar performance. This indicates that most of the work in creating the duobinary bit correlation is performed by the narrow optical filters at the transmitter and receiver. Indeed, an electrical LPF may not be needed at all if the optical filters are narrow enough. For example, a single ultra-narrow optical filter at the receiver with $B_{opt}$ ~ 0.6R was found to be sufficient to produce a duobinary signal from a DPSK signal, with excellent ASE noise-limited performance [37].

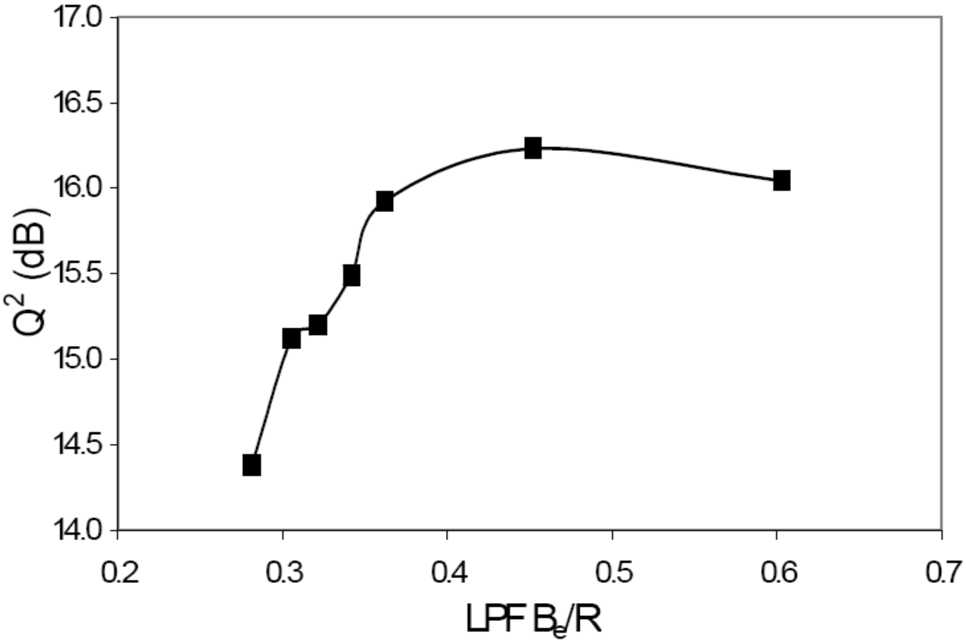


Figure 4.8: Measurement of Q as a function of electrical LPF bandwidth. OSNR is kept fixed at 15 dB/0.1nm.

One possible drawback of using narrow bandwidth optical filtering to tailor the optimum duobinary pulse shape is the penalty that may be incurred when the carrier frequency drifts away from the filter center frequency. Since both the transmitter laser and optical filters can drift off the ITU grid due to aging and/or environmental factors, this effect must be considered in the design of an optimum duobinary system. Figure 4.9 shows a measurement of Q versus transmitter carrier frequency detuning for the optimum duobinary system. In this experiment, OSNR is fixed at 15 dB/0.1nm, while the transmitter laser wavelength is tuned in steps of ~ 2 pm. This measurement shows that the carrier frequency must be aligned to the optical filters with +/- 0.5 GHz accuracy over the lifetime of the system to ensure less than 0.5 dB Q penalty.

The technology already exists for locking the DFB laser wavelength to the ITU grid with ~ +/- 2 pm (+/- 0.25 GHz) accuracy over the system lifetime [38]. Since the wavelength locking sub-systems themselves depend on a very stable narrow optical frequency discriminating filter as the basis for their operation, it is reasonable to presume that optical filters can be locked to the ITU grid with similar or better accuracy.

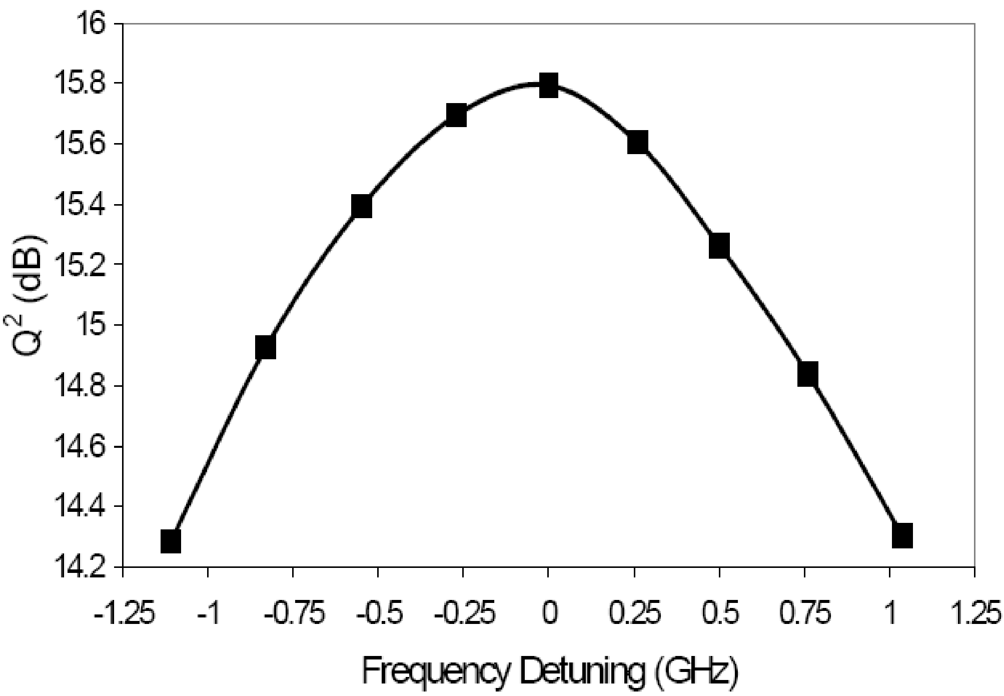


Figure 4.9: Measurement of Q as a function of carrier frequency detuning from optimum. OSNR is kept fixed at 15 dB/0.1nm.

Since the optimum duobinary generating LPF bandwidth, Tx and Rx bandpass filter bandwidth are obtained, the performance comparisons are conducted below. Figure 4.10 shows our results for back-to-back (B2B) optically pre-amplified receiver sensitivity measurements. The optical BPF bandwidth for NRZ and RZ is set close to optimum at 15 GHz and 23 GHz, respectively. The BPF bandwidth for conventional duobinary ( Conv. Duob.) is purposefully kept the same as for NRZ, to maintain the typical setup used in previously demonstrated duobinary systems. The receiver sensitivity for optimum duobinary (Opt. Duob.), with LPF, Tx BPF, and Rx BPF bandwidth values set close to the theoretical optimum [39], is also shown in figure 4.10. The measured eye diagrams shown in figure 4.10 are taken after the receiver BPF for each modulation format, with optical signal-to-noise ratio (OSNR) set to its maximum value.

The receiver sensitivity (BER = $10^{-9}$) is measured to be –38, -36.2, and –32.6 dBm for RZ, NRZ, and conventional duobinary, respectively. Thus, RZ performs 1.8 dB better than NRZ, which is in turn 3.6 dB better than conventional duobinary. These measurements confirm the widely held belief regarding the relative performance of RZ, NRZ and duobinary [14, 22, 90]. However, our optimum duobinary receiver sensitivity measurement results provide unambiguous evidence to the contrary. The optimum duobinary system achieves a receiver sensitivity of – 37 dBm, which is ~ 4.4 dB better compared to conventional duobinary. More importantly, optimum duobinary surpasses NRZ, and comes to within only ~ 1 dB of RZ. Note that the OSNR in our experiment corresponding to the RZ sensitivity of –38 dBm is 13.5 dB/0.1nm, which is close to the quantum limit for RZ/NRZ.

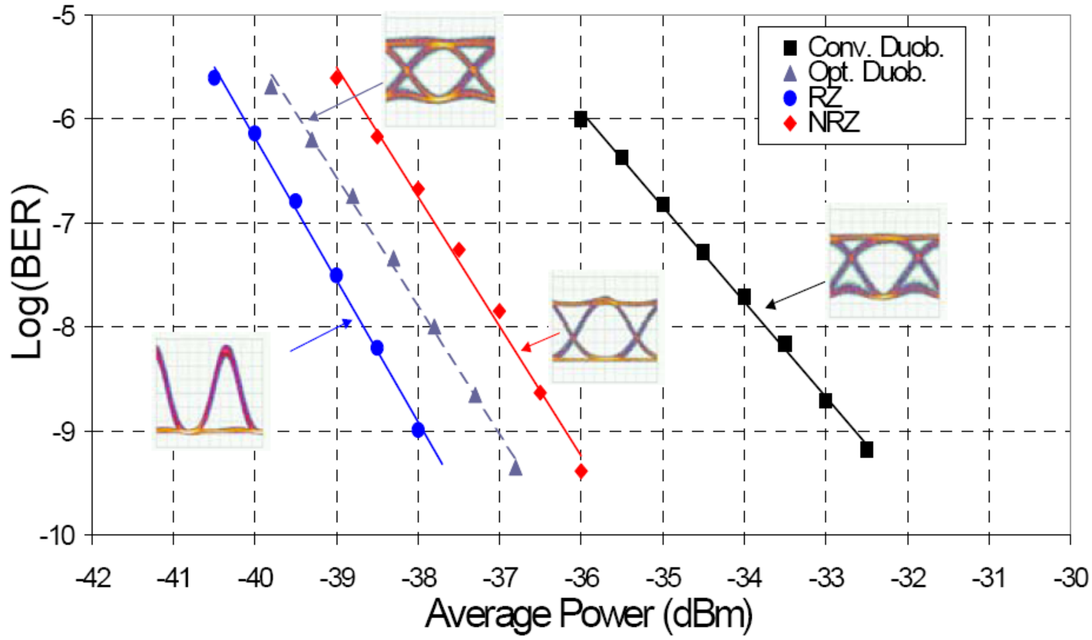


Figure 4.10: Optically pre-amplified receiver sensitivities and eye diagrams for RZ (circles), NRZ (diamonds), conventional duobinary (squares), and optimum duobinary (triangles). The eye diagrams are measured after the receiver optical bandpass filter.

Conventional LPF generated duobinary suffers an ASE noise-limited receiver sensitivity penalty compared to NRZ due to its pulse shape, which has an eye crossing level higher than NRZ, and a narrower space valley [27]. We have demonstrated that this is not a fundamental limitation for duobinary. It is possible to optimize the duobinary pulse shape to have its crossing level near 50%, while widening the space valley, as can be clearly seen in comparing the eyes shown in figure 4.10 for optimal and conventional duobinary. Moreover, the narrow bandwidth 8.5 GHz Rx BPF, which plays an important role in beneficially shaping the optimum duobinary signal, also serves to reduce the amount of ASE noise that enters the receiver. It is this unique combination of beneficial pulse shaping, and ASE noise reduction that results in excellent ASE noise-limited performance.

The dispersion tolerance is obtained by measuring receiver sensitivity with different lengths of conventional single mode fiber (SMF) inserted between transmitter and VOA. The launch power is fixed at a relatively low value of – 6.5 dBm to avoid self-phase modulation effects in the fiber. Figure 4.11 shows the measured dispersion tolerance of the different modulation formats. Conventional duobinary has the best dispersion tolerance. RZ has the worst dispersion tolerance, with NRZ slightly better. However, RZ and NRZ still beat conventional duobinary at SMF distances up to ~ 40-50 km due to their great advantage in ASE noise-tolerance. The most striking result in figure 4.11 is the performance of optimum duobinary. While occupying only ~ 1/4 as much spectral real estate as RZ, optimum duobinary almost reaches RZ performance B2B, and already surpasses it after ~ 20 km of SMF.

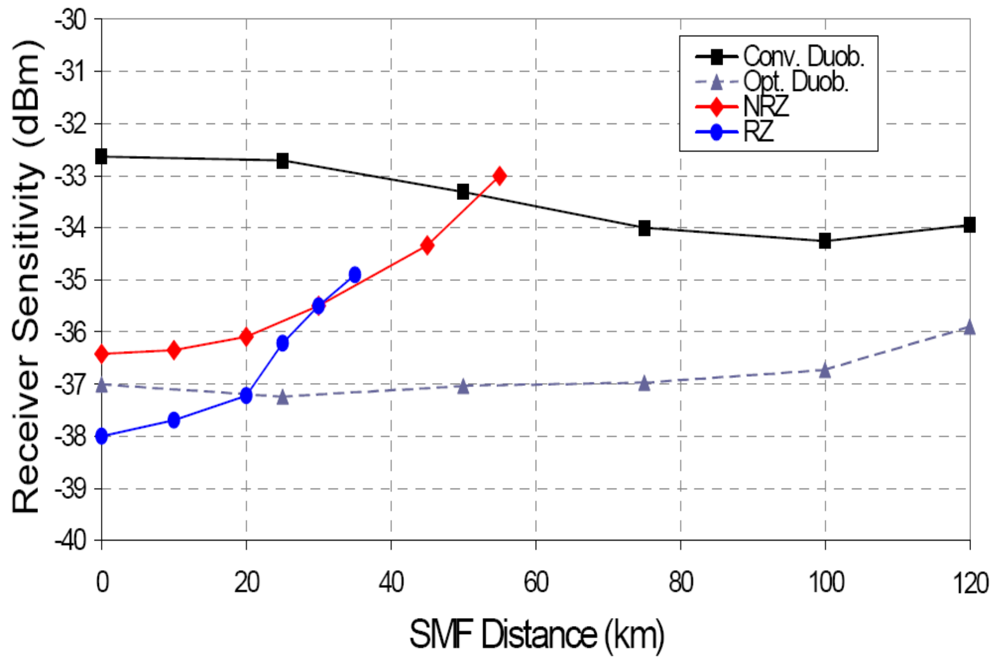


Figure 4.11: Optically pre-amplified receiver sensitivities as a function of SMF transmission distance.

From figure 4.11, we can also see that the pulse shape improves with dispersion for the conventional duobinary system up to ~ 100km SMF, and receiver sensitivity improves as well. In contrast, the optimum duobinary pulse shape degrades with dispersion, and receiver sensitivity suffers a ~ 1 dB penalty at 120km SMF. However, despite the dispersion penalty, optimum duobinary maintains a ~ 2 dB advantage over conventional duobinary even at 120km SMF.

Why is it that fiber dispersion of up to ~ 100km SMF produces beneficial pulse shaping for conventional duobinary, while degrading the optimum duobinary signal? Our studies of narrow optical filtering can provide a qualitative answer. In the linear transmission regime, it is possible to define a fiber transfer function for optical pulses, which has the same effect as an optical bandpass filter with bandwidth inversely proportional to transmission distance L [10]. Thus, conventional duobinary pulse shape benefits from additional optical filtering produced by fiber dispersion up to L ~ 100km. The optimum duobinary pulse shape is already optimized in terms of optical filtering. Thus, any additional optical filtering effects induced by fiber dispersion, which become noticeable at L ~ 100 km, tend to degrade the optimum duobinary signal.

We plot the spectrum of duobinary compared with NRZ-OOK and 50% duty cycle RZ-OOK. In figure 4.12, we can see that duobinary has the narrowest spectrum, which is approximately half of the NRZ-OOK signal spectrum. The narrower the spectrum (i.e. the less component of frequency it carriers) would enhance the tolerance of chromatic dispersion. The narrow spectrum not only allows packing more WDM channels in a signal fiber, but also allows tighter optical filtering, which also reduce the noise from receiving by receiver more. Another characteristic is that the optical carrier tone/frequency is absent from the duobinary spectrum.

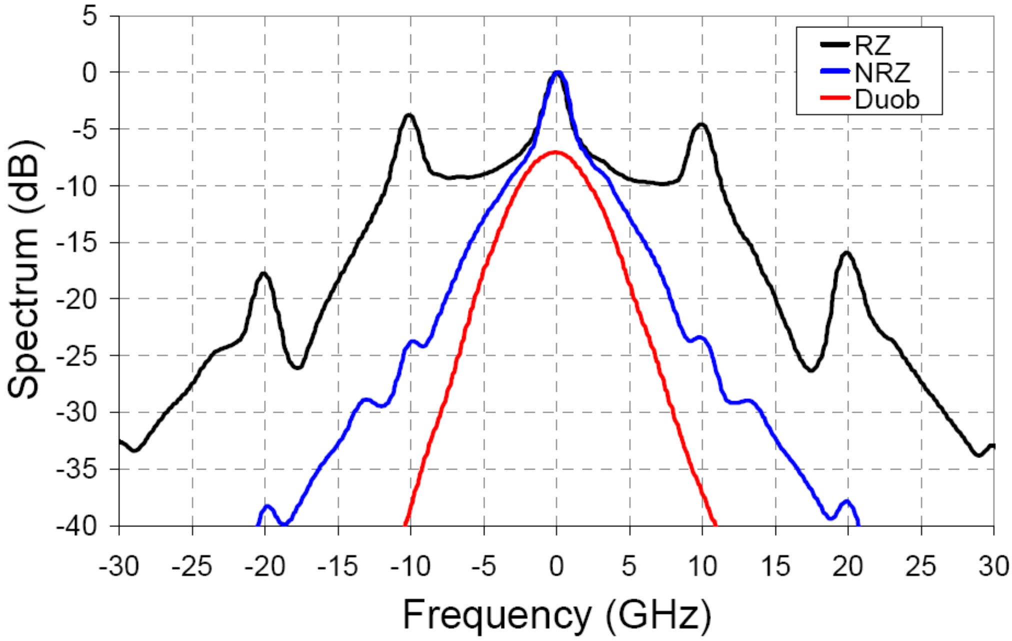


Figure 4.12: Measured signal spectra for 10 Gb/s RZ (black), NRZ (blue), and duobinary (red). Note that frequency axis is displayed relative to the optical carrier frequency. The spectra are captured using an optical spectrum analyzer with ~ 10 pm resolution.

## 4.2 RZ-Duobinary

An important choice in the design and optimization of any optical modulation format is the pulse shape to be used. For practical reasons, this choice often boils down to return-to-zero (RZ) versus nonreturn-to-zero (NRZ) pulse shapes, with possible variations in duty cycle. Much previous research has focused on comparing RZ versus NRZ pulse shapes for on–off keyed (OOK) transmission [15, 90, 94]. In particular, we now know that RZ-OOK enjoys an 1–2 dB advantage over NRZ-OOK in amplified spontaneous emission (ASE) noise limited systems due to an inherent tolerance of the RZ-OOK pulse shape to ISI in the receiver [41]. A similar conclusion was found to hold true for the differential phase-shift keying format [95]. Interestingly, while the duobinary format has been studied extensively for many years now [20, 23, 29, 36, 91, 96, 97], there is a lack of experimental data on a direct comparison between RZ and NRZ pulse shapes in duobinary transmission. In this dissertation, we attempt to fill this knowledge gap by conducting systematic experimental studies on RZ versus NRZ pulse shapes in duobinary transmission systems that are dominated by ASE noise, fiber chromatic dispersion, and self-phase modulation (SPM). Our experiments are designed to isolate various transmission impairments, thus providing physical insight into the optimum pulse shape for duobinary transmission under different transmission conditions.

### 4.2.1 RZ-Duobinary Precoder and Decoder

RZ-duobinary shares the same decoding and decoding processes with NRZ-duobinary. Please refer to chapter 4.1.1 and 4.1.3 for NRZ-duobinary precoder and decoder.

### 4.2.2 RZ-Duobinary Encoder

An RZ-duobinary signal can be generated similarly by incorporating a pulse carver modulator, as shown in Fig. 4.13, to produce an RZ pulse train (instead of continuous wave) input into the NRZ-duobinary modulator.

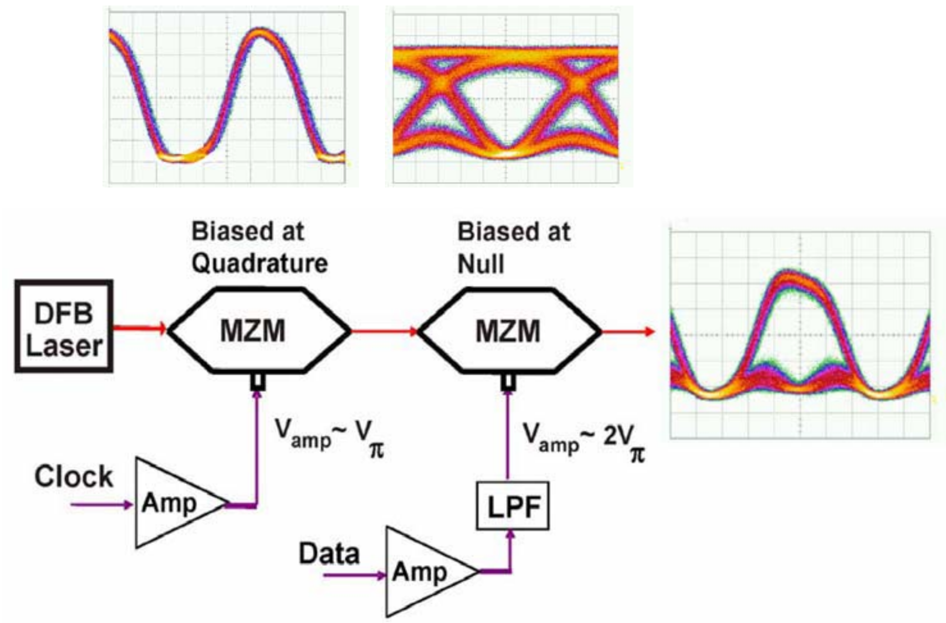


Figure 4.13: Schematic diagram of an RZ-duobinary transmitter and measured output eye at 10 Gb/s.

### 4.2.3 Results

Fig. 4.14 shows our 10-Gb/s transmitter setup for generating RZ- and NRZ-duobinary modulation. A DFB laser emits an optical carrier wave at ~1550 nm, which is modulated in two stages to produce RZ (in one stage for NRZ). First, a periodic RZ pulse train with 50% duty cycle is produced by driving an x-cut lithium niobate MZM, which is biased at quadrature, with the CLOCK signal from a pulse-pattern generator that is amplified to $\sim V\pi$. The duobinary data is impressed on the RZ pulse train in a second-stage MZM, which is physically identical to the first but biased at a null, and driven with an electrical duobinary signal that is amplified to $\sim 2V\pi$. The duobinary LPF bandwidth is varied in our experiments by employing different-bandwidth Bessel–Thomson-type filters that were obtained from the same manufacturer. The RZ- or NRZ-duobinary optical signal is fed into a variable optical attenuator (VOA1), which controls the launch power into conventional single-mode fiber (SMF) spools of variable lengths. A second variable optical attenuator (VOA2) sets the input optical power into an erbium-doped fiber amplifier (EDFA). An optical spectrum analyzer monitors the optical signal-to-noise ratio (OSNR) at the output of the EDFA. The EDFA optical preamplifier is followed by a variable-bandwidth optical filter based on free-space grating technology. The receiver in the experimental setup is a commercially available 10-Gb/s p-type-intrinsic-n-type (p-i-n) photodetector with integrated transimpedance amplifier and limiting amplifier and is specified to have an electrical bandwidth of 9 GHz. This represents a typical receiver for 10-G transmission systems. The p-i-n receiver output is fed into a 12.5-GHz error detector. Clock recovery (CR) is achieved by taping off a fraction of the optical signal at the input to the p-i-n detector into a commercial instrumental receiver that includes CR circuitry.

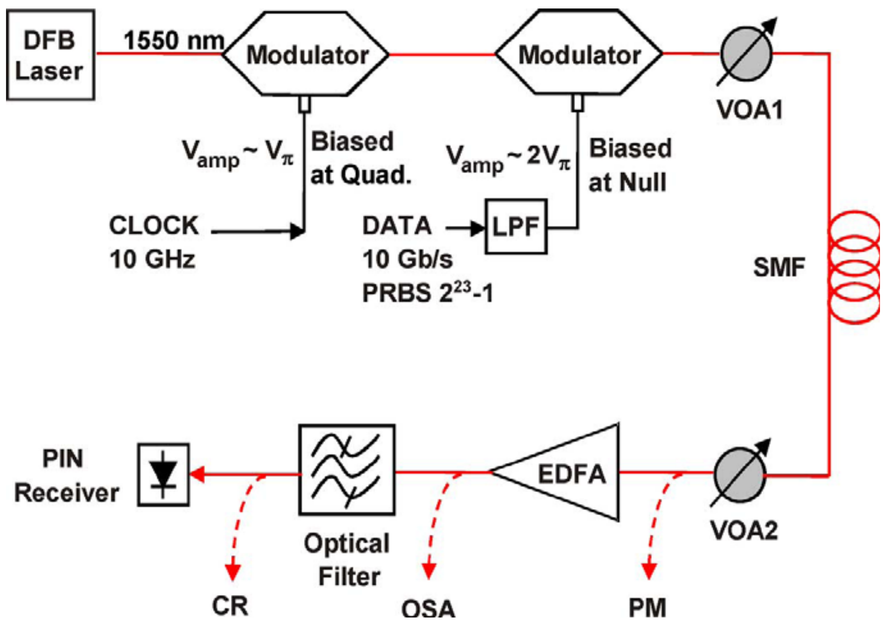


Figure 4.14: Experiment setup of 10-Gb/s NRZ-duobinary transmitter and direct detection.

Fig. 4.15 shows the measured spectra at 10 Gb/s for RZ- and NRZ-duobinary and OOK for comparison. As with the NRZ-duobinary, the RZ-duobinary shows a clear spectral compression compared to its OOK counterpart. This spectral compression results in better dispersion tolerance for duobinary compared to OOK [40]. We also note that the RZ-duobinary spectrum is significantly broader compared with the NRZ duobinary one. In the case of OOK, the wider spectral content of RZ creates a pulse shape that is more tolerant to ISI in the receiver and, hence, to a 1–2 dB advantage in performance compared with the NRZ [41]. This begs the following question: should we see a similar benefit for RZ-duobinary?

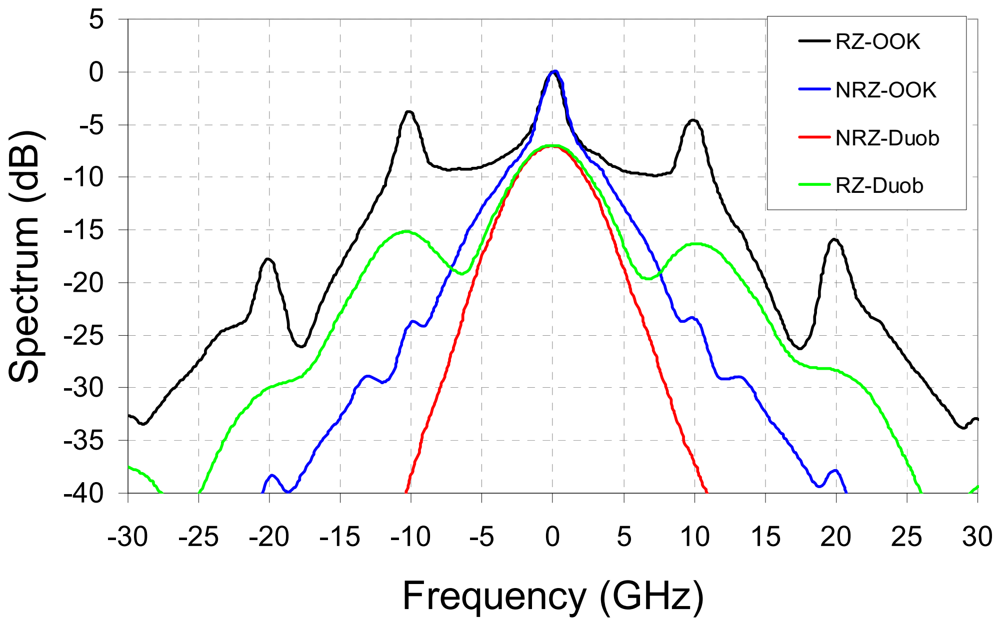


Figure 4.15: Spectra of different modulation Formats

A key element in the duobinary transmitter is the duobinary generating electrical LPF. Thus, to ensure a fair comparison between RZ and NRZ pulse shapes, we conduct measurements of bit-error-rate-equivalent $Q$-factor versus LPF bandwidth in an ASE-noise-loaded system. The measured $Q$-factor versus LPF bandwidth, with the OSNR fixed at 14 dB/0.1 nm, is shown in figure 4.16.

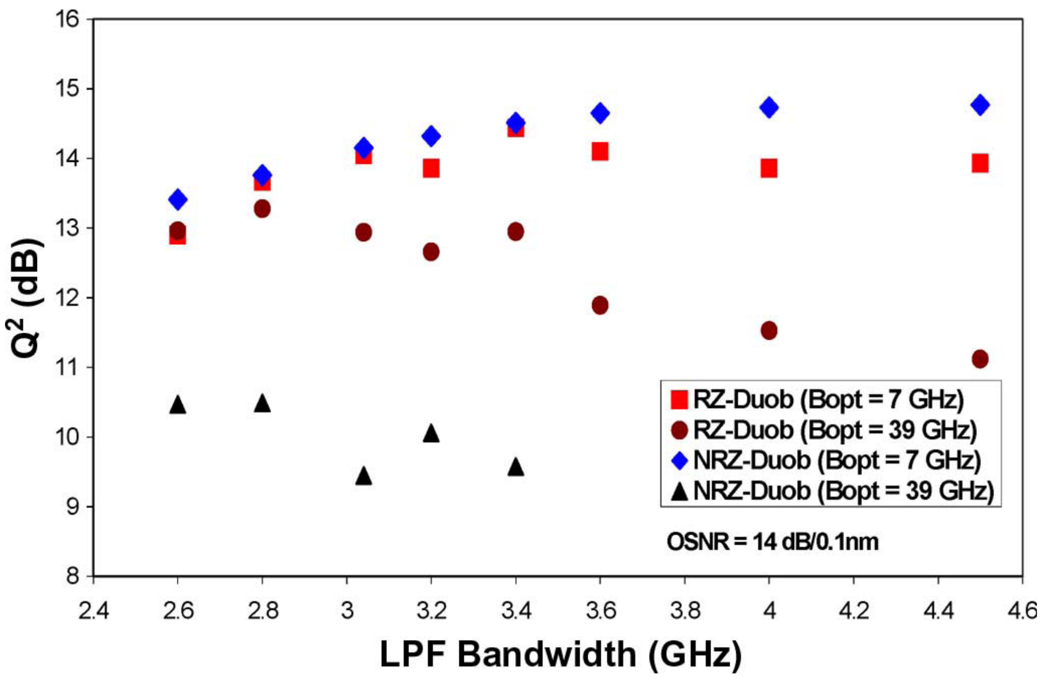


Figure 4.16: Optimization of LPF bandwidth for RZ- and NRZ-duobinary, with Optical filter fixed at either 7 GHz or 39 GHz

Two sets of data are shown for both RZ and NRZ pulse shapes, corresponding to receiver optical filter bandwidths of 39 and 7 GHz. We see that, for a relatively wide 39-GHz optical filter, the optimum LPF bandwidth is close to a quarter of the bit rate (2.8 GHz in our experiments) for both RZ- and NRZ-duobinary. In this case, the RZ pulse shape enjoys a ~2–3 dBQ advantage in performance. However, we find that the back-to-back (B2B) performance can be greatly improved by employing a narrow

7-GHz optical filter in tandem with an LPF bandwidth that is significantly greater than a quarter of the bit rate. In this optimum regime, the NRZ pulse shape shows slightly better performance compared with RZ. The overall optimum LPF bandwidth, which was obtained with a nearly matched optical filter, is roughly 34% and 40% of the bit rate for RZ- and NRZ-duobinary, respectively.

Fig. 4.17 shows measurements of the $Q$-factor versus receiver optical filter bandwidth in ASE-noise-limited regime, with the RZ- and NRZ- duobinary LPF bandwidths fixed at 3.4 GHz. The corresponding computer simulation results, which were obtained using the OptSim software, are also plotted for comparison. There are several interesting features in the data. First, we observe two distinct maxima in the B2B $Q$-factor versus optical filter bandwidth curve for RZ-duobinary. The more optimum peak occurs at the same narrow optical bandwidth ( ~7 GHz, as predicted by the theory) for both RZ- and NRZ-duobinary. However, RZ-duobinary also shows a second peak at an optical bandwidth that is roughly twice the bit rate. The second peak corresponds to a "matched" filter for the RZ pulse shape, which unfortunately does not correspond to the optimum duobinary pulse shape. Indeed, the data in Fig. 4.17 clearly shows that the RZ-duobinary obtains its optimum ASE-noise-limited performance at the same optical filter bandwidth as NRZ duobinary, where the

RZ-duobinary pulse shape is actually converted into an NRZ-duobinary by the ultra narrow optical filtering process. This provides clear evidence in favor of the NRZ pulse shape for duobinary systems that are limited by ASE noise. Indeed, the smooth single-lobe NRZ-duobinary spectrum is well matched to a Gaussian-shaped optical filter.

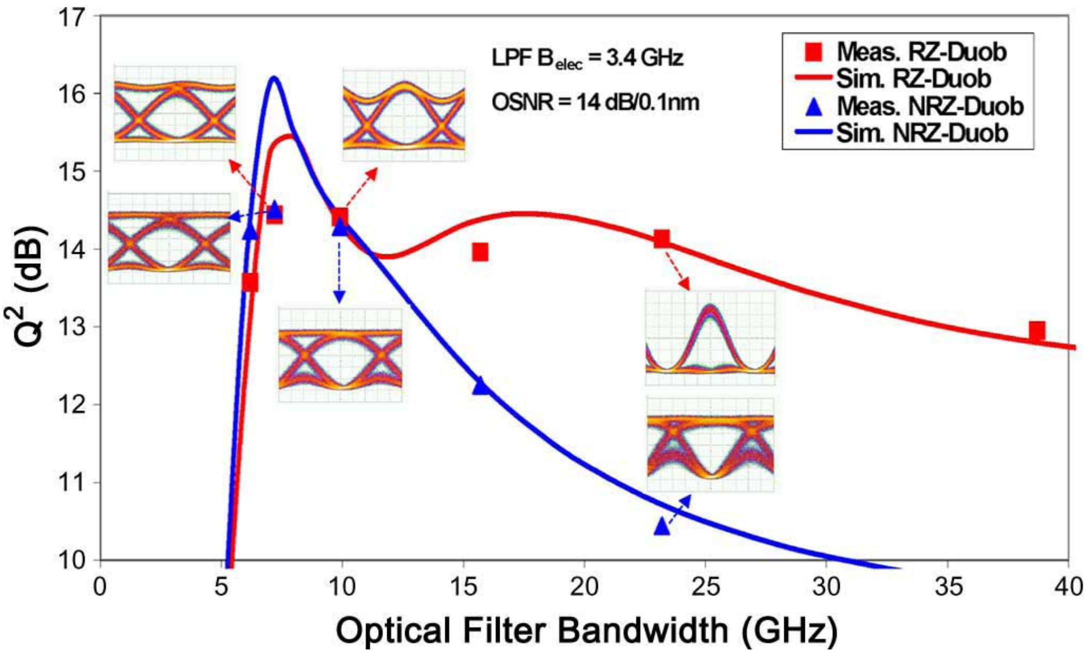


Figure 4.17: Measurement and simulation results of receiver sensitivity

An experimental comparison of dispersion tolerance for NRZ- and RZ-duobinary is shown in Fig. 4.18, where the $Q$ factor is measured as a function of SMF ($D$ ~ 17 ps/nm/km) distance with the OSNR fixed at 14 dB/0.1 nm. To avoid nonlinear effects in this experiment, the launch power into SMF is reduced to a relatively low value of ~ −5 dBm using VOA1 in Fig. 4.14, while OSNR is controlled with VOA2. We observe that the NRZ-duobinary is able to span 100 km of SMF with no dispersion penalty, while the RZ-duobinary suffers a ~2 dBQ penalty. Thus, while the RZ-to-NRZ duobinary conversion at the receiver using ultra narrow optical filtering is sufficient to give roughly the same performance B2B, there are still some high-frequency components that are present in the RZ-duobinary spectral sidelobes (generated as a result of the RZ modulation process) that may leak into the filter bandwidth to produce the greater dispersion penalty for RZ-duobinary compared with NRZ-duobinary.

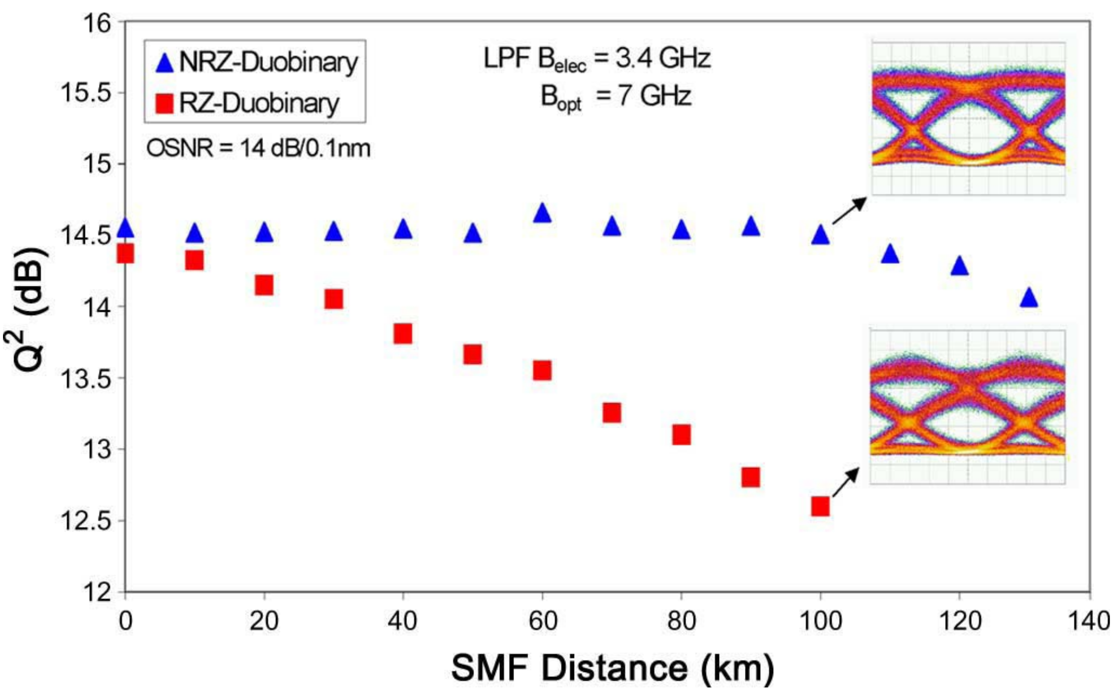


Figure 4.18: Dispersion penalty of RZ- and NRZ-duobinary

Fig. 4.19 shows our setup for studying the impact of SPM. To generate sufficient SPM, we transmit the duobinary signal through two spans, each composed of 11.4-km DCF, followed by 70-km SMF. The overall dispersion is roughly balanced at the receiver. Note that in order to increase the SPM effect, we launch high power into the DCF, which has a factor of ~5 greater nonlinearity coefficient compared with SMF [42]. By launching $P$ ~10 dBm into each span, we achieve a significant effective nonlinear phase shift of ~1 rad. The VOA before the last EDFA is used to keep the received OSNR fixed at 14 dB/0.1 nm.

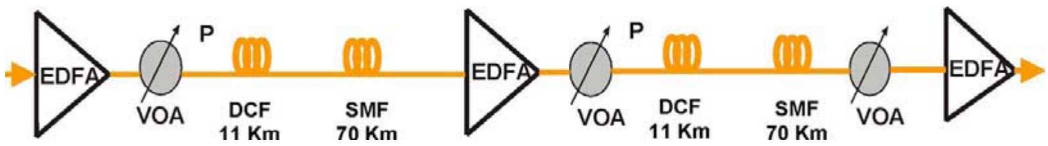


Figure 4.19: Experimental setup of self phase modulation effect on duobinary

Figs. 4.20 and 4.21 show the measured $Q$-factor versus optical filter bandwidth for RZ- and NRZ-duobinary, respectively, with the LPF bandwidth fixed at 3.4 GHz. The lines that were drawn through the data points are included as guides for the eye. We plot a series of data corresponding to different launch powers and, thus, different amounts of SPM-induced nonlinear phase shift. As shown in Fig. 4.20, in the case of RZ-duobinary, SPM clearly hurts the performance even at a relatively modest launch power of 4 dBm. RZ-duobinary suffers a ~1 dBQ penalty at a launch power of 10 dBm.

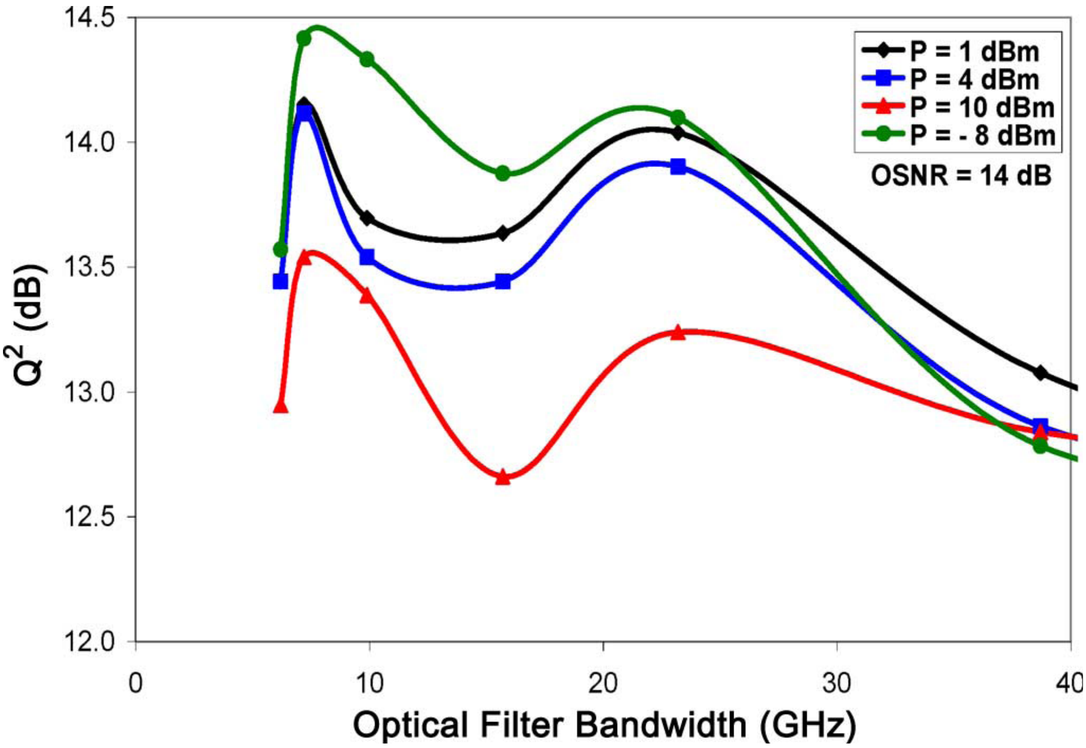


Figure 4.20: Experiment results of SPM effect on RZ-duobinary

In the contrast to RZ-duobinary, the performance of NRZ-duobinary initially improves as the launch power increases [43]. Even at a high launch power of 10 dBm, the NRZ-duobinary shows an improvement in *Q*-factor compared with B2B. The optimum NRZ-duobinary performance is obtained at a launch power of 7 dBm, where NRZ-duobinary outperforms RZ-duobinary by ~1.5 dBQ, shown in figure 4.21. These measurements demonstrate that the SPM nonlinearity can, in fact, be utilized to improve the NRZ-duobinary system performance, as long as the launch power is properly controlled. The SPM seems to provide a beneficial pulse-shaping mechanism for NRZ-duobinary [44]. On the other hand, the spectral sidelobes in the RZ-duobinary optical spectrum may contribute to its relatively poor tolerance to SPM. The SPM nonlinearity tends to broaden the signal spectrum, including a broadening of the sidelobes in RZ-duobinary. Thus, additional high-frequency components are "aliased" from the sidelobes into the main duobinary spectral lobe, producing deleterious distortion for RZ-duobinary.

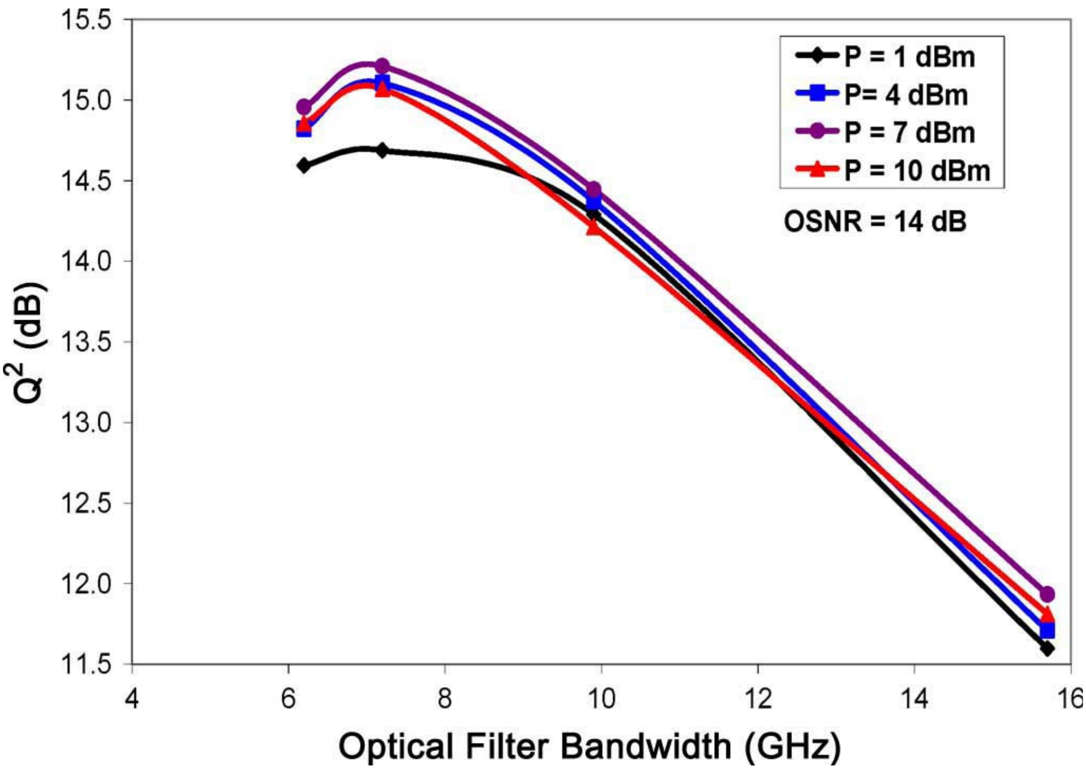


Figure 4.21: Experiment results of SPM effect on NRZ-duobinary

# Chapter 5

# Phase Modulation Formats

Phase modulation formats are an attractive alternative other than intensity modulation formats, which may provide better spectral efficiency. Differential phase-shift keying (DPSK) modulation, differential quadrature phase-shift keying (DQPSK), and polarization multiplexing differential phase-shift keying (PolMul DQPSK) modulation are covered in this character.

## 5.1 Differential Phase Shift Keying (DPSK)

Differential phase-shift keying (DPSK) is emerging as an important modulation format for fiber-optic communication systems [44]. In DPSK, information is encoded by impressing phase shifts onto an optical carrier wave. A critical element in any DPSK system is the demodulator, which converts phase modulation into intensity modulation for detection at the receiver. The most common DPSK demodulator is based on a Mach–Zehnder interferometer with a bit period delay between the two arms [49]. This arrangement can be used for single-ended direct detection, or balanced detection, by utilizing both constructive and destructive interferometer output ports [48]. DPSK with balanced detection yields a 3-dB advantage in amplified spontaneous emission (ASE) noise-limited performance over ON–OFF keying (OOK) [57]. However, this advantage in performance must be weighed against the increased complexity and cost of the Mach–Zehnder interferometer with balanced detection. It would be highly desirable to develop a DPSK demodulator for direct detection, which also maintains an ASE noise-limited performance advantage over OOK. An interesting recent proposal involves using phase-to-polarization conversion followed by a polarizer and direct detection [56].However, this scheme shows equivalent receiver sensitivity to OOK. In this work, we demonstrate a 10-Gb/s DPSK demodulator based on an optical discriminator filter followed by direct detection. While this technique is well known [52-54], it has received relatively little attention compared to the delay interferometer. The discriminator filter demodulator is suitable for integrating the functions of wavelength-division-multiplexing (WDM) demultiplexing, ASE noise suppression, and DPSK demodulation in a single filter element. Furthermore, our study shows that this DPSK demodulation scheme may hold a significant ASE noise-limited performance advantage over OOK, even though conventional direct detection is used.

### 5.1.1 DPSK Precoder

A precoder is needed at transmitter side in order to recover the transmitted data at the receiver side [21, 45]. Fig. 5.1 shows an optical DPSK system with a precoder scheme on the bottom left. The precoder contains a XOR gate with a one bit delay feedback loop form its output. The precoding function could be expressed as:

$$b_K = a_K \oplus b_{K-1} \tag{5.1}$$

where $a_K \in \{0, 1\}$ is the original transmitted binary data sequence. $b_K \in \{0, 1\}$ is the precoded binary sequence and $\oplus$ is logic XOR gate. After a DC block and an amplifier, $b_K$ sequence is shifted to $c_K \in \{+1, -1\}$, which is used to drive DPSK modulator.

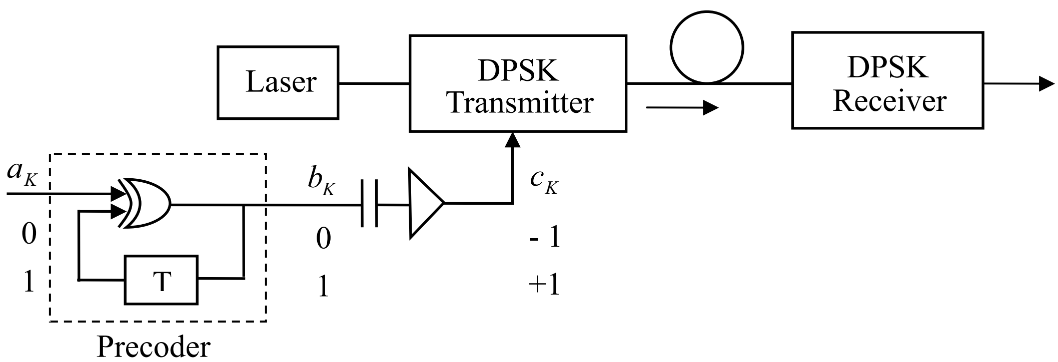


Figure 5.1: Scheme diagram of a DPSK transmitter

Table 1 illustrates how digital signals are converted at different stages of a DPSK transmission system. A reference bit is needed to initial the differential encoding process. This reference bit could be set to logic "0" or "1". In our case, we set it to be logic "0" at the instant $K = -1$.

| Time instant $K$ | -1 | 0 | 1 | 2 | 3 | 4 | 5 | 6 |
|---|---|---|---|---|---|---|---|---|
| Transmitted data $a_K$ | | 0 | 1 | 1 | 0 | 1 | 0 | 0 |
| Diff. Encoded data $b_K$ | 0 | 0 | 1 | 0 | 0 | 1 | 1 | 1 |
| MZM drive signal $c_K$ | -1 | -1 | +1 | -1 | -1 | +1 | +1 | +1 |
| MZM drive voltage $\pm V_\pi$ | $-V_\pi$ | $-V_\pi$ | $+V_\pi$ | $-V_\pi$ | $-V_\pi$ | $+V_\pi$ | $+V_\pi$ | $+V_\pi$ |
| MZM electric field $\pm E$ | $+E$ | $+E$ | $-E$ | $+E$ | $+E$ | $-E$ | $-E$ | $-E$ |
| Transmitted phase $\phi$ | 0 | 0 | $\pi$ | 0 | 0 | $\pi$ | $\pi$ | $\pi$ |
| Phase difference $\lvert\phi\rvert$ | | 0 | $\pi$ | $\pi$ | 0 | $\pi$ | 0 | 0 |

Table 1: Different digital signals at different stage for DPSK modulation

### 5.1.2 DPSK Encoder

DPSK (or more correctly NRZ-DPSK) can be generated using a single MZM. The MZM must be biased at a null, and the electrical NRZ drive signal amplitude is amplified to 2V$_\pi$ [46, 47, 48]. The output phase actually varies between 0 and $\pi$ for successive intensity peaks in the MZM transmission curve. Thus, by biasing the MZM at a null, and using a high-power RF driver amplifier with Vp-p ~ 2V$_\pi$ we can modulate the output phase between 0 and $\pi$, producing an optical phase-shift-keying

(PSK) signal. When the electrical data signal is differentially encoded prior to the MZM driver amplifier, the MZM optical output becomes DPSK. Figure 5.2 shows the experimental 10 Gb/s DPSK transmitter realized in our laboratory.

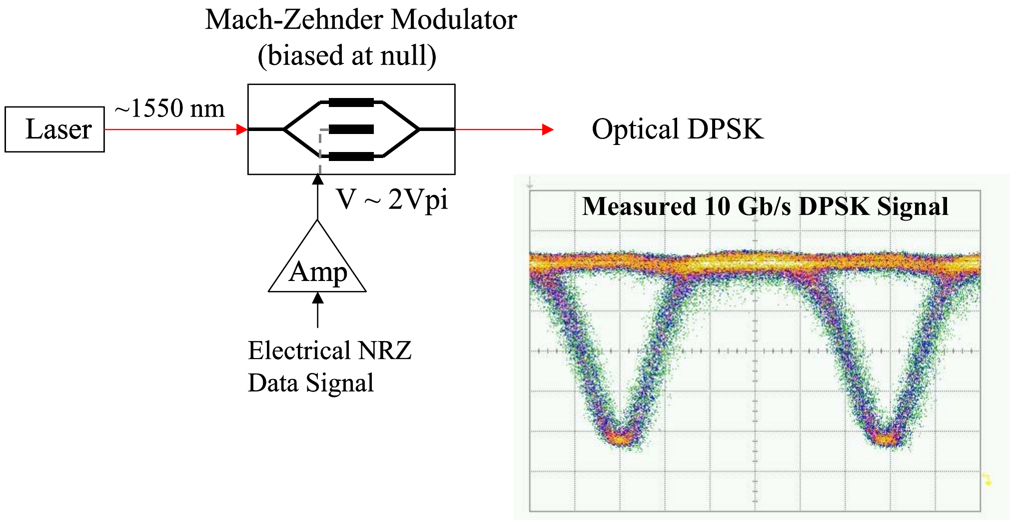


Figure 5.2: Experimental 10 Gb/s DPSK transmitter, and measured DPSK eye diagram.

Employing an intensity modulator (instead of a pure phase modulator) to generate optical DPSK has the advantage that *exact* $\pi$-phase shifts are produced. However, as can be seen in figure 5.2, some residual intensity modulation is present in the signal. This usually poses no problems in decoding the DPSK signal at the receiver since the residual intensity modulation occurs between the bits (i.e. at the bit boundaries). Note that DPSK can also be produced with RZ pulses by employing an RZ pulse carver in addition to the DPSK modulator shown in figure 5.2. In this case, the transmitter output is a periodic RZ pulse train, with the phase of each pulse modulated between 0 and $\pi$ according to the data. Thus, there are actually two flavors of DPSK: so-called NRZ-DPSK and RZ-DPSK. In the following discussions, the reader may assume that DPSK always refers to NRZ-DPSK.

### 5.1.3 DPSK Decoder

A critical element in any phase modulator system is the demodulator, which converts phase modulation into intensity modulation for detection by photodiode. Two types of DPSK receivers are shown in figure 5.3. The conventional DPSK demodulator is based on a Mach-Zehnder delay interferometer (MZDI) with 1-bit delay in one arm and followed by either two identical photodiodes for balanced detection [ 47, 49, 50, 57], as shown in Fig. 5.3(a) or simply one photodiode for direct detection (single-end detection) at either one of the two output ports of delay interferometer. However, balanced detection yields a 3-dB receiver sensitivity over single-end detection. In this configuration, MZDI plays an important part of demodulation. First, the difference of two uneven arm lengths should be equal to one bit period, which is determined by the baud rate of transmitter. The one bit delay MZDI enable interference occurred between two adjacent bits, which also turns phase modulation into intensity modulation. Second, the two arms should have roughly equal power at the output of MZDI to gain the best efficiency of interferometer. One (or two) of the arms is heated by micro-heater to control the optical phase (i.e. the optical path length) in order to gain a constructive interference, where there is optical power presented, in one output and a destructive interference, where optical power is absent, in another output.

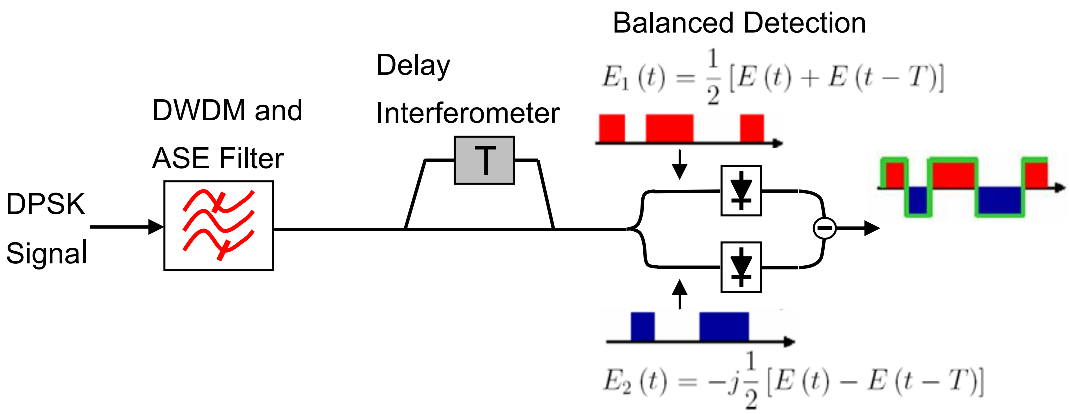


(a)

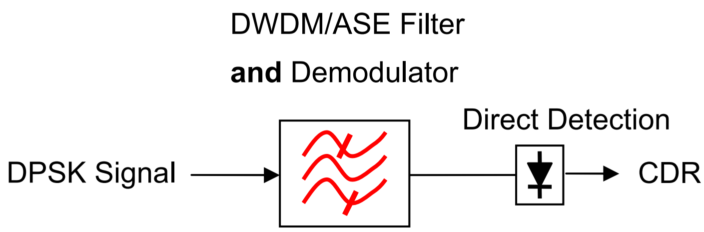


(b)

Figure 5.3: (a) Conventional DPSK demodulator, and (b) Our approach (as simple as NRZ)-discriminator filter followed by direct detection

Our proposed DPSK demodulator based on an optical discriminator filter followed by direct detection is shown in Fig. 5.3(b). While this technique is well known [51, 52, 53, 54, 56, 58], it has received relatively little attention compared to the delay interferometer. The discriminator filter demodulator has a potential advantage: a possibility for integrating the functions of ASE noise suppression, wavelength-division-multiplexing (WDM) demultiplexing, and DPSK demodulation in a single filter element. Furthermore, we show below that this DPSK demodulation scheme may hold a significant ASE noise-limited performance advantage over OOK, even though conventional direct detection is used.

### 5.1.4 Results

Fig. 5.4 shows our experimental setup of DPSK transmission system. Nonreturn-to-zero (NRZ)-DPSK modulation is produced at 10 Gb/s by driving an x-cut Lithium Niobate modulator, biased at a null, with electrical NRZ data of $\sim 2V_{\pi}$ amplitude. The pulse-pattern generator is set to produce pseudorandom binary sequence pattern of length $2^{23}-1$. After modulation, the optical signal passes through a variable optical attenuator (VOA) and an erbium-doped fiber amplifier (EDFA). The VOA is used to set the optical power into the EDFA optically preamplified receiver. An ultranarrow optical bandpass filter (BPF) follows the EDFA.

The optical BPF has a full-width at half-maximum (FWHM) bandwidth of 6.2 GHz, and serves the dual purpose of ASE noise rejection *and* DPSK demodulation. The optical BPF is realized with an Agilent 86146B optical spectrum analyzer (OSA), operated in WDM filter mode.

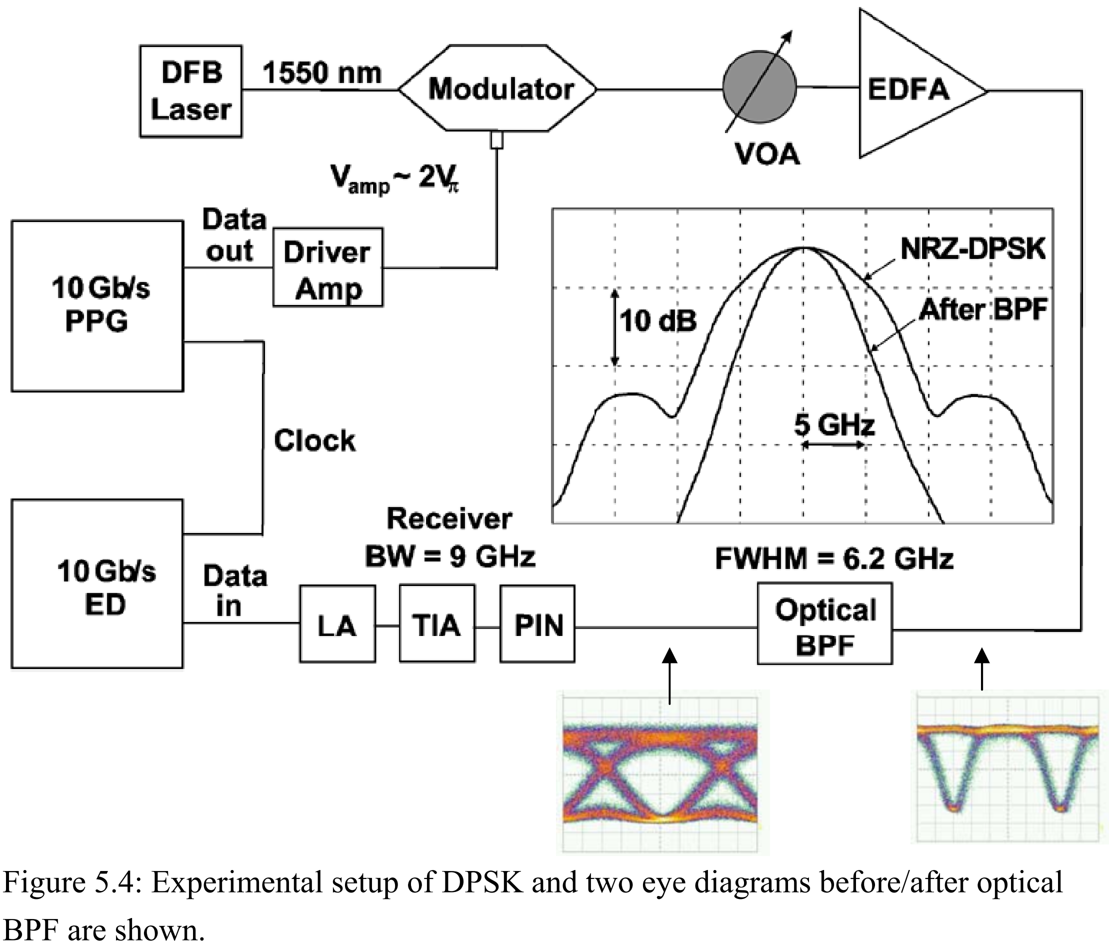


Figure 5.4: Experimental setup of DPSK and two eye diagrams before/after optical BPF are shown.

The inset in Fig 5.4 shows the NRZ-DPSK spectrum, measured with 10-pm resolution, before and after the optical BPF. The ultranarrow optical BPF operates as a frequency discriminator [58], demodulating the DPSK signal into an intensity modulated signal. From another point of view, the optical BPF effectively carves out a duobinary spectrum from the original DPSK [53]. The receiver chain in our experimental setup employs a commercial p-i-n photodetector with integrated transimpedance amplifier, and a limiting amplifier (LA), followed by a 12.5-GHz error detector (ED). The receiver is specified to have a 9-GHz electrical bandwidth. Both LA threshold voltage and ED sampling instant are optimized for each measurement of bit-error rate (BER).

Fig. 5.5 shows the measured receiver sensitivity and demodulated eye diagram for the NRZ-DPSK and NRZ-OOK. To ensure a fair comparison, an optical BPF with FWHM bandwidth of 15 GHz is used for NRZ-OOK. The electrical bandwidth of $B_e = 9$ GHz and optical BPF bandwidth of $B_o = 15$ GHz are close to theoretical optimum for NRZ-OOK [13]. The eye diagram shown in Fig. 5.5 for NRZ-OOK is taken after the 15-GHz optical BPF. Using the optical BPF frequency discriminator technique, we achieve a receiver sensitivity of -37.4 dBm for NRZ-DPSK, corresponding to optical signal-to-noise ratio (OSNR) =14.1 dB/0.1nm. In comparison, the NRZ-OOK measures a receiver sensitivity of -36.2 dBm, corresponding to OSNR= 15.3 dB/0.1 nm. Thus, despite using direct detection, the NRZ-DPSK achieves 1.2 dB better ASE noise-limited performance compared to

NRZ-OOK. The reason for the superior ASE noise-limited performance for NRZ-DPSK in our experiment lies in the ultranarrow optical BPF used to demodulate the DPSK signal, which is also very effective in blocking ASE noise from reaching the p-i-n receiver. It is not possible to use such a narrow optical BPF for ASE noise suppression in NRZ-OOK, as it would result in severe penalty due to intersymbol interference [14].

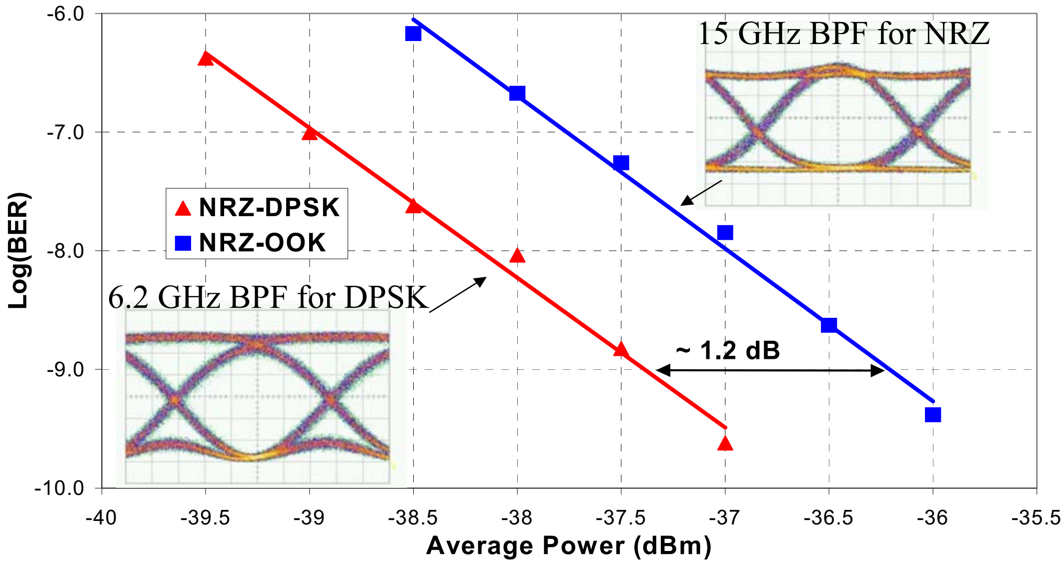


Figure 5.5: Measured receiver sensitivity for DPSK (triangles) and NRZ-OOK (squares). Corresponding measured eye diagrams are also shown.

The above results and analysis beg the following question: Is the 1.2-dB gain that we see for NRZ-DPSK over NRZ-OOK a fundamental advantage, or just an artifact of a suboptimum NRZ-OOK system? The former hypothesis is supported by recent theoretical work by Bosco *et al.* [36], which proves that the quantum limit for duobinary is 1 dB below OOK in ASE noise-limited regime. The connection with duobinary is plausible since the optical discriminator BPF converts NRZ-DPSK into an NRZ-duobinary signal at the receiver. Of course, we cannot rule out the possibility that our receiver is somehow biased against NRZ-OOK, although the optical and electrical receiver bandwidths used for the NRZ-OOK measurements are very close to the theoretical optimum values $B_o = 14\,\mathrm{GHz}$ and $B_e = 8.5\,\mathrm{GHz}$ [13]. Moreover, according to [55], the NRZ-OOK system would have to be significantly off from the optimum to explain a 1.2-dB difference. For example, the optical bandwidth can be anywhere from 10 to 20 GHz with only a ~0.5-dB penalty relative to the optimum (see [14, Fig. 2]). Thus, the experimental evidence points to a fundamental 1-dB advantage for NRZ-DPSK, although more work is needed to give a definitive answer.

Fig. 5.6 shows a measurement of BER-equivalent Q–factor for DPSK as a function of optical BPF demodulator bandwidth. Two distinct 86146B units, each with slightly different filter bandwidths (due to manufacturing tolerances), are used to realize the various filter bandwidths corresponding to the data points in Fig.5.6. For comparison, we also plot simulation results obtained with Optsim commercial software package, where the optical BPFs are modeled by Gaussian (dashed line) and fifth-order Bessel (solid line) filter shapes. In both measurements and simulations, OSNR is kept fixed at 14 dB/0.1 nm. Fig. 5.6 also shows the measured eye diagrams corresponding to several different BPF bandwidths. The optimum demodulator BPF bandwidth is found to be near ~6 GHz. Using a narrower bandwidth leads to eye closure, while a wider bandwidth results in a less efficient frequency discriminator.

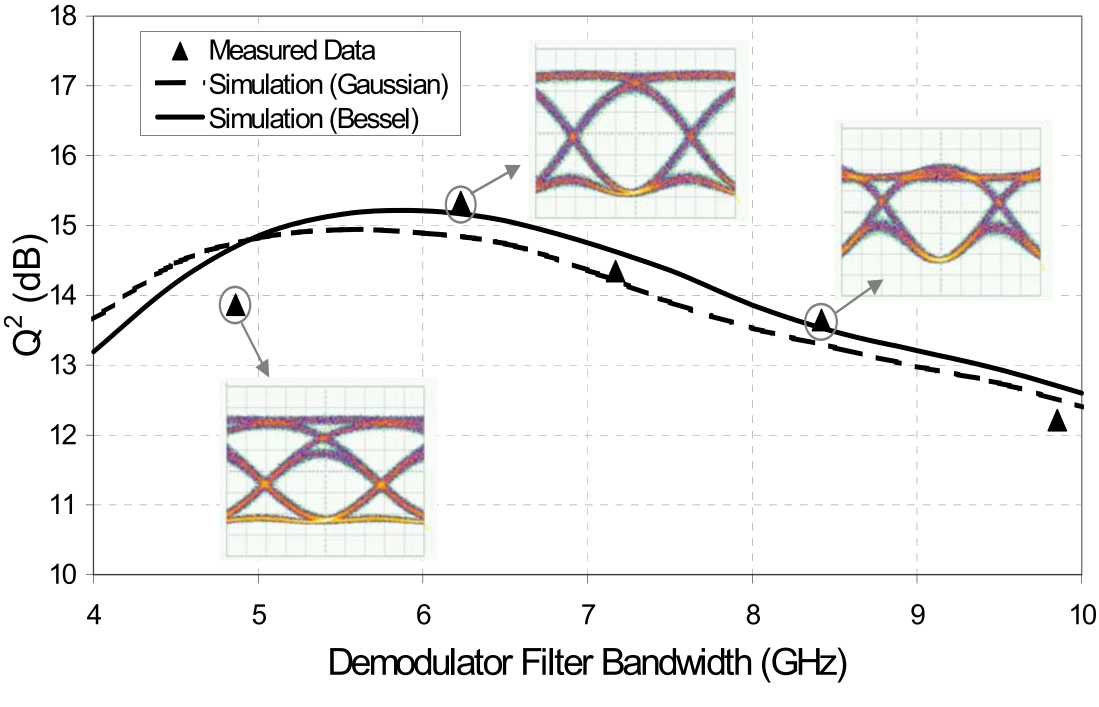


Figure 5.6: Measured $Q^2$ as a function of DPSK demodulator BPF bandwidth (triangles), and simulation results (dashed and solid curves). Measured eye diagrams are also shown for several BPF bandwidth points.

Fig. 5.7 shows the amplitude response of the 6.2-GHz BPF used in the experiment, as well as the corresponding Gaussian and Bessel filter models. The

Bessel model approximates more closely the 86146B filter shape, and also gives slightly better agreement between simulated and measured Q as a function of BPF bandwidth.

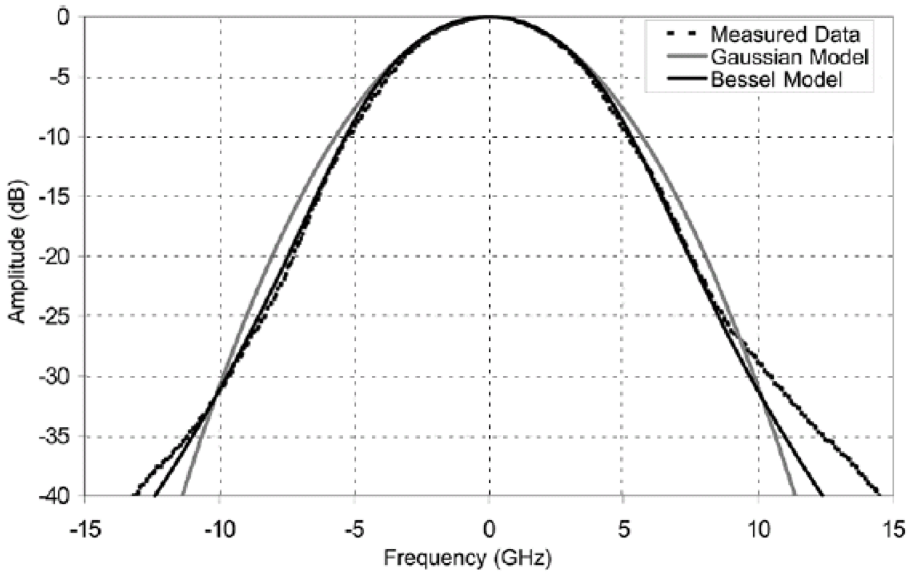


Figure 5.7: Measured amplitude response for 86 146B optical BPF with 6.2-GHz bandwidth. The corresponding Gaussian and Bessel filter models used in the simulations are also shown for comparison.

Fig. 5.8 shows a measurement of BER-equivalent Q-factor as a function of DPSK carrier frequency detuning from optimum. In this measurement, OSNR is kept fixed at 14 dB/0.1 nm while the DFB laser transmitter wavelength is varied in increments of 1 pm. As seen in Fig. 5.8, the laser transmitter wavelength and optical BPF must be aligned with $\pm 0.6$-GHz accuracy over the lifetime of the system to ensure less than ~0.5-dB Q-penalty. Although such a strict requirement on frequency stability is challenging, it should be technically feasible [38]. Finally, we note that the conventional DPSK demodulator based on delay-interferometer has similarly strict requirements on frequency stability [55].

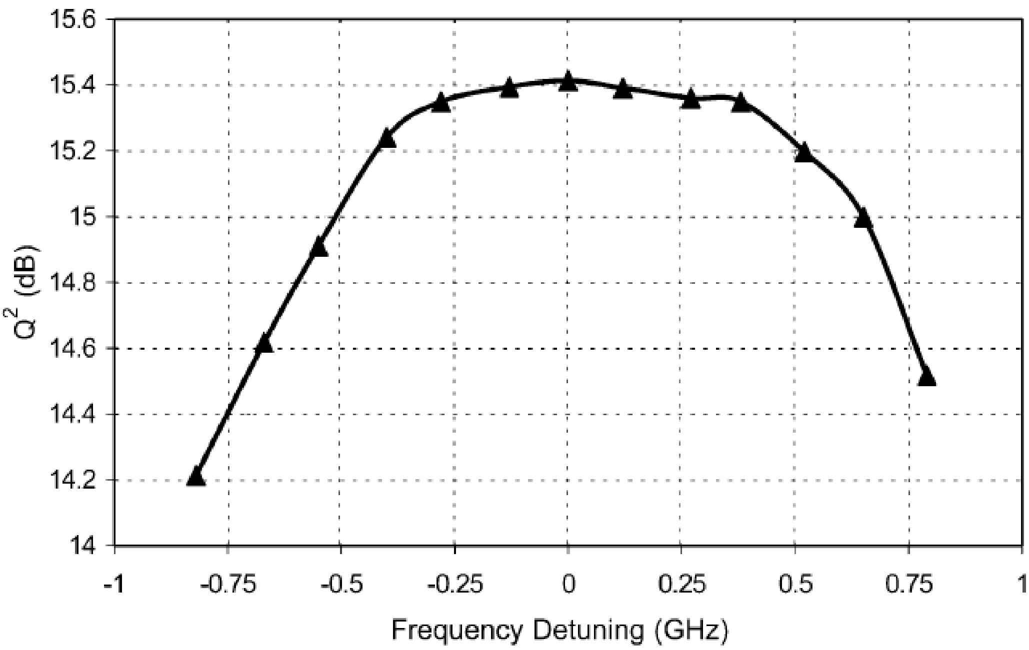


Figure 5.8: Measured Q as a function of transmitter laser frequency detuning.

Figure 5.9 compares the measured 10 Gb/s optical spectra of the different modulation formats described above. The spectra are measured using an optical spectrum analyzer (OSA) with ~ 10 pm (or ~ 1 GHz) resolution. RZ modulation has the broadest spectrum, about a factor of two wider than NRZ. Duobinary clearly has the narrowest spectrum. Thus, we expect duobinary to give the best spectral efficiency, i.e. the tightest packing of WDM channels on a single optical fiber. The DPSK spectrum is similar to NRZ, except for the absence of a carrier tone. DPSK modulation has a lower peak power compared to NRZ, and thus, reduced nonlinear effects. Moreover, the DPSK 3 dB advantage in receiver sensitivity makes it possible to lower the launch power of WDM channels to further reduce nonlinear effects. Thus, both DPSK and duobinary have some interesting features that need to be explored further to determine which modulation format is more optimal for ultra-dense WDM (UDWDM).

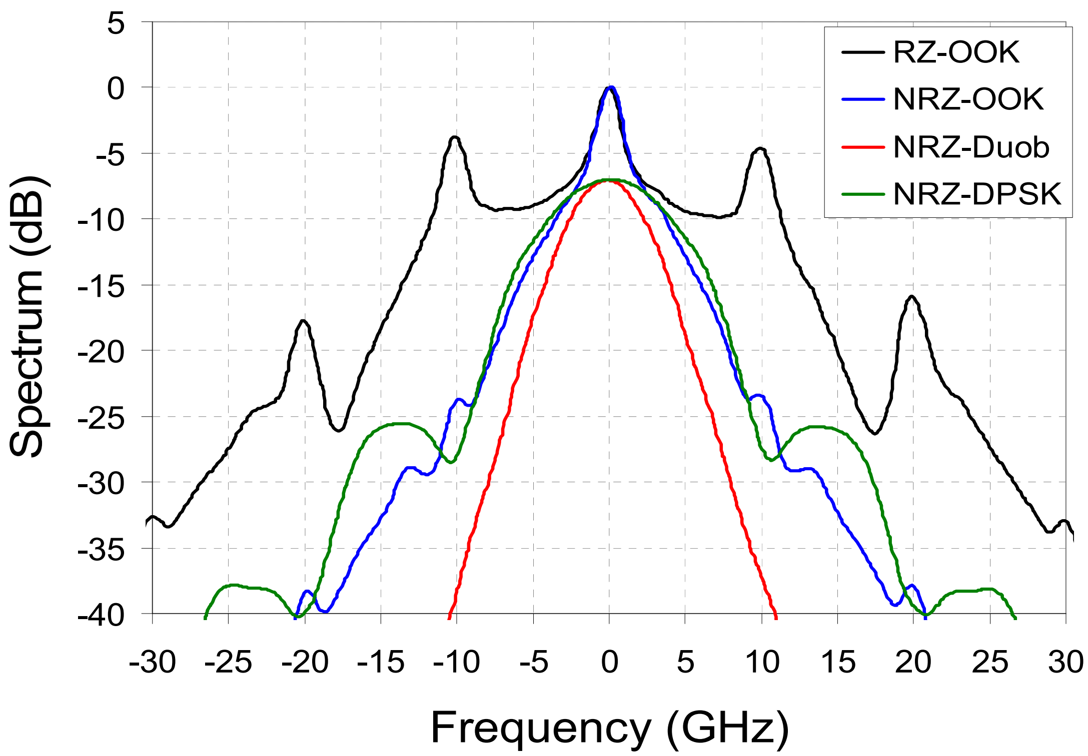


Figure 5.9: Measured 10 Gb/s optical spectra for RZ (black), NRZ (blue), DPSK (green), and duobinary (red). OSA resolution is ~ 10 pm. Note that frequency axis is plotted relative to carrier frequency.

## 5.2 Differential Quadrature Phase Shift Keying (DQPSK)

The development of advanced multilevel modulation and detection technologies is important for enabling efficient lightwave transmission of high-bit rate services, such as 40G Synchronous Optical Network (SONET/SDH) and 100G Ethernet. Multilevel modulation formats allow signal-channel data rates to exceed the limits of high-speed optoelectronics technology. As multilevel intensity modulation formats have proven not beneficial for optical fiber transmission application so far, mainly due to a back-to-back receiver sensitivity penalty compared to binary on-off-keying. Differential Quadrature Phase Shift Keying (DQPSK) has received considerable attention recently [59, 60, 61, 71, 81] and is one of the most promising multilevel optical modulation formats [64, 67, 68, 69, 78]. In DQPSK transmission, information is encoded into optical phase shifts in both quadratures of the optical carrier, thus doubling spectral efficiency compared to binary modulation formats such as differential phase shift keying (DPSK) [75, 76, 77]. The DQPSK demodulator is a key component for converting the optical phase modulation into intensity modulation for square-law detection at the receiver. The conventional “self-homodyne” DQPSK receiver includes two Mach-Zehnder delay interferometers (DIs) for demodulation of each quadrature, followed by balanced detection [46, 60, 61, 62]. The two DIs each have a delay of a symbol period $T_s$, but must be phase shifted differently (by +/- π/4) to decode the two signal quadratures correctly. Note that the opposite phases of the two DIs are equivalent to opposite frequency detuning of δf = +/- S/8 relative to signal, where S = $1/T_s$ is the symbol rate.

In this dissertation we demonstrate experimentally a lower complexity DQPSK demodulator, which also provides for a significantly greater tolerance to fiber chromatic dispersion, enabling transmission over 80 km of SMF without dispersion compensation or electronic signal processing.

### 5.2.1 DQPSK Precoder

Figure 5.10 shows a schematic of an optical DQPSK precoder. Like DPSK, a DQPSK precoder is needed in order to provide a direct mapping of data from the original input to received output. The precoder only needs to operate at the symbol rate, which is half of the transmitted data rate.

The operation of DQPSK precoder is described in [45, 60, 100], and has the logic functions as below:

$$I_K = U_K V_K I_{K-1} + \overline{U}_K V_K Q_{K-1} + U_K \overline{V}_K \overline{Q}_{K-1} + \overline{U}_K \overline{V}_K \overline{I}_{K-1}$$

$$Q_K = U_K V_K Q_{K-1} + \overline{U}_K V_K \overline{I}_{K-1} + U_K \overline{V}_K I_{K-1} + \overline{U}_K \overline{V}_K \overline{Q}_{K-1}$$

where $U_K$ and $V_K$ are original input binary data streams, $I_K$ and $Q_K$ are precoded data streams after precoder, $I_{K-1}$ and $Q_{K-1}$ are one bit delay version of precoder outputs, $I_K$ and $Q_K$. The two precoded signals $I_K$ and $Q_K$ are used to drive MZM to produce optical DQPSK signals.

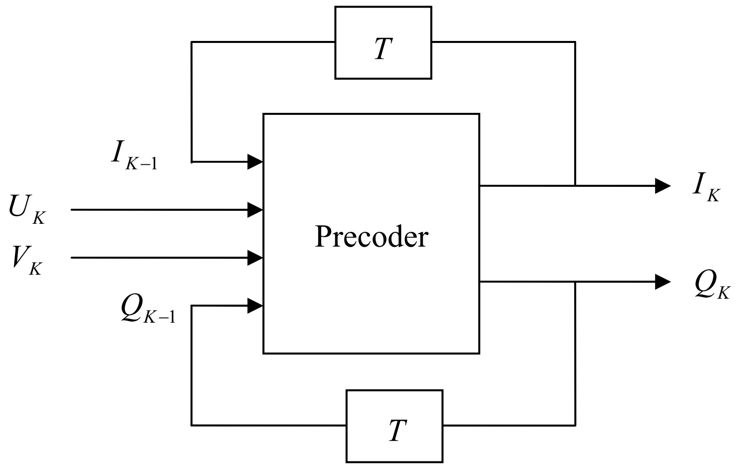


Figure 5.10: Schematic of an optical DQPSK precoder

## 5.2.2 DQPSK Encoder

A common implementation of the optical DQPSK encoder is based on integrating two parallel DPSK modulators to form a Mach-Zehnder superstructure as shown in figure 5.11 [60, 71]. The superstructure has quadrature control electrodes in order to adjust the optical phase difference $\frac{\pi}{2}$ between two DPSK signals. Each MZM is biased at minimum transmission and driven by a binary NRZ signal with peak-to-peak amplitude of $2V_\pi$. One MZM produces the optical field $\mathrm{Re}(E)$ with normalized filed amplitude {+1, -1} similar to DPSK. Another MZM also produces a DPSK signal with $\frac{\pi}{2}$ phase shifted, therefore donated as $\mathrm{Im}(E)$. The output field of optical DQPSK modulator is $E_o = \mathrm{Re}(E) + j\,\mathrm{Im}(E)$, which is a four-level phase modulated signal $\{\pm 1 \pm j\}$ and could be presented as phase values $\{\frac{\pi}{4}, \frac{3\pi}{4}, \frac{5\pi}{4}, \frac{7\pi}{4}\}$ as shown in table 2.

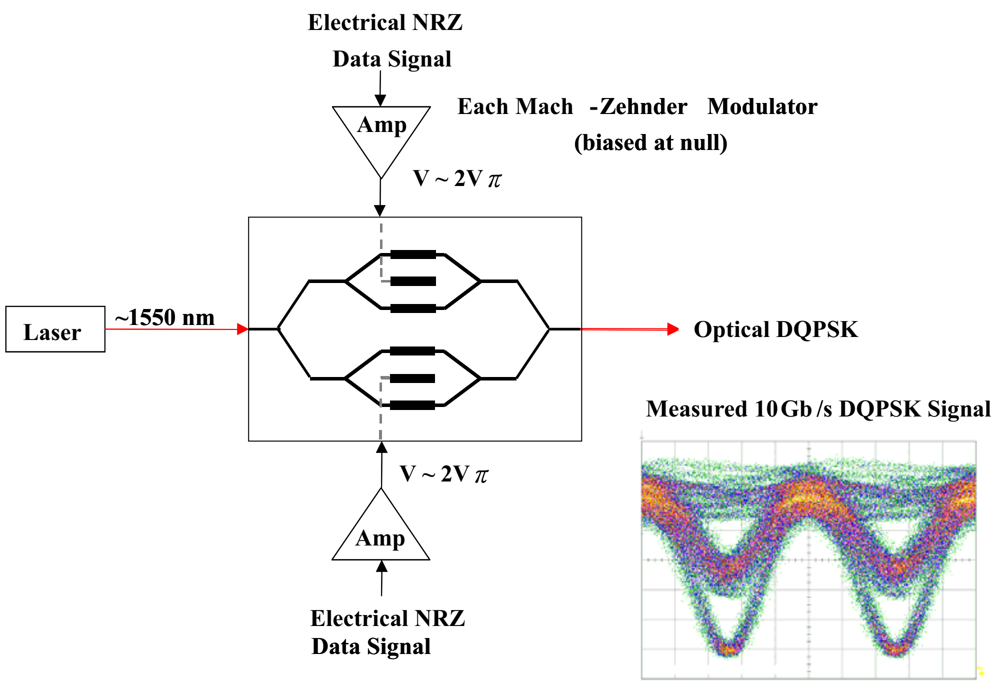


Figure 5.11: DQPSK transmitter setup. An optical DQPSK eye diagram is also shown.

| $I_K$ | $Q_K$ | $E_o$ | $\Phi_K$ |
|---|---|---|---|
| 0 | 0 | +1+ j | $\pi / 4$ |
| 1 | 0 | -1+ j | $3\pi / 4$ |
| 0 | 1 | +1- j | $7\pi / 4$ |
| 1 | 1 | -1- j | $5\pi / 4$ |

Table 2: Mapping of modulator input signals ($I_K$ and $Q_K$) to corresponded optical electric field ($E_o$) and generated phase state ($\Phi_K$) of DQPSK modulator

With the use of a precoder before the optical encoder, the original input data signals ($U_K$ and $V_K$) is mapping to the phase changes ($\Delta\Phi_K$) as shown in table 3. The phase change $\Delta\Phi_K$ corresponds to the phase difference between the current phase $\Phi_K$ and the previous phase $\Phi_{K-1}$. This phase difference contains the transmitted information that can be extracted at the receiver by the DQPSK decoder.

| $U_K$ | $V_K$ | $d_K$ | $\Delta\Phi_K$ |
|---|---|---|---|
| 0 | 0 | 1 | $\pi$ |
| 1 | 0 | 2 | $\pi / 2$ |
| 0 | 1 | 3 | $3\pi / 2$ |
| 1 | 1 | 4 | 0 |

Table 3: Mapping of initial input signals ($U_K$ and $V_K$) to corresponded optical phase changed ($\Delta\Phi_K$) of DQPSK modulation

### 5.2.3 DQPSK Decoder

The optical DQPSK signals can be decoded by using two optical delay and add interferometers followed by two balanced detectors for each quadrature. The two DIs each have a delay of a symbol period Ts, but must be phase shifted differently (by +/- $\pi$ /4) to decode the two signal quadratures correctly [46], shown in 5.12(a).

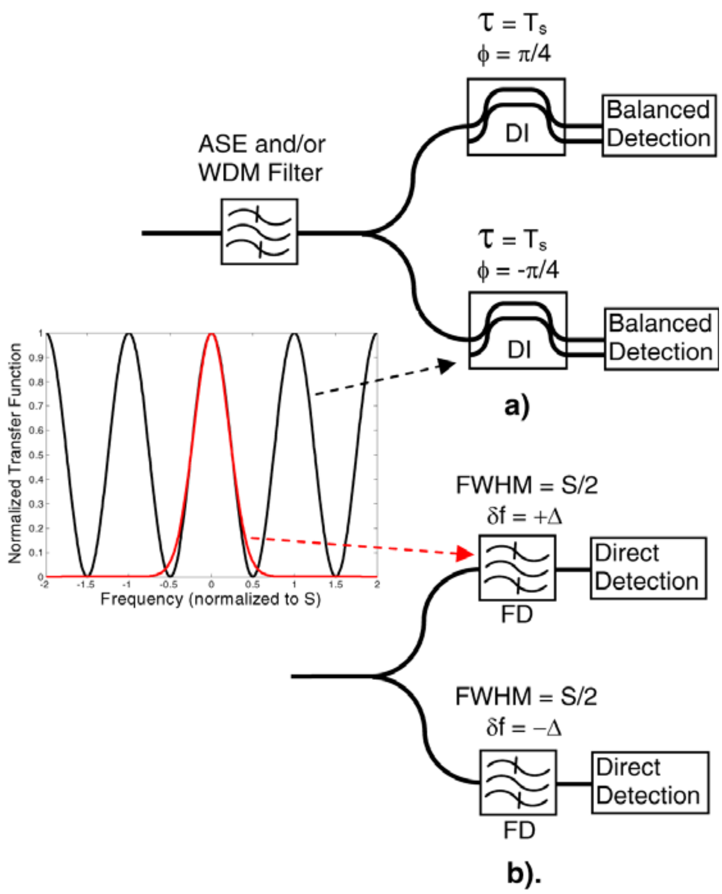


Figure 5.12: Schematic diagram for (a) conventional DQPSK receiver based on DI demodulators and balanced detection, and (b) proposed DQPSK receiver based on frequency discriminator (FD) filters and direct detection.

If the input signals to modulator have the form $E_0 e^{-j(\omega_0 + \Delta\Phi_K)}$, the output signals after balanced detection for each interferometer are proportional to $[\cos(\Delta\Phi_K) + \sin(\Delta\Phi_K)]$ and $[\cos(\Delta\Phi_K) - \sin(\Delta\Phi_K)]$ [60, 79, 98, 99, 100]. The transmitted and received data bit streams at different stages for an optical DQPSK system are also shown in table 4. Note that the opposite phases of the two DIs are equivalent to opposite frequency detuning of Δf = +/- S/8 relative to signal, where S = 1/Ts is the symbol rate, shown in 5.12(b).

| Time Instant $k$ | -1 | 0 | 1 | 2 | 3 | 4 | 5 | 6 | 7 |
|---|---|---|---|---|---|---|---|---|---|
| Binary Data $U_k$ | | 1 | 0 | 0 | 1 | 1 | 1 | 0 | 1 |
| Binary Data $V_k$ | | 0 | 0 | 1 | 1 | 0 | 1 | 1 | 0 |
| Precoded Data $I_k$ | 0 | 1 | 0 | 1 | 1 | 0 | 0 | 1 | 0 |
| Precoded Data $Q_k$ | 0 | 0 | 1 | 1 | 1 | 1 | 1 | 1 | 1 |
| I/P Voltage to MZM ($I$) | $-V_\pi$ | $+V_\pi$ | $-V_\pi$ | $+V_\pi$ | $+V_\pi$ | $-V_\pi$ | $-V_\pi$ | $+V_\pi$ | $-V_\pi$ |
| I/P Voltage to MZM ($Q$) | $-V_\pi$ | $-V_\pi$ | $+V_\pi$ | $+V_\pi$ | $+V_\pi$ | $+V_\pi$ | $+V_\pi$ | $+V_\pi$ | $+V_\pi$ |
| O/P Electrical Field $E_0$ | +1+j | -1+j | +1-j | -1-j | -1-j | +1-j | +1-j | -1-j | +1-j |
| Transmitted Phase Φ | $\pi/4$ | $3\pi/4$ | $7\pi/4$ | $5\pi/4$ | $5\pi/4$ | $7\pi/4$ | $7\pi/4$ | $5\pi/4$ | $7\pi/4$ |
| Phase Difference $\Delta\Phi$ | | $\pi/2$ | $\pi$ | $3\pi/2$ | 0 | $\pi/2$ | 0 | $3\pi/2$ | $\pi/2$ |
| Received Data $u_k$ | | 1 | 0 | 0 | 1 | 1 | 1 | 0 | 1 |
| Received Data $v_k$ | | 0 | 0 | 1 | 1 | 0 | 1 | 1 | 0 |

Table 4: The transmitted and received data bit streams at different stages for an optical DQPSK system.

In this dissertation, we proposed and demonstrated experimentally a lower complexity DQPSK demodulator. The receiver architecture of DIs are replaced by Gaussian shaped band-pass optical filters with full width of half maximum (FWHM)

~ S/2, and opposite frequency detuning of +/- Δ. The Gaussian shaped filter approximates one spectral lobe of the periodic DI filter. However, the optimum frequency detuning $\Delta \sim 0.173 \cdot S$ is slightly greater than S/8 [63]. The narrow optical filters act as *frequency discriminators*, and depending on the sign of frequency detuning, can convert phase modulation of the in-phase or quadrature signal components into an intensity modulation, which is detected using simple direct-detection receivers.

### 5.2.4 Results

Our 20 Gb/s (10 Gbaud) DQPSK experimental setup is shown schematically in Fig. 5.13. The DQPSK modulator is based on a nested Mach-Zehnder modulator (MZM) structure in Lithium Niobate, and is specified to have a bandwidth of 8 GHz. The I and Q arms of the modulator are driven by the two complementary 10 Gb/s NRZ data outputs of a pulse pattern generator (PPG), amplified to 2Vpi . The PPG generates a pseudo random bit sequence (PRBS) pattern of length $2^{15}$-1, with a 26 bit delay inserted between I and Q data streams for de-correlation. The optical DQPSK signal output of modulator is fed into a variable optical attenuator (VOA1), which controls the launch power into conventional single mode fiber (SMF) spools of various lengths; launch power is fixed at –3 dBm. A second variable optical attenuator (VOA2) sets the input optical power into an erbium doped fiber amplifier (EDFA). The EDFA pre-amplifier is followed by either an optical frequency discriminator filter or DI demodulator. We utilize an optical spectrum analyzer (OSA) operating in a filter mode to realize the required narrow optical bandpass filter for the frequency discriminator demodulator, shown in Fig. 5.13(a). The optical filter bandwidth is set by the OSA resolution. At an OSA resolution of 0.04 nm, we obtain an approximately Gaussian shaped optical filter with ~ 6 GHz bandwidth [63]. The frequency discriminator demodulator is followed by a standard 10 Gb/s OOK receiver, including p-i-n photodetector, integrated trans-impedance amplifier (TIA), and limiting amplifier (LA), specified to have an electrical bandwidth of ~ 9 GHz. The receiver electrical output is fed into an error detector (ED), programmed for the proper data pattern after demodulation. Clock recovery (CR) is achieved by tapping a portion of the signal at output of discriminator filter demodulator into a commercial instrumental OOK receiver. The simplicity of frequency discriminator direct detection (FD-DD) receiver compared with conventional DI balanced detection (DI-BD) receiver is evident in Fig. 5.13(b). However, the lower complexity comes at the cost of OSNR sensitivity.

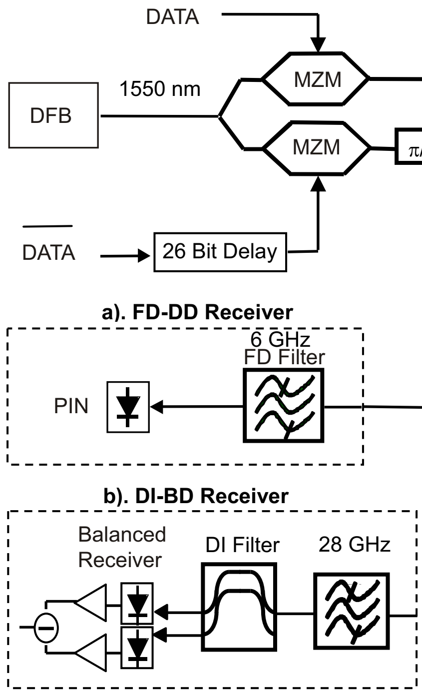


Figure 5.13: Experimental setup for testing 20 Gb/s DQPSK modulation format, demodulated by a). Frequency discriminator with direct detection (FD-DD), or b). Delay interferometer with balanced detection (DI-BD).

Fig. 5.14 shows the data on back-to-back (B2B) bit error rate (BER) versus optical signal to noise ratio (OSNR). The OSNR is measured at output of EDFA pre-amplifier (defined over a 0.1 nm noise bandwidth including both polarizations). For FD-DD receiver, the I and Q tributaries are demodulated by detuning the discriminator filter center by ~ ± 1.7 GHz relative to laser carrier frequency, while in DI-BD receiver, the DI phase is tuned for ± π/4. The BER is measured separately for I and Q, and averaged to obtain the composite BER displayed in Fig. 5.14. We tested two different DIs, one DI with FSR exactly matched to baud rate, and a second DI with a 20% wider FSR. The wider FSR DI is interesting to study due to previous theoretical predictions of an enhanced dispersion tolerance in DPSK systems using DI demodulator with differential delay less than a symbol period [72]. At a BER of $10^{-3}$, the required OSNR of DI-BD receiver is measured to be ~ 11.7 dB for both DI designs. Note that theory predicts a slight ~ 0.25 dB B2B penalty for the 20% wider FSR DI [73]. We surmise that the wider FSR DI suffers no B2B penalty in our system because the IQ modulator has a relatively narrow ~ 8 GHz bandwidth; a wider FSR DI can compensate for a narrowing of signal bandwidth, as shown in [74] with optical filters.

The FD-DD receiver required an OSNR ~ 14.9 dB to achieve BER of $10^{-3}$, ~ 3.2 dB more than DI-BD receiver. The ~ 3 dB gain in OSNR sensitivity for DI-BD over FD-DD receiver is expected due to the advantage of balanced detection over direct detection. The noise free demodulated eye diagrams for a quadrature tributary are also shown in the inset of Fig. 5.14; note that the DI-BD eye is measured after the LA of balanced receiver, and thus appears “square” due to the limiting action of LA. Interestingly, the FD-DD demodulated eye (measured directly after frequency discriminator filter using digital communications analyzer high-speed optical plug-in) appears somewhat similar to a duobinary eye, which portends well for a good dispersion tolerance.

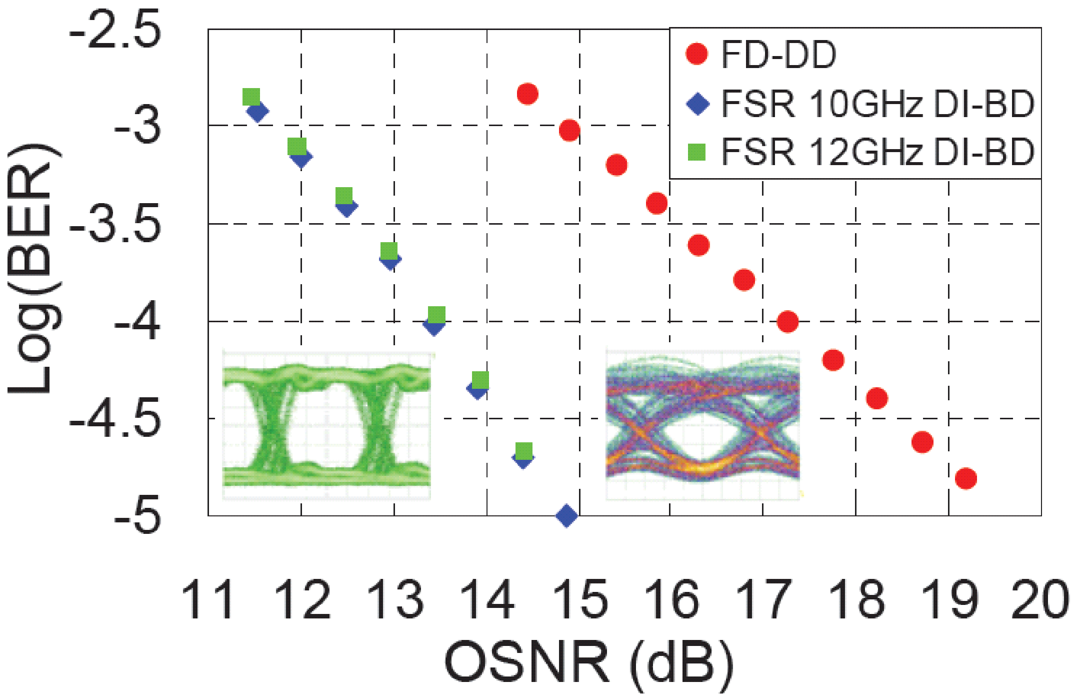


Figure 5.14: Back-to-back BER versus required OSNR for DQPSK

The tolerance to fiber chromatic dispersion (CD) is illustrated in Fig. 5.15, where we plot the measured OSNR penalty as a function of SMF (D ~ 17 ps/nm/km) transmission distance. OSNR penalty is defined relative to B2B performance at a BER = $10^{-3}$. As seen in Fig. 5.15, the FD-DD received shows a factor of 2x advantage in dispersion tolerance compared with DI-BD receiver. This experimental data confirms our previous theoretical predictions [63].

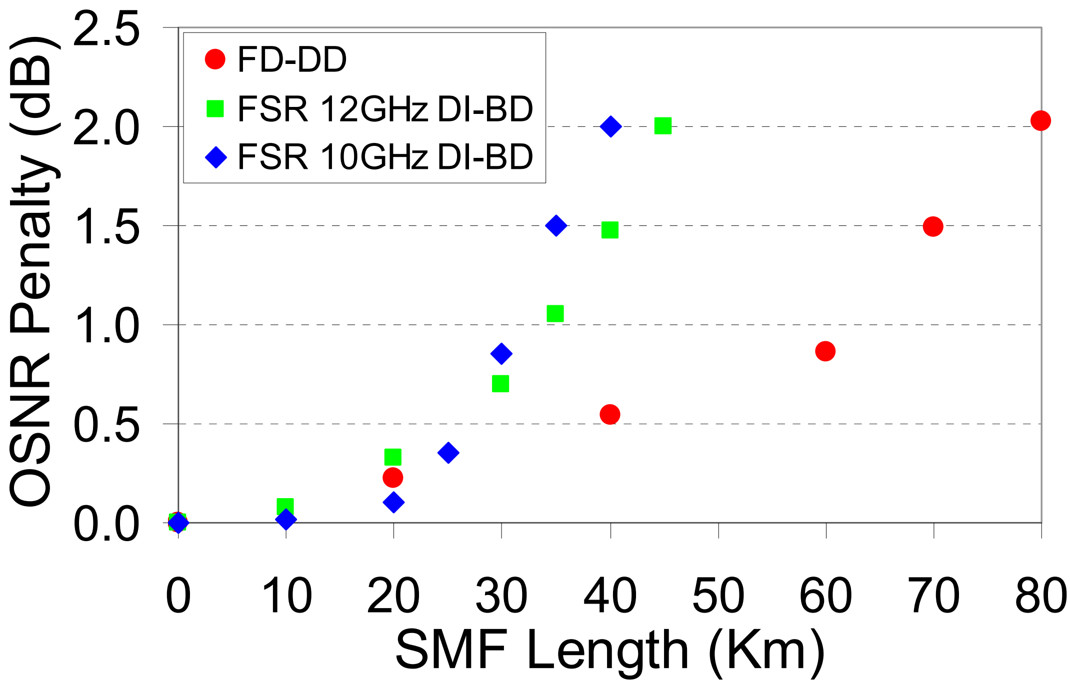


Figure 5.15: Measured OSNR penalty versus SMF transmission distance.

It is also interesting to compare the impact of FSR on the dispersion tolerance of DI-BD receiver. The 20% wider FSR DI shows a ~ 12.5% improvement in CD tolerance at 2 dB OSNR penalty, roughly in line with the theoretical predictions in [72] for DPSK. Comparing the DI-BD and FD-DD receivers, the wider FSR DI enables uncompensated 10 Gbaud DQPSK transmission over ~ 44 km of SMF at 2 dB OSNR penalty, while the FD-DD receiver supports an impressive ~ 80km SMF transmission distance. The ultra-narrow frequency discriminator filter can suppress deleterious high frequency signal components more effectively compared with DI filter [79, 80]; even with an optimized FSR one cannot completely avoid deleterious high frequency components from entering the receiver due to periodic response of DI filter.

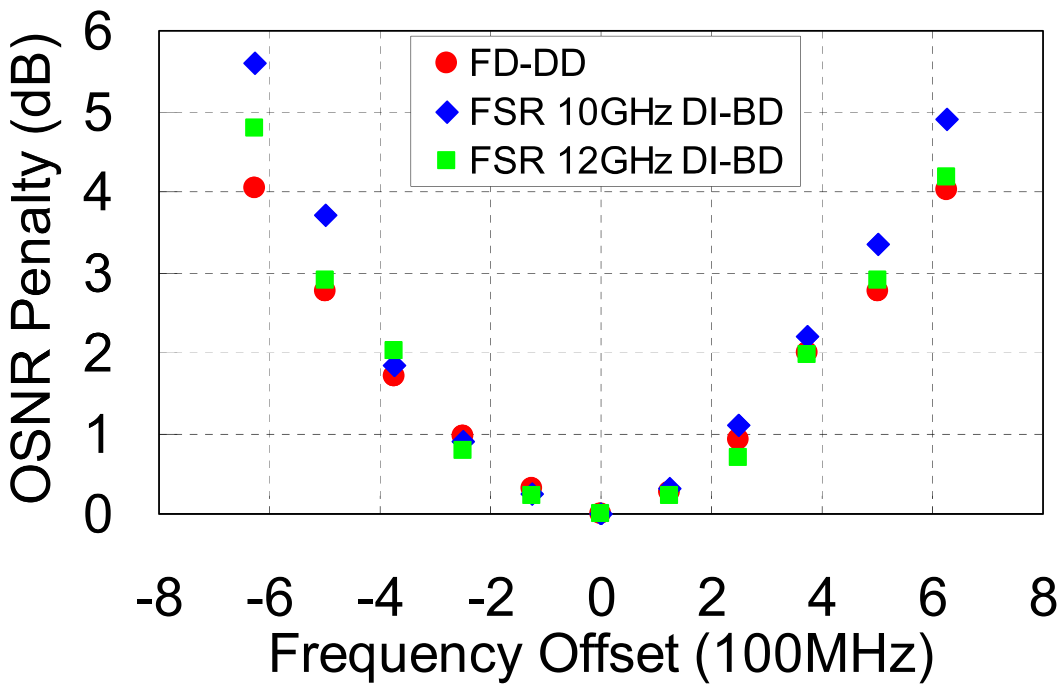


Figure 5.16: Measured OSNR penalty versus laser frequency offset.

An additional concern with DQPSK systems, especially at 10 Gbaud, is the tight tolerance to frequency offsets between signal and demodulator filter. Fig. 5.16 shows experimental data assessing the sensitivity to frequency offsets for both DI-BD and FD-DD receivers. The OSNR penalty is measured versus laser frequency detuning from the optimum. As demonstrated in Fig. 5.16, the frequency discriminator demodulator shows the best tolerance to frequency offsets compared with DI demodulator, with the 20% wider FSR DI fairing slightly better than conventional DI. However, the differences are rather small, and only observable at relatively large OSNR penalties. For all of the DQPSK receivers tested, frequency offsets should be controlled to approximately ~ 100 MHz to ensure less than ~ 0.5 dB penalty.

## 5.3 Polarization Multiplexing DQPSK

A doubling of spectral efficiency can be achieved by combining two DQPSK signals with two orthogonal polarizations of carrier waves by Polarization Division Multiplex (PolDM) [82-89]. By combining multilevel DQPSK modulation with polarization multiplexing, we quadruple spectral efficiency compared with single polarization binary formats. However, a polarization controller would be needed which results in a more complex receiver. A 40 Gbit/s Dual-Polarization (DP) DQPSK signal can be generated by combining two 20 Gbit/s DQPSK signals, which are originally formed by two DPSK signals for each in quadrature phases.

### 5.3.1 DP-DQPSK Encoder

Fig. 5.17 shows the DP-DQPSK transmitter scheme. The optical carrier wave is split into two polarizations (X and Y) through the polarization beam splitter (PBS). Each carrier wave is then modulated by a DQPSK modulator driven by two 10 Gbit/s PRBS data streams with proper bit mutual delay resulting in the generation of an optical DQPSK signal. Two DQPSK signals are then combined in orthogonal polarizations by a polarization beam combiner (PBC). The resultant signal is a $2\times2\times10$ Gbit/s DP-DQPSK signal.

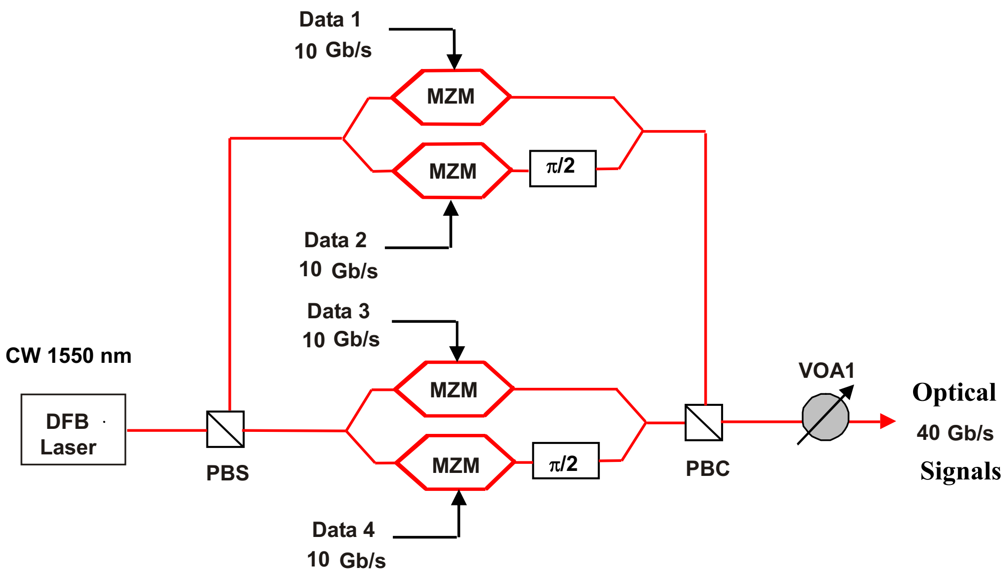


Figure 5.17: A $2 \times 2 \times 10$ Gb/s DP-DQPSK transmitter setup

## 5.3.2 DP-DQPSK Decoder

In order to detect the signals carried by different polarizations, a polarization controller, which controls a proper polarization, followed by a polarizer, which filters out undesired polarization component, is needed for a DP-DQPSK receiver. Since the polarization of light inside fiber is time-variable, a dynamic polarization controller is helpful to stabilize the polarization of carrier wave. In a practical implementation, a polarization beam splitter would be employed instead of a polarizer in order to receive the signals in both polarizations simultaneously. Then each signal is received by a separate DQPSK receiver to extract the transmitted information. Like DQPSK, two types of demodulator schemes, delay interferometer plus balanced detection (DI-BD) and frequency discriminator plus direct detection (FD-DD), could be employed to covert optical phase signals into intensity signals for detection. As figure 5.18(a) shows below, four DIs and eight photodiodes are needed to demodulated DP-DQPSK signals simultaneously. Meanwhile, four frequency discriminators and four photodiodes are needed to do the same job in the second scheme, shown in 5.18(b).

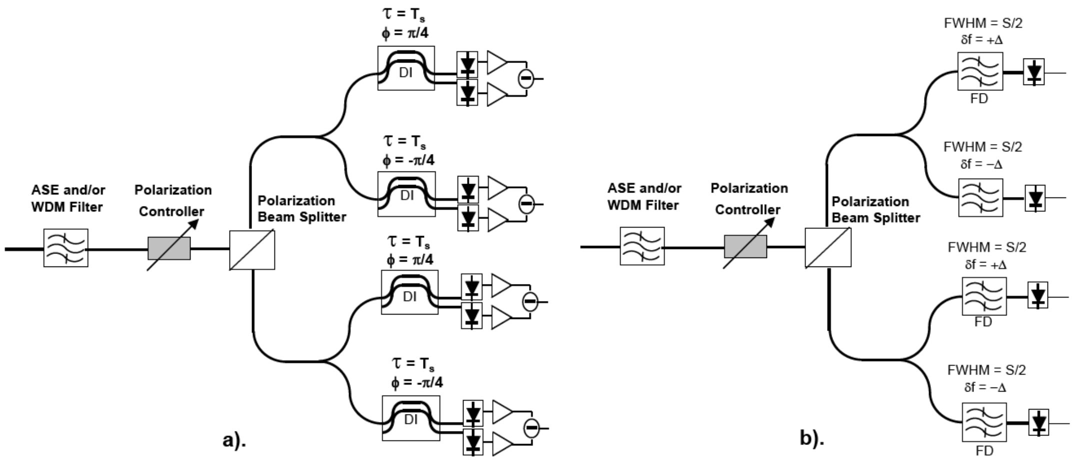


Figure 5.18: Two demodulator schemes of a). DI+BD, and b). FD+DD for DP-DQPSK

### 5.3.3 Results

Our 40 Gb/s (10 Gbaud) DP-DQPSK experimental setup is shown schematically in Fig. 5.19. The DQPSK modulator is based on a nested MZM structure in Lithium Niobate, and is specified to have a bandwidth of 8 GHz. The I and Q arms of the modulator are driven by the two complementary 10 Gb/s NRZ data outputs of a pulse pattern generator, amplified to 2Vπ. We tested both PRBS $2^7$-1

(PRBS-7) and $2^{15}$-1 (PRBS-15) data patterns, with a 15 bits delay between I and Q data streams for de-correlation.

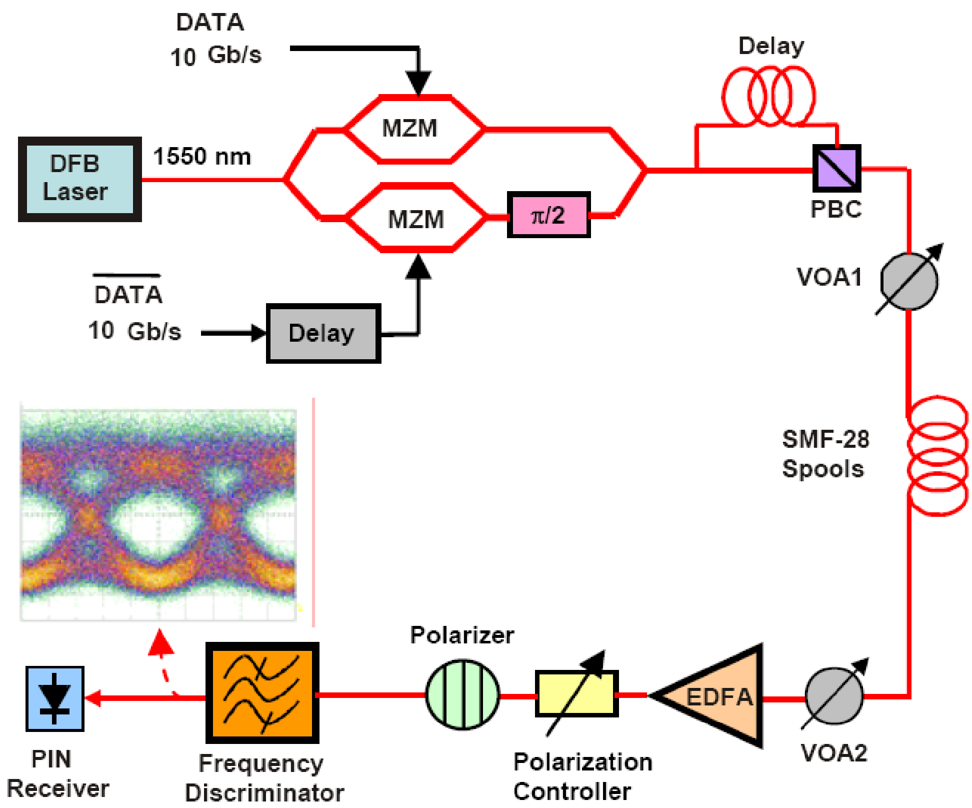


Figure 5.19: 40 Gb/s DP-DQPSK experimental setup with frequency discriminator. The B2B demodulated eye diagram is also showed in inset.

The optical signal output from modulator is further processed to produce the dual-polarization DQPSK format by splitting and combining in a PBC, with an appropriate optical delay for de-correlation. The DP-DQPSK signal is then transmitted through various lengths of conventional single mode fiber (D ~ 17 ps/nm/km). Two variable optical attenuators (VOA1 and VOA2) are used to control the input optical power into the fiber span (< -3 dBm), and OSNR at the output of

EDFA pre-amplifier. The EDFA pre-amplifier is followed by a polarizer for demultiplexing one of the two polarization channels, and then an optical frequency discriminator filter with ~ 6 GHz bandwidth for demodulating one of the two signal quadratures. A measured demodulated eye diagram for one of the signal quadratures is shown in the inset of Fig. 5.19. The receiver in the experimental setup is a commercially available 10 Gb/s p-i-n photodetector with integrated trans-impedance amplifier (TIA), and limiting amplifier (LA), and is specified to have an electrical bandwidth of ~ 9 GHz. The receiver output is fed into an error detector (ED), programmed for the proper data pattern after DQPSK demodulation. Clock recovery (CR) is achieved by taping off a fraction of the optical signal at input to p-i-n detector into a commercial instrumental receiver that includes clock recovery circuitry.

Fig. 5.20 shows the measured bit error ratio (BER) versus OSNR performance back-to-back (B2B). The OSNR is defined in a 0.1 nm noise bandwidth, and referenced to the output of EDFA pre-amplifier. Both Single Polarization (SP) and DP-DQPSK are tested with a PRBS-15 data pattern. As expected, the DP-DQPSK shows a ~ 3-dB penalty compared with SP-DQPSK. We observed only a small ~ 0.5 dB improvement in performance when using a PRBS-7 pattern instead of PRBS-15, most likely due to modulator imperfections.

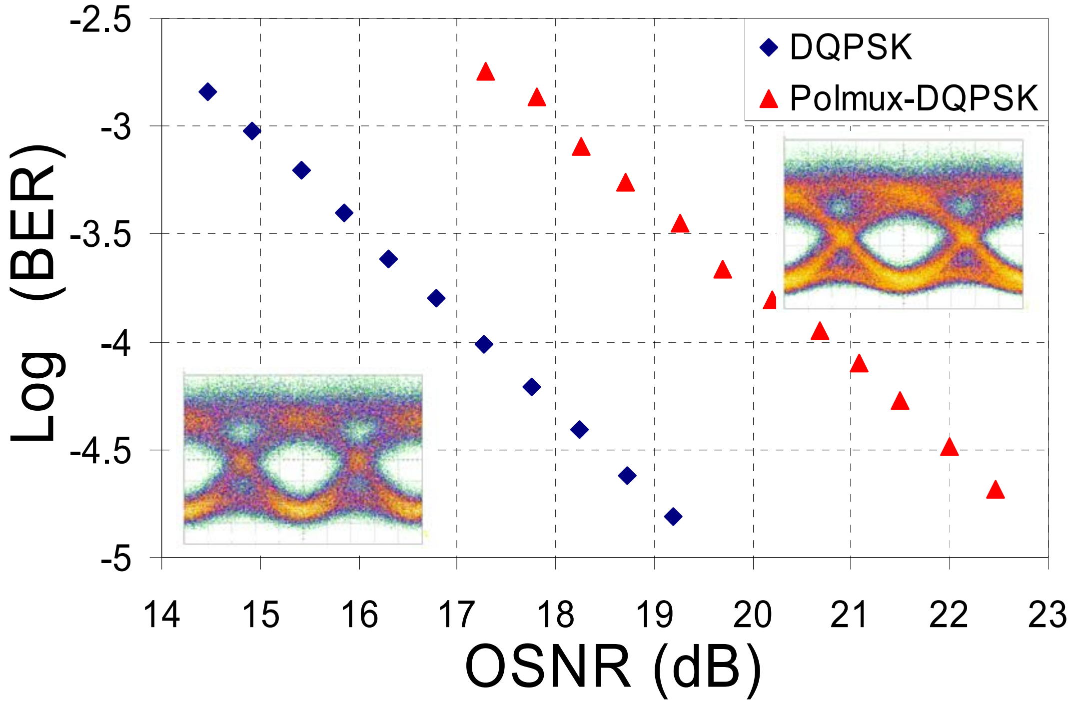


Figure 5.20: B2B performance for SP- and DP-DQPSK with frequency discriminator demodulator.

The tolerance to fiber chromatic dispersion is demonstrated in Fig. 5.21, where we plot the measured OSNR penalty relative to B2B as a function of SMF length in km. The penalty is determined by measuring the required OSNR to achieve a BER = $10^{-3}$. As seen in Fig. 5.21, we have demonstrated 40 Gb/s DP-DQPSK transmitted over 80 km of SMF with ~ 2 dB penalty, without using any optical dispersion compensation or electronic signal processing. Thus, our 40 Gb/s system has an equivalent dispersion tolerance to 10 Gb/s NRZ.

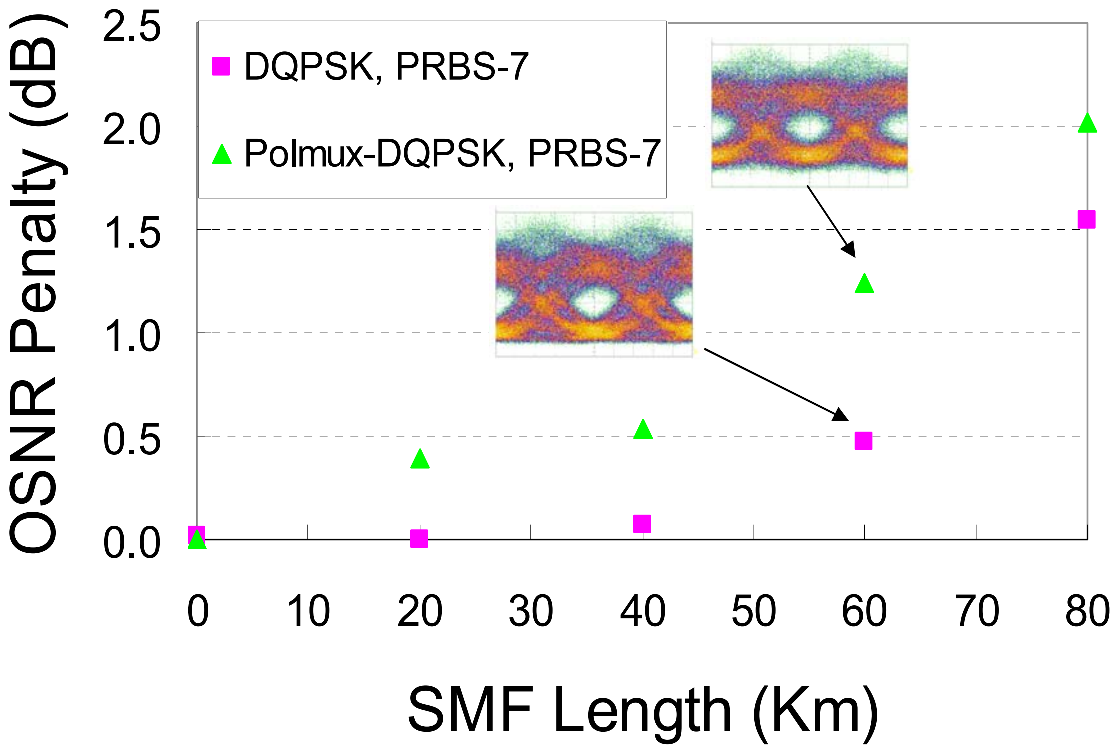


Figure 5.21: Dispersion penalty for SP- and DP-DQPSK.

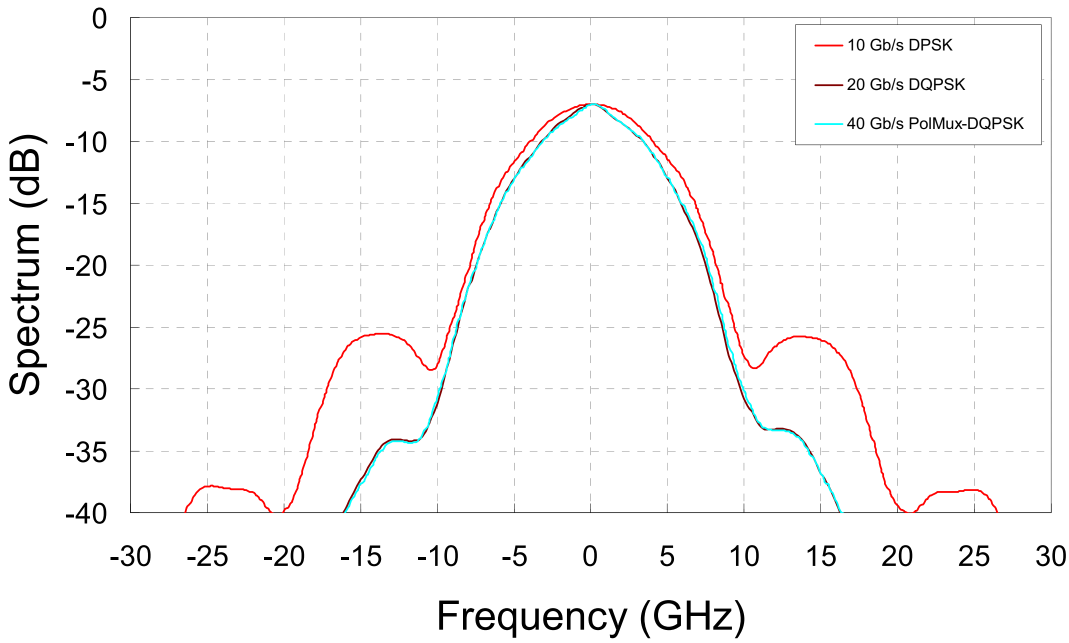


Figure 5.22: Spectra of NRZ-DPSK, DQPSK and DP-DQPSK.

Fig 5.22 shows spectra of different modulation formats, NRZ-DPSK, NRZ-DQPSK, and DP-DQPSK (i.e. PolMux DQPSK). As we expected, DP-DQPSK has the same spectrum bandwidth with SP-DQPSK. Meanwhile, the data rate of DP-DQPSK is two time higher than NRZ-DQPSK, which doubles the spectrum efficiency by a factor of two.

# Chapter 6

# Conclusions

## 1. NRZ-Duobinary

Our results of an experimental investigation on the optimum duobinary system for ASE noise-limited transmission are presented. The optimum transmitter and receiver optical filter bandwidths are found to be near or slightly less than bit rate ~ R in agreement with theory. A nearly optimum duobinary transmission system is demonstrated B2B to operate within 3.4 dB of the matched filter limit for duobinary. The optimum duobinary system is compared to a conventional duobinary system in ASE noise-limited and dispersion-limited regimes. The optimum duobinary shows a ~ 4.4 dB optically pre-amplified receiver sensitivity advantage B2B, and a ~ 2 dB advantage after 120km transmission over SMF.

Finally, we point out that to obtain the optimum duobinary pulse shape at the receiver, one must view the entire channel, including all electrical/optical filtering effects and fiber dispersion, as the “duobinary filter,” and each element in the system must be optimized accordingly.

2. RZ-Duobinary:

Optimized 10-Gb/s RZ- and NRZ-duobinary transmitters and matched receivers are experimentally demonstrated. The RZ versus NRZ pulse shape is compared for duobinary systems that are dominated by ASE noise, fiber chromatic dispersion, and SPM nonlinearity. Surprisingly, and in stark contrast to the case of OOK, in all cases that were considered, the NRZ pulse shape is found to be superior to RZ for duobinary transmission. These experiments highlight the unique properties of the duobinary modulation format.

3. DPSK:

A simple DPSK demodulation technique based on an optical discriminator filter followed by a direct detection (FD-DD) is demonstrated, while showing a 1.2-dB advantage over OOK in our experiments. This scheme has the potential for integrating DPSK demodulator, ASE filter, and WDM demultiplexer functionality in a single element.

4. DQPSK:

A novel low complexity DQPSK demodulator based on frequency discriminator filtering and direct detection is demonstrated experimentally, and compared with conventional DI demodulator with balanced detection. While the FD-DD receiver requires a higher OSNR to achieve an equivalent BER compared with the conventional DI-BD scheme, it is less sensitive to non-optimum frequency offsets, and shows a factor of 2 times better dispersion tolerance. The dispersion tolerance of DI-BD receiver can be improved by increasing DI FSR to be greater than baud rate, although the performance gain is modest compared with the 2x improvement demonstrated with FD-DD. The excellent dispersion tolerance of FD-DD, taken together with the lower complexity receiver structure, may offer a promising alternative for future applications where OSNR sensitivity is not the major driver.

5. PolMux DQPSK:

A DP-DQPSK system operating at 40 Gb/s was realized, while keeping almost the same spectrum bandwidth of NRZ-OOK, thus quadrupling the spectral efficiency of NRZ-OOK. Our proposed frequency discriminator filter demodulator scheme is suitable for DP-DQPSK. Our experimental results show 40 Gb/s DP-DQPSK system only suffering small penalty compared to 20 Gb/s SP-DQPSK in fiber chromatic dispersion.

# Bibliography


[1] J.-P. Hamaide, “Linear and Nonlinear Effects in Lightwave Transmission: Dispersion Management in Terrestrial and Submarine Systems,” Optical Fiber Communications Conference, tutorial paper, Anaheim, CA, 2002.

[2] J. M. Kahn and K.-P. Ho, “Spectral efficiency limits in DWDM systems”, in 31st European Conference on Optical Communication (ECOC 2005), Glasgow, vol. 4, pp. 843 – 846, September 2005.

[3] K. Petermann and S. Randel, “Strategies for spectrally efficient optical fiber communication systems with direct detection”, in International Conference on Transparent Optical Networks (ICTON 2003), Warsaw, Poland, vol. 2, pp. 58 – 63, 2003.

[4] H. Louchet, K. Petermann, A. Robinson, and R. Epworth, “On the spectral information distribution in optical fibers”, in IEEE Lasers and Electro-Optics Society Annual Meeting (LEOS 2004), Rio Grande, Puerto Rico, vol. 1, pp. 17 – 18, 2004.

[5] N. Kikuchi, “Amplitude and phase modulated 8-ary and 16-ary multilevel signaling technologies for high-speed optical fiber communication”, in SPIE Proceedings, vol. 6021, pp. 17 – 18, 2005.

[6] S. K. Ibrahim, S. Bhandare, and R. Noé, “Performance of 20 Gbit/s Quaternary Intensity Modulation Based on Binary or Duobinary Modulation in Two Quadratures With Unequal Amplitudes”, IEEE Journal of Selected Topics in Quantum Electronics, vol. 12, no. 4, pp. 596 – 602, 2006.

[7] T. Kataoka, Y. Miyamota, K. Hagimoto, and K. Noguchi, “20 Gbit/s long distance transmission using a 270 photon/bit optical preamplifier receiver”, IEE Electronic Letters, vol. 30, no. 9, pp. 715 – 716, April 1994.

[8] M. Daikoku, N. Yoshikane, and I. Morita, “Performance comparison of modulation formats for 40 Gbit/s DWDM transmission systems”, in Optical

Fiber Communications Conference (OFC 2005), Anaheim, CA, USA, OFN2, March 2005.

[9] A. Hodzic, B. Konrad, and K. Petermann, “Alternative Modulation Formats in N×40 Gb/s WDM Standard Fiber RZ-Transmission Systems”, IEEE Journal of Lightwave Technology, vol. 20, no. 4, pp. 598 – 607, April 2002.

[10] G. P. Agrawal, Fiber-Optics Communication Systems, Wiley-Interscience, 2002, ISBN 0-471-21571-6

[11] G. L. Li and P. K. L. Yu, “Optical Intensity Modulators for Digital and Analog Applications”, IEEE Journal of Lightwave Technology, vol. 21, no. 9, pp. 2010 – 2030, September 2003.

[12] E. L. Wooten, et. al., “A Review of Lithium Niobate Modulators for Fiber-Optic Communications Systems,” Sel. Top. in Quant. Elec., vol. 6, pp. 69-82, 2000.

[13] G. Bosco, R. Gaudino, and P. Poggiolini, “An Exact Analysis of RZ Versus NRZ Sensitivity in ASE Noise Limited Optical Systems,” European Conference on Optical Communications, vol. 4, pp. 526-527, Amsterdam, 2001.

[14] M. Pfennigbauer, M. Pauer, P. J. Winzer, and M. M. Strasser, ‘Performance Optimization of Optically Preamplified Receivers for Return-to-Zero and Non Return-to-Zero Coding’, Int. J. Electron. Commun., vol. 56, pp. 261–267, 2002.

[15] M. I. Hayee and A. E. Willner, “NRZ vs RZ in 10–40 Gb/s dispersion-managed WDM transmission systems,” IEEE Photon. Technol. Lett., vol. 11, pp. 991-993, 1999.

[16] G. P. Agrawal, Nonlinear Fiber Optics, 3rd ed., Academic Press, San Diego, CA, 2001

[17] A. Hodzic, Investigations of high bit rate optical transmission systems employing

a channel data rate of 40 Gb/s, Ph.D. thesis, Technische Universität Berlin, Berlin, Germany, 2004.

[18] T. Ono, Y. Yano, and K. Fukuchi, “Demonstration of high-dispersion tolerance of 20 Gbit/s optical duobinary signal generated by a low-pass filtering method”, in Optical Fiber Communications Conference (OFC 1997), Dallas, USA, ThH1, pp. 268 – 269, February 1997.

[19] K. Yonenaga, S. Kuwano, S. Norimatsu, and N. Shibata, “Optical duobinary transmission system with no receiver sensitivity degradation”, IEE Electronic Letters, vol. 31, no. 4, pp. 302 – 304, Feb. 1995.

[20] T. Ono, Y. Yano, K. Fukuchi, T. Ito, H. Yamazaki, M. Yamaguchi, and K. Emura, “Characteristics of Optical Duobinary Signals in Terabit/s Capacity, High-Spectral Efficiency WDM Systems”, IEEE Journal of Lightwave Technology, vol. 16, no. 5, pp. 788 – 797, May 1998.

[21] S. Bigo, G. Charlet, and E. Corbel, “What has hybrid phase/intensity encoding brought to 40 Gbit/s ultralong-haul systems?”, in 30th European Conference on Optical Communication (ECOC 2004), Stockholm, Sweden, pp. 872 – 875, 2004.

[22] M. W. Chbat, and Denis Penninckx, “High-Spectral-Efficiency Transmission Systems,” OFC’00, vol. 1, pp. 134-136, 2000.

[23] K. Yonenaga and S. Kuwano, “Dispersion-Tolerant Optical Transmission System Using Duobinary Transmitter and Binary Receiver”, IEEE Journal of Lightwave Technology, vol. 15, no. 8, pp. 1530 – 1537, August 1997.

[24] X. Gu and L. C. Blank, “10 Gbit/s unrepeated optical transmission over 100 km of standard fiber,” Electron. Lett., vol. 29, no. 9, pp. 2209–2211, Dec. 1993.

[25] D. Penninckx et al., “The Phase-shaped Binary Transmission (PSBT): A new technique to transmit far beyond the chromatic dispersion limit,” in Proc. ECOC’96, vol. 2, Oslo, pp. 173–176.

[26] H. Bissesur et al., "3.2 Tb/s (80_40 Gb/s) C-band transmission over 3_100 km with 0.8 bit/s/Hz efficiency," presented at the Proc. ECOC'01, Amsterdam, The Netherlands, 2001, Postdeadline Paper PD.M.1.11.

[27] L. Moller, C. Xie, X. Wei, X. Liu, C. Stook, J. Wood, P. Bravetti, P. Bergamini, and C. Gualandi, "A Novel 10-Gb/s Duobinary Receiver with Improved Back-to-Back Performance and Large Chromatic Dispersion Tolerance," Phot. Tech. Lett., vol. 16, pp. 1152-1154, 2004.

[28] G. Charlet, J.-C. Antona, S. Lanne, P. Tran, W. Idler, M. Gorlier, S. Borne, A. Klekamp, C. Simonneau, L. Pierre, Y. Frignac, M. Molina, F. Beaumont, J.- P. Hamaide, and S. Bigo, "6.4Tb/s (159×42.7Gb/s) Capacity over 21×100 km using Bandwidth-limited Phase-Shaped Binary Transmission", in 28th European Conference on Optical Communication (ECOC 2002), Copenhagen, Denmark, PD4.1, September 2002.

[29] W. Kaiser, T. Wuth, M. Wichers, and W. Rosenkranz, "Reduced Complexity Optical Duobinary 10-Gb/s Transmitter Setup Resulting in an Increased Transmission Distance", IEEE Photonics Technology Letters, vol. 13, no. 8, pp. 884 – 886, August 2001.

[30] W. Rosenkranz, "High Capacity Optical Communication Networks - Approaches for Efficient Utilization of Fiber Bandwidth", in First Joint Symposium on Opto- & Microelectronic Devices and Circuits (SODC 2000), Nanjing, China, pp. 106 – 107, April 2000.

[31] A. J. Price and N. L. Mercier, "Reduced bandwidth optical intensity modulation with improved chromatic dispersion tolerance", IEE Electronic Letters, vol. 31, no. 1, pp. 58 – 59, January 1995.

[32] A. J. Price, L. Pierre, R. Uhel, and V. Havard, "210 km Repeaterless 10 Gb/s Transmission Experiment Through Nondispersion-Shifted Fiber Using Partial Response Scheme", IEEE Photonics Technology Letters, vol. 7, no. 10, pp. 1219 – 1221, October 1995.

[33] H. Kim and C. X. Yu, "Optical Duobinary Transmission System Featuring

Improved Receiver Sensitivity and Reduced Optical Bandwidth", IEEE Photonics Technology Letters, vol. 14, no. 8, pp. 1205 – 1207, August 2002.

[34] H. Kim, C. X. Yu, and D. T. Neilson, "Demonstration of Optical Duobinary Transmission System Using Phase Modulator and Optical Filter", IEEE Photonics Technology Letters, vol. 14, no. 7, pp. 1010 – 1012, July 2002.

[35] N. S. Bergano, F. W. Kerfoot, and C. R. Davidson, "Margin measurements in optical amplifier systems," Phot. Tech. Lett., vol. 5, pp. 304-306, 1993.

[36] G. Bosco, A. Carena, V. Curri, R. Gaudino, and P. Poggiolini, "Quantum limit of direct-detection receivers using duobinary transmission," Photon. Tech. Lett., vol. 15, pp. 102–104, 2003.

[37] I. Lyubomirsky, and C.-C. Chien, "DPSK Demodulator Based on Optical Discriminator Filter," Phot. Tech. Lett., vol. 17, pp. 492-494, 2005.

[38] H. Nasu, T. Mukaihara, T. Nomura, and A. Kasukawa, "25GHz-spacing wavelength monitor integrated DFB laser module using standard 14-pin butterfly package," in proc. Optical Fiber Communications Conf., Anaheim, CA, 2002, WF5.

[39] L. Moller, C. Xie, R. Ryf, X. Liu, and X. Wei, "10 Gb/s duobinary receiver with a record sensitivity of 88 photons per bit," in proc. Optical Fiber Communications conf., 2004, PDP30.

[40] I. Lyubomirsky and C.-C. Chien, "Optical duobinary spectral efficiency versus transmission performance: Is there a tradeoff?" presented at the Conf. Lasers Electro-Optics/Quantum Electron. Laser Science Conf. (CLEO/QELS), Baltimore, MD, 2005, Paper JThE72.

[41] M. Pfennigbauer et al., "Dependence of optically preamplified receiver sensitivity on optical and electrical filter bandwidths: Measurement and simulation," IEEE Photon. Technol. Lett., vol. 14, no. 6, pp. 831–833, Jun. 2002.

[42] R. J. Nuyts, Y. K. Park, and P. Gallion, “Performance improvement of 10 Gb/s standard fiber transmission system by using the SPM effect in the dispersion compensating fiber,” IEEE Photon. Technol. Lett., vol. 8, no. 10, pp. 1406–1408, Oct. 1996.

[43] T. Wuth, K. Kaiser, and W. Rosenkranz, “Impact of self-phase modulation on bandwidth efficient modulation formats,” presented at the Optical Fiber Commun. Conf. (OFC), Anaheim, CA, 2001, Paper MM6.

[44] N. Yoshikane, I. Morita, and N. Edagawa, “Improvement of dispersion tolerance by SPM-based all-optical reshaping in receiver,” IEEE Photon. Technol. Lett., vol. 15, no. 1, pp. 111–113, Jan. 2003.

[44] A. H. Gnauck, and P. J. Winzer, ”Phase-Shift-Keyed Transmission,” Optical Fiber Communications Conf., paper TuF4, Los Angeles, CA, 2004.

[45] K.-P. Ho, Phase-Modulated Optical Communication Systems, Springer, 2005, ISBN 0-387-24392-5.

[46] A. H. Gnauck and P. J. Winzer, “Optical Phase-Shift-Keyed Transmission”, IEEE Journal of Lightwave Technology, vol. 23, no. 1, pp. 115 – 130, January 2005.

[47] H. Kim, “Differential Phase Shift Keying for 10-Gb/s and 40-Gb/s Systems”, in IEEE Lasers and Electro-Optics Society Annual Meeting (LEOS 2004), Rio Grande, Puerto Rico, ThC1, pp. 13 – 14, 2004.

[48] A. H. Gnauck, S. Chandrasekhar, J. Leuthold, and L. Stulz, “Demonstration of 42.7 Gb/s DPSK Receiver With 45 Photons/Bit Sensitivity”, IEEE Photonics Technology Letters, vol. 15, no. 1, pp. 99 – 101, January 2003.

[49] E. A. Swanson, J. C. Livas, and R. S. Bondurant, “High Sensitivity Optically Preamplified Direct Detection DPSK Receiver with Active Delay-Line Stabilization”, IEEE Photonics Technology Letters, vol. 6, no. 2, pp. 263 – 265, February 1994.

[50] A. Gnauck, “40-Gb/s RZ-Differential Phase Shift Keyed Transmission”, in Optical Fiber Communications Conference (OFC 2003), Atlanta, Georgia, USA, ThE1, March 2003.

[51] G. Bosco and P. Poggiolini, “The Impact of Receiver Imperfections on the Performance of Optical Direct-Detection DPSK”, IEEE Journal of Lightwave Technology, vol. 23, no. 2, pp. 842 – 848, February 2005.

[52] A. Royset and D. R. Hjelme, “Novel dispersion tolerant optical duobinary transmitter using phase modulator and Bragg grating filter,” in Proc. Eur. Conf. Opt. Commun., Madrid, Spain, 1998, pp. 225–226.

[53] D. Penninckx, H. Bissessur, P. Brindel, E. Gohin, and F. Bakhti, “Optical differential phase shift keying (DPSK) direct detection considered as a duobinary signal,” in Proc. Eur. Conf. Opt. Commun., Amsterdam, The Netherlands, 2001, pp. 456–457.

[54] H. Bissessur, G. Charlet, E. Gohin, C. Simonneau, L. Pierre, and W. Idler, “1.6 Tb/s (40_40 Gb/s) DPSK transmission with direct detection,” in Proc. Eur. Conf. Opt. Commun., Copenhagen, Denmark, 2002, Paper 8.1.2.

[55] P. J. Winzer and H. Kim, “Degradations in balanced DPSK receivers,” IEEE Photon. Technol. Lett., vol. 15, no. 9, pp. 1282–1284, Sep. 2003.

[56] E. Ciaramella, G. Contestabile, and A. D’Errico, “A novel scheme to detect optical DPSK signals,” IEEE Photon. Technol. Lett., vol. 16, no. 9, pp. 2138–2140, Sep. 2004.

[57] P. A. Humblet and M. Azizoglu, “On the bit error rate of lightwave systems with optical amplifiers,” J. Lightw. Technol., vol. 9, no. 11, pp 1576–1582, Nov. 1991.

[58] W. V. Sorin, K.W. Chang, G. A. Conrad, and P. R. Hernday, “Frequency domain analysis of an optical FM discriminator,” J. Lightw. Technol., vol. 10, no. 6, pp. 787–793, Jun. 1992.

[59] M. Daioku, I. Morita, H. Taga, H. Tanaka, T. Kawanishi, T. Sakamoto, T. Miyazaki, and T. Fujita, "100-Gb/s DQPSK transmission experiment without OTDM for 100G ethernet transport," J. Lightw. Technol., vol. 25, no. 1, pp. 139–145, Jan. 2007.

[60] R. A. Griffin and A. C. Carter, "Optical differential quadrature phase shift key (oDQPSK) for high capacity optical transmission," OFC, Anaheim, CA, 2002.

[61] A. H. Gnauck, P. J. Winzer, C. Dorrer, and S. Chandrasekhar, "Linear and nonlinear performance of 42.7-Gb/s single-polarization RZ-DQPSK format," IEEE Photon. Technol. Lett., vol. 18, no. 7, pp. 883–885, Apr. 1, 2006.

[62] C. Wree, J. Leibrich, J. Eick, and W. Rosenkranz, "Experimental investigation of receiver sensitivity of RZ-DQPSK modulation format using balanced detection", in Optical Fiber Communications Conference (OFC 2003), Atlanta, Georgia, USA, vol. 2, pp. 456 – 457, March 2003.

[63] I. Lyubomirsky, C.-C. Chien and Y.-H. Wang, "Optical DQPSK Receiver with Enhanced Dispersion Tolerance," IEEE Phot. Tech. Lett., vol. 20, pp. 511-513, 2008.

[64] P. J. Winzer , "Advanced Modulation Formats for High-Capacity Optical Transport Networks," JLT vol. 24, no. 12, Dec. 2006

[65] D. Penninckx, "Dispersion-tolerant modulation techniques for optical communications", in 24th European Conference on Optical Communication (ECOC 1998), Madrid, Spain, vol. 1, pp. 509 – 510, September 1998.

[66] J.-P. Elbers, H.Wernz, H. Griesser, C. Glingener, A. Faerbert, S. Langenbach, N. Stojanovic, C. Dorschky, T. Kupfer, and C. Schulien, "Measurement of the dispersion tolerance of optical duobinary with an MLSE receiver at 10.7 Gb/s", in Optical Fiber Communications Conference (OFC 2005), Anaheim, CA, USA, OThJ4, March 2005.

[67] S. Hayase, N. Kikuchi, K. Sekine, and S. Sasaki, "Proposal of 8-state per symbol (binary ASK and QPSK) 30-Gbit/s optical modulation/demodulation scheme",

in 29th European Conference on Optical Communication (ECOC 2003), Rimini, Italy, Th2.6.4, September 2003.

[68] K.-P. Ho and H.-W. Cuei, “Generation of Arbitrary Quadrature Signals Using One Dual-Drive Modulator”, IEEE Journal of Lightwave Technology, vol. 23, no. 2, pp. 764 – 770, February 2005.

[69] R. A. Griffin, “Integrated DQPSK Transmitters”, in Optical Fiber Communications Conference (OFC 2005), Anaheim, CA, USA, OWE3, March 2005.

[70] G. Kramer, A. Ashikhmin, A. J. van Wijngaarden, and X. Wei, “Spectral Efficiency of Coded Phase-Shift Keying for Fiber-Optic Communication”, IEEE Journal of Lightwave Technology, vol. 21, no. 10, pp. 2438 – 2445, October 2003.

[71] P. S. Cho, V. S. Grigoryan, Y. A. Godin, A. Salamon, and Y. Achiam, “Transmission of 25-Gb/s RZ-DQPSK Signals With 25-GHz Channel Spacing Over 1000 km of SMF-28 Fiber”, IEEE Photonics Technology Letters, vol. 15, no. 3, pp. 473 – 475, March 2003.

[72] Y. K. Lizé, L. Christen, X. Wu, J.-Y. Yang, S. Nuccio, T. Wu, A. E. Willner, R. Kashyap, “Free Spectral Range Optimization of Return-to-Zero Differential Phase Shift Keyed Demodulation in the Presence of Chromatic Dispersion,” Optics Express, vol. 15, No. 11, pp. 6817-6822, 2007.

[73] G. Bosco, and P. Poggiolini, “On the Joint Effect of Receiver Impairments on Direct-Detection DQPSK Systems,” IEEE J. Light. Tech., vol. 24, pp. 1323-1333, 2006.

[74] X. Zhou, J. Yu, T. Wang, and G. Zhang, “Impact of Strong Optical Filtering on DQPSK Modulation Formats”, in Proc. ECOC, paper Po94, 2007.

[75] D. van-den Borne, et. al., “1.6-b/s/Hz Spectrally Efficient Transmission Over 1700 km of SSMF Using 40 x 85.6-Gb/s PolMux-RZ-DQPSK,” IEEE J. Lightwave Tech., vol. 25, p. 222, 2007.

[76] E. B. Desurvire, "Capacity Demand and Technology Challenges for Lightwave Systems in the Next Two Decades," IEEE J. Lightwave Tech., vol. 24, p. 4697, 2006.

[77] J. M. Kahn and K.-P. Ho, "Spectral Efficiency Limits and Modulation/Detection Techniques for DWDM Systems," IEEE J. Sel. Top. Quant. Elec., vol. 10, no. 2, p. 259, 2004.

[78] D. van den Borne, S. L. Jansen, E. Gottwald, E. D. Schmidt, G. D. Khoe, and H. de Waardt, "DQPSK modulation for robust optical transmission," Paper OMQ1, OFC, San Diego, USA, 2008.

[79] J. M. Gené, M. Soler, R. I. Killey, and J. Prat, "Investigation of 10-Gb/s Optical DQPSK Systems in Presence of Chromatic Dispersion, Fiber Nonlinearities, and Phase Noise", IEEE Photonics Technology Letters, vol. 16, no. 3, pp. 924 – 926, March 2004.

[80] D. van den Borne, S. L. Jansen, E. Gottwald, P. M. Krummrich, P. Leisching, G. D. Khoe, and H. de Waardt, "A robust modulation format for 42.8-Gbit/s long-haul transmission: RZ-DPSK or RZ-DQPSK?", in 7th ITG Fachtagung on Photonic Networks, Leipzig, Germany, pp. 51 – 56, April 2006.

[81] G. Charlet and S. Bigo, "Upgrading WDM Submarine Systems to 40-Gbit/s Channel Bitrate," Proc. IEEE, vol. 94, p.935, 2006.

[82] S. Bhandare, D. Sandel, B. Milivojevic, A. Hidayat, A. Fauzi, H. Zhang, S. K. Ibrahim, F. Wüst, and R. Noé, "5.94-Tb/s 1.49-b/s/Hz (40×2×2×40 Gb/s) RZDQPSK Polarization-Division Multiplex C-Band Transmission Over 324 km", IEEE PTL, vol. 17, no. 4, pp. 914 – 916, April 2005.

[83] S. Bhandare, D. Sandel, B. Milivojevic, A. Hidayat, A. Fauzi, H. Zhang, S. K. Ibrahim, F. Wüst, and R. Noé, "5.94 Tbit/s (40×2×2×40 Gbit/s) C-Band Transmission over 324 km using RZ-DQPSK Combined with Polarization Division Multiplex", in 6th ITG Fachtagung on Photonic Networks

"Photonische Netze", Leipzig, Germany, pp. 87 – 90, May 2005.

[84] B. Milivojevic, A. F. Abas, A. Hidayat, S. Bhandare, D. Sandel, R. Noé, M. Guy, and M. Lapointe, “1.6-b/s/Hz 160-Gb/s 230-km RZ-DQPSK Polarization Multiplex Transmission With Tunable Dispersion Compensation”, IEEE Photonics Technology Letters, vol. 17, no. 2, pp. 495 – 497, February 2005.

[85] D. van den Borne, S. L. Jansen, E. Gottwald, P. M. Krummrich, G. D. Khoe, and H. de Waardt, “1.6-b/s/Hz Spectrally Efficient 40×85.6-Gb/s Transmission Over 1,700 km of SSMF Using POLMUX-RZ-DQPSK”, in OFC 2006, Anaheim, CA, USA, PDP34, March 2006.

[86] Y. Zhu, K. Cordina, N. Jolley, R. Feced, H. Kee, R. Rickard, and A. Hadjifotiou, “1.6 bit/s/Hz orthogonally polarized CSRZ-DQPSK transmission of 8×40 Gbit/s over 320 km NDSF”, OFC 2004, Los Angeles, CA, USA, TuF1, February 2004.

[87] P. S. Cho, G. Harston, C. J. Kerr, A. S. Greenblatt, A. Kaplan, Y. Achiam, G. Levy-Yurista, M. Margalit, Y. Gross, and J. B. Khurgin, “Investigation of 2-b/s/Hz 40-Gb/s DWDM Transmission Over 4×100 km SMF-28 Fiber Using RZ-DQPSK and Polarization Multiplexing”, IEEE Photonics Technology Letters, vol. 16, no. 2, pp. 656 –658, February 2004.

[88] C. Wree, N. Hecker-Denschlag, E. Gottwald, P. Krummrich, J. Leibrich, E.-D. Schmidt, B. Lankl, and W. Rosenkranz, “High Spectral Efficiency 1.6-b/s/Hz Transmission (8×40 Gb/s With a 25-GHz Grid) Over 200-km SSMF Using RZ-DQPSK and Polarization Multiplexing”, IEEE Photonics Technology Letters, vol. 15, no. 9, pp. 1303 – 1305, September 2003.

[89] N. Yoshikane and I. Morita, “1.14 b/s/Hz spectrally-efficient 50×85.4 Gb/s transmission over 300 km using copolarized CS-RZ DQPSK signals”, OFC 2004, Los Angeles, CA, USA, PDP38, February 2004.

[90] T. Matsuda, et. al., “Comparison between NRZ and RZ signal formats for in-line amplifier transmission in the zero-dispersion regime,” IEEE J. Light. Technol., vol. 16, pp. 340-348, 1998.

[91] G. Charlet, S. Lanne, L. Pierre, C. Simonneau, P. Tran, H. Mardoyan, P. Brindel, M. Gorlier, J.-C. Antona, M. Molina, P. Sillard, J. Godin, W. Idler, and S. Bigo, "Cost-optimized 6.3 Tbit/s-capacity terrestrial link over 17x100km using phase-shaped binary transmission in a conventional all-EDFA SMF-based system," in proc. Optical Fiber Communications Conf., Atlanta, GA, 2003, PD25-1.

[92] I. Lyubomirsky, and B. Pitchumani, "Impact of optical filtering on duobinary transmission," Phot. Tech. Lett., vol. 16, pp. 1969-1971, 2004.

[93] K. Fukuchi, "Wideband and Ultra-Dense WDM Transmission Technologies Toward over 10-Tb/s Capacity," OFC'02, paper ThX5, 2002.

[94] P. J. Winzer *et al.*, "Optimum filter bandwidths for optically preamplified (N)RZ receivers," IEEE J. Lightwave Tech., vol. 19, no. 9, pp. 1263–1273, Sep. 2001.

[95] W. Atia and R. S. Bondurant, "Demonstration of return-to-zero signaling in both OOK and DPSK formats to improve receiver sensitivity in an optically preamplified receiver," in Proc. LEOS, 1999, pp. 226–227.

[96] M. Shtaif and A. H. Gnauck, "The relationship between optical duobinary modulation and spectral efficiency in WDM systems," IEEE Photon. Tech. Lett., vol. 11, no. 6, pp. 712–714, Jun. 1999.

[97] S. Walkin and J. Conradi, "On the relationship between chromatic dispersion and transmitter filter response in duobinary optical communication systems," IEEE Photon. Tech. Lett., vol. 9, no. 7, pp. 1005–1007, Jul. 1997.

[98] B. Milivojevic, Study of Optical Differential Phase Shift Keying Transmission Techniques at 40 Gbit/s and beyond, Ph.D. thesis, University of Paderborn, EIM-E, Paderborn, Germany, 2005.

[99] T. Tokle, Optimised Dispersion Management and Modulation Formats for High Speed Optical Communication Systems, Ph.D. thesis, Research Center COM, Technical University of Denmark, Denmark, 2004.

[100] S. K. Ibrahim, Study of Multilevel Modulation Formats for High Speed Digital Optical Communication Systems, Ph.D. thesis, University of Paderborn, Germany, 2007